FOULING OF MICROFILTRATION MEMBRANES DURING FILTRATION OF WASTEWATER EFFLUENT FOR WATER REUSE: MECHANISMS, EFFECTS, AND CONTROL

A Dissertation

by

KUNAL GUPTA

Submitted to the Office of Graduate and Professional Studies of
Texas A&M University
in partial fulfillment of the requirements for the degree of

DOCTOR OF PHILOSOPHY

Chair of Committee,	Shankaramaan Chellam
Committee Members,	Scott Socolofsky
	Ying Li
	Jacqueline Ann Aitkenhead-Peterson
Head of Department,	Robin Autenrieth

May 2021

Major Subject: Civil Engineering

ABSTRACT

This research investigates the performance of polyvinylidene fluoride (PVDF) microfiltration (MF) membranes during its utilization for direct filtration of wastewater treatment plant (WWTP) effluent for potable water reuse. The research primarily focuses on the fouling of PVDF MF membranes and explores the mechanisms, long-term effects, and strategies for control and mitigation. The overall hypothesis of the research is that irreversible fouling of microfiltration membranes is influenced by specific effluent organic matter (EfOM) – membrane interactions and the progressive accumulation of these foulants plays a primary role in the long-term productivity loss of microfilters.

The research demonstrated that fouling of PVDF microfilters by EfOM proceeded via a two-step mechanism involving the initial deposition of relatively hydrophobic organics to the membrane followed by the attachment of relatively hydrophilic organics. It was also shown that the fouling is critically dependent on the attachment of a small specific fraction of EfOM. Clues to the identity of this specific fraction were obtained using high-resolution mass spectrometry and shown to possibly belong to the lipid chemical class. Potential mechanisms of fouling were evaluated via surface characterization techniques (e.g. attenuated total reflection - Fourier transform infrared spectroscopy, scanning electron microscopy, electrokinetic analysis) along with mathematical modeling (constant flux blocking laws). The analysis revealed the detrimental role of internal pore fouling in irreversible fouling with surface fouling working as a secondary dynamic membrane preventing pore exposure. Further, the analysis of backwash performance of different backwashing solutions underscored non-electrostatic EfOM-membrane interactions as the dominant mechanism of irreversible fouling.

Investigations on the long-term performance (fouling propensity and water permeability) of the membranes revealed that while multiple chemical cleaning cycles led to no change in membrane productivity, progressive chemically irreversible fouling led to the loss in productivity, confirming the hypothesis of the research. The irreversible fouling was also accompanied by progressive loss in membrane mechanical strength (measured as Young's modulus and dynamic storage modulus). Additionally, pre-chlorination of wastewater effluent was an effective pretreatment strategy for fouling control. However, fouling control was dose-dependent and transitional in nature with fouling exacerbated at chlorine doses below a threshold dose. This transitional behavior originated from the dose-dependent alterations in EfOM character and was validated by extended Derjaguin-Landau-Verwey-Overbeek theory calculations of EfOM-membrane free energy of adhesion.

DEDICATION

To my Father and Mother,

Your sacrifices and support led me here.

Forever indebted.

ACKNOWLEDGEMENTS

I would like to begin by expressing my sincerest gratitude to my advisor, Dr. Shankar Chellam. Without his tremendous patience, support, and guidance this Ph.D. study and related research would not have been completed. I cannot thank him enough for providing me the opportunity to explore independent research avenues while relentlessly pushing me to expand the limits of my skills and intellectual curiosity. His immense knowledge, strong work ethic, curiosity to science, and attention to detail will continue to inspire me.

Besides my advisor, I would like to thank the rest of my dissertation committee: Prof. Scott Socolofsky, Prof. Ying Li, and Prof. Jacqueline Aitkenhead-Peterson, for their insightful comments and encouragement, but also for the hard questions which incented me to widen my research from various perspectives.

I would also like to thank the faculty and staff of Texas A&M Civil and Environmental Engineering Department. To Laura Byrd, Chris Grunkemeyer, Sherry Hoffman, James Mras, Dave Dillon, and Larry John, thank you very much for your patience and kind assistance.

I was fortunate to get a chance to work with the most motivated and hardworking students in Dr. Chellam's group. Special thanks to my fellow lab mates and friends, Kyungho Kim, Sourav Das, and Bilal Abada, for the stimulating discussions, for the sleepless nights we were working together, and for all the fun we have had in the last four years or so. I wish them all the very best for their future and hope we remain connected as lifelong friends. I would also like to thank the previous students in Dr. Chellam's group, Dr. Nernaga Gamage and Dr. Ayu Sari, for their transfer of knowledge and very useful advice.

I would also like to thank my family: my parents, Navin Gupta and Prabha Gupta, my brother, Praneet Gupta, and his family (his wife Deepshikha Gupta and my nephew Pranshik Gupta) for supporting me spiritually throughout writing this dissertation and my life in general. A special thanks to Geetika Bharadwaj, for her continuous love and support. Thank you for being by my side even though we were thousands of miles apart. And finally, a special mention to the Academic Twitter community, which became my support and introduced me to some amazing mentors throughout this journey and journey to come.

Additionally, this research was made possible through funding by a grant from the National Science Foundation (CBET 1636104), which is greatly acknowledged.

CONTRIBUTORS AND FUNDING SOURCES

Contributors

This work was supervised by a dissertation committee consisting of Professor Shankar Chellam (advisor) and Professor Scott Socolofsky of the Department of Civil and Environmental Engineering, Professor Ying Li of the Department of Mechanical Engineering, and Professor Jacqueline Ann Aitkenhead-Peterson of the Department of Soil and Crop Science.

All work for the dissertation was completed independently by the student.

Funding Sources

This work was made possible in part by National Science Foundation (Grant CBET 1636104). Its contents are solely the responsibility of the author and do not necessarily represent the official views of the sponsors.

TABLE OF CONTENTS

Page

LIST OF FIGURES

Page

LIST OF TABLES

Page

CHAPTER I

INTRODUCTION

Introduction

Growing population and climate change have put pressure on typical drinking water supplies. In the past few years, water shortages and its subsequent rationing in large cities around the world, such as Cape Town, South Africa [1]; Sydney, Australia [2]; and Chennai, India [3] exemplify the severity of water scarcity facing the world. It is estimated that if the unsustainable pressures on global water resources continue to rise, more than half of the world's population will be at risk by 2050 [4]. A key strategy to tackle this challenge is improved water management especially in urban settings [5], one important component of which is potable reuse of municipal wastewater [6, 7].

Municipal wastewater reuse within this work implies the treatment of municipal wastewater effluent to a level acceptable for potable use. The treatment is accomplished by a 'multiple barrier approach,' i.e., a sequence of treatment processes in series termed together as a treatment train [8-11]. Different types of treatment trains are utilized around the world and within United States [8, 9]. The choice of technologies depends on multiple factors including wastewater quality, economic viability, and regulatory constraints [10, 11]. In any case, one of the more commonly employed treatment trains is shown in **Figure 1** [10, 11]. The focus of my research is low-pressure membrane filtration.

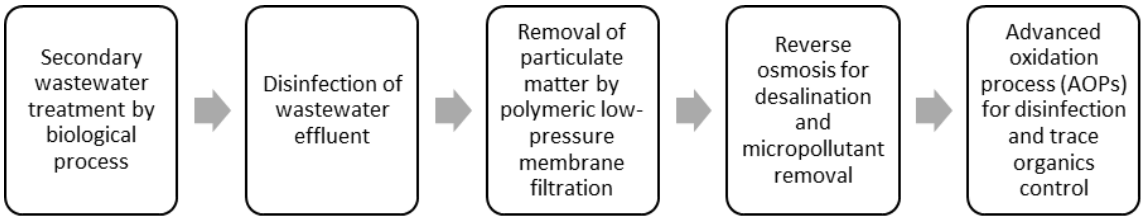

Figure 1 Block diagram illustration of water reuse treatment train.

Low-pressure membrane filtration is the broad term used for ultrafiltration (UF) and microfiltration (MF) [12]. Both these membrane processes affect filtration predominantly by sieving, i.e., remove particles greater than their pore size (typical range of pore sizes in UF is 0.01 – 0.1 µm and MF is 0.1 – 1 µm) [11, 13]. The work presented here has employed polymeric MF membranes (nominal pore size of 0.1 µm); nevertheless, the results and inferences can be extrapolated to UF membranes composed of the same polymer owing to the same filtration mechanism. The primary role of these membrane filters is the removal of particulate matter including bacteria, protozoa, and other suspended particles [14, 15]. However, a major impediment to the performance of these membranes is 'fouling' [16]. Fouling can be defined as the deposition of suspended or dissolved feed water constituents (foulants) on the membrane surface, at its pore openings or inside membrane pores, resulting in loss of performance of a membrane, i.e., increasing the resistance to the flow of water [17]. Prolonged fouling during the filtration process necessitates a stoppage in operation to perform fouling control measures. One of the most common measures is 'hydraulic backwashing,' basically the reversal of flow of water to remove or dislodge the foulants [18, 19]. While backwashing has proven quite effective with universal acceptance across the water treatment industry, it does not remove all

foulants and does not restore membrane permeability completely, resulting in 'hydraulically irreversible fouling' [18, 20-22].

One important cause of irreversible fouling during potable reuse is the hydraulically irreversible attachment of effluent organic matter (EfOM) [23, 24]. In the past, multiple works have identified different fractions of EfOM responsible for fouling [25-27] and even categorically associated the EfOM components to various extents of fouling and its reversibility [28, 29]. However, an important limitation of these earlier works is that they have been based on single filtration cycles [25-27], which by definition do not address long-term fouling behavior that is highly detrimental to membrane life. Another shortcoming of earlier research focusing on individual EfOM fractions is that although it provides insights into their interactions with membranes, it completely ignores foulant-foulant interactions, which is key to understanding long-term fouling [21, 29, 30]. For these reasons, a lab-scale apparatus was designed using hollow-fiber membranes and custom-built to facilitate flow reversal and membrane surface analysis to better understand reversible and irreversible fouling over multiple backwashing-filtration cycles.

Apart from our lack of understanding of fouling mechanisms, there is insufficient coherence about the identity of dominant EfOM fractions responsible for fouling. Four classes of EfOM are typically recognized; namely biopolymers, humic substances, microbial building blocks, and low molecular weight organics [31, 32]. Using this classification, different researchers have implicated different fractions for fouling. While biopolymers have been the usual suspects in majority of cases, the possible role of humic substances has been reported inconsistently [31-33]. Also, the use of biopolymer

concentration as a potential predictor of fouling propensity has been reported contradictorily [31, 32]. The main reason for the incoherence and contradictions across the body of research is the complex nature of EfOM, which is basically a concoction of numerous organic compounds of yet unknown structure and composition [34]. Thus, a broad and generic classification of EfOM is unable to account for its specific interactions with membranes that play a major role in determining the fouling behavior of a given feed water [21, 30, 35]. Hence, a molecular level characterization of EfOM is required to provide clues to the identity of organic species responsible for fouling, which may serve as potential predictor of fouling propensity.

Irreversible fouling during long-term operation even with backwashing results in the gradual loss in membrane permeability, which is countered by chemical cleaning. Chemical cleaning typically includes sodium hydroxide, sodium hypochlorite, and dilute (HCl) or weak acids (e.g. citric acid) [36, 37]. The chemical cleaning agents employed, their respective concentrations, and the protocol used is typically recommended by the membrane manufacturer. Chemical cleaning requires the complete stoppage of filtration soaking and flushing of the membranes with cleaning agents for a few hours, and rinsing them thoroughly before filtration can be resumed [37]. Chemical cleaning also contributes to membrane aging [36]. Thus, ‘aging’ can be defined as the long-term irreversible deteriorations in membranes (character and performance) brought about by exposure to physical, chemical, and biological stressors during operation [38, 39].

The aging of membranes due to exposure to harsh chemicals and associated degradation has received significant attention in the past decade [36]. While this is an

important facet, the critical role of irreversibly attached foulants also needs to be considered especially since this has been established by membrane autopsies of full-scale facilities at different stages in their operational lifetime [40, 41]. Now, although directly characterizing surface foulants from full-scale plants present a truer picture of membrane aging, they are typically more difficult logistically owing to costs associated with element replacement and plant downtime and the need for coordination between academics and municipalities [42, 43]. Thus, laboratory studies can facilitate the better understanding of the role of irreversible foulants in aging.

Regardless of the mechanisms of fouling, it has to be controlled for engineering applications. One of the mainstays of fouling mitigation is pretreatment [44-47]. Drinking water facilities routinely employ chemical coagulation-flocculation as pretreatment prior to membrane filtration [44, 45], which is often not the case in potable reuse [8, 9]. However, the wastewater effluent is almost universally disinfected with chlorine (a strong oxidant) prior to MF to control biofouling throughout the treatment train [9, 48, 49]. Importantly, hypochlorite can alter the overall character of EfOM and thus their interactions with membranes [50, 51]. Paradoxically, MF fouling by pre-chlorinated wastewater effluent has not been studied to date.

The above literature review and background of current research demonstrates that further investigations are required to develop a more holistic understanding of the long-term performance of MF membranes during potable reuse. This dissertation enunciates fouling mechanisms and sets forth molecular insights about organic foulants. To our knowledge, this is amongst the first rigorous and systematic investigations of the aging of

membranes, from an irreversible fouling aspect. The analysis of sodium hypochlorite addition as a fouling mitigation strategy presents a pragmatic tool for utilities adopting water reuse. In this research, different facets of MF membrane fouling during potable water reuse, including the mechanisms, the consequence (aging), and its control and mitigation were investigated.

Research goals and objectives

The overarching hypothesis of the research is that irreversible fouling of microfilters stems from EfOM-membrane interactions, influenced predominantly by a small fraction of specifically interacting species. Persistent attachment of these foulants can alter membrane surface and bulk character leading to membrane aging. The main goal of my research is to understand the underlying mechanisms of irreversible MF membrane fouling, identify responsible foulants, understand how this fouling affects membrane productivity in the long-term, and analyze a possible approach for fouling mitigation. To achieve this goal, the following specific objectives were formulated:

a. Investigate the mechanisms of progressive irreversible fouling of MF membranes during the filtration of municipal wastewater effluent.

b. Implement a non-targeted molecular level organic matter characterization technique to identify dominant organic species responsible for fouling.

c. Carefully investigate the aging of membranes over multiple fouling and cleaning cycles.

d. Analyze the role of sodium hypochlorite when used for MF pretreatment to control and mitigate fouling.

Dissertation organization

The main components of this dissertation are five manuscripts dedicated to research findings (chapter II – VI), chapter II and III have already been published and others (IV – VI) are being prepared for submission for peer-review before possible publication. The format of each of these chapters is the same as journal articles; each beginning with an introduction, followed by the material and methods, results and discussion, and finally the concluding remarks. The final chapter (chapter VII) in the dissertation summarizes the important conclusions drawn from the entire study along with recommendations for future research directions.

Chapter II focuses on elucidation of the mechanisms of progressive irreversible fouling during microfiltration of wastewater filtration over multiple filtration-backwashing cycles. These findings can be found in Gupta, K. and S. Chellam, Contributions of surface and pore deposition to (ir)reversible fouling during constant flux microfiltration of secondary municipal wastewater effluent. *Journal of Membrane Science*, 2020. **610**: p. 118231.

Chapter III investigates the use of pre-chlorination (addition of sodium hypochlorite prior to MF) as a pretreatment strategy to mitigate fouling during wastewater effluent microfiltration. These findings can be found in Gupta, K. and S. Chellam, Pre-

chlorination effects on fouling during microfiltration of secondary municipal wastewater effluent. *Journal of Membrane Science*, 2021. **620**: p. 118969.

Chapter IV explores the use of high-resolution mass spectrometry to characterize EfOM (molecular fingerprinting) as a tool to identify species predominantly responsible for MF fouling. Research work has been completed and manuscript for this work is under preparation.

Chapter V discusses the bench-scale progressive aging of membranes as brought about by fouling and chemical cleaning over long-term operation. The work compares and discusses the differences between typical laboratory-based membrane aging experimental designs. Research work has been completed and manuscript for this work is also in preparation.

Chapter VI investigates the relative contributions of typically invoked mechanisms for irreversible fouling (non-electrostatic membrane-foulant interactions and multivalent cation influenced foulant-membrane bridging) of microfiltration membranes. The work employs various backwash water compositions (salt solutions, acids, alkalis, and oxidizers) and analyzes and compares their efficacy in fouling removal to peer into the mechanisms responsible for irreversible fouling. Research work has also been completed and the manuscript is in preparation.

CHAPTER II

CONTRIBUTIONS OF SURFACE AND PORE DEPOSITION TO (IR)REVERSIBLE FOULING DURING CONSTANT FLUX MICROFILTRATION OF SECONDARY MUNICIPAL WASTEWATER EFFLUENT *

Introduction

Although microfiltration (MF) is commonly employed during wastewater reclamation to remove suspended solids, bacteria, and protozoa, its fouling continues to be an unresolved problem [8, 14, 15]. Short-term fouling of MF and ultrafiltration (UF) membranes by effluent organic matter (EfOM) during forward filtration has been principally attributed to colloidal [23, 52-54] or acidic [24, 55, 56] fractions. However, MF/UF systems are backwashed periodically to control fouling [19], which needs to be incorporated in the experimental design to differentiate EfOM fouling during short-term forward filtration and long-term operation. In this context, process engineering and statistical techniques have been implemented to operationally extend chemical cleaning intervals by optimizing backwashing (e.g. frequency and duration) and pretreatment (e.g. ozonation and coagulation) parameters during MF of wastewater effluent [57-63]. Simply monitoring flux decline caused by individual EfOM fractions and varying pretreatment type have suggested that colloidal matter [29], biopolymers [64], and humics [28] are

* Reprinted with permission from "Contributions of surface and pore deposition to (ir)reversible fouling during constant flux microfiltration of secondary municipal wastewater effluent", Gupta, K and S. Chellam, Journal of Membrane Science, 610, 118231, Copyright 2020 by Elsevier.

principally responsible for longer-term hydraulically irreversible fouling. However, these earlier efforts were largely directed towards developing overall fouling indices or identifying specific EfOM components that caused the maximum extent of fouling, and as such do not provide mechanistic insights into irreversible fouling. Further, EfOM fractionation may obfuscate specific foulant-foulant interactions [29, 30, 65] and forward filtration experiments alone do not capture intricacies of fouling progression over multiple backwashing cycles. For example, humics and low molecular weight species were inferred to not cause short-term fouling [30, 53] but were implicated in long-term irreversible MF fouling [28, 66]. Fractionation also negates interactions between different foulant types, which has been shown to be critical in surface water MF [21, 35] necessitating experiments with the whole water (i.e. not just individual components).

Typically, pretreatment is used to reduce fouling e.g. [67] but it can also be used to operationally identify dominant fouling mechanisms. For example, differences in MF fouling following iron coagulation and powdered activated carbon (PAC) adsorption of EfOM revealed the importance of the colloidal fraction on fouling [54, 68]. Prefiltration, iron coagulation, and anion exchange have also been used to show that low molecular weight EfOM was not responsible for flux decline [52]. Similarly, I also employ several pretreatment scenarios herein to investigate long-term MF fouling mechanisms during filtration of secondary-treated municipal wastewater.

The principal objective of this research is to systematically elucidate specific membrane-foulants and foulant-foulant interactions leading to long-term hydraulically irreversible fouling during hollow fiber MF of municipal wastewater secondary effluent.

Fouling progression over multiple filtration-backwashing cycles was characterized in terms of EfOM functionalities accumulated on the membrane surface using attenuated total reflectance-Fourier transform infrared (ATR-FTIR) spectroscopy and blocking law modeling. Changes in organic functionalities were analyzed to identify dominant foulants as the pressure increased during constant flux MF over multiple forward filtration and backwashing cycles. Clues to hydraulically irreversible fouling mechanisms were also obtained by comparing pressure profiles after different adsorption pretreatments (PAC, heated aluminum oxide particles (HAOPs), and colloidal polyvinylidene fluoride (cPVDF)).

Materials and methods

Source water

Secondary effluent from Carter's Creek conventional activated sludge Treatment Plant in College Station, Texas after ultraviolet (UV) disinfection was employed not only because of proximity but also because the State water plan has estimated that potable reuse will account for > 10% of all new drinking water supplies by 2070 [69]. Important water quality parameters for the sample collected on February 2018 were: pH 8.0 ± 0.2, turbidity 5.2 ± 0.6 NTU, silicon 3.1 ± 0.3 mg/L, alkalinity 159.2 mg/L as $CaCO_3$, chemical oxygen demand (COD) 14 mg/L, dissolved organic carbon (DOC) 9.1 ± 0.5 mg/L, and UV_{254} 0.188 ± 0.020 cm^{-1}. Carbohydrates and proteins were measured to be 3.36 mg/L as glucose and 1.03 mg/L as bovine serum albumin, respectively [21]. The average specific UV absorbance (SUVA, the ratio of UV_{254} in m^{-1} and DOC in mg/L) was 2.066 L/(mg.m)

indicating EfOM (measured as DOC) was largely of low hydrophobicity and low molecular weight [70]. Note that as is universally practiced [23, 24, 29, 34, 53, 71, 72], EfOM concentration was quantified as DOC.

Membrane and modules

Four polyvinylidene fluoride (PVDF) hollow fiber membranes nominally rated at 0.1 μm with 1.293 mm outer diameter and 0.711 mm inner diameter (Aria™, Pall Corp.) were potted in a transparent 15 mm polyvinyl chloride tube using epoxy resin. Fiber lumens were closed at one end and open at the other to accomplish outside-in filtration. The exposed length of each fiber was 18.5 cm resulting in a total active filtration area of 30 cm^2. Following manufacturer recommendations, modules were thoroughly rinsed first with ultrapure water to remove the biocide preservative (NaN_3), followed by a 50% ethanol solution to wet all the pores since these are highly hydrophobic with an air-water contact angle measured as 112.8 ± 0.14° (Attention Tensiometer, Biolin Scientific), and finally rinsed again three times with ultrapure water prior to experimentation with wastewater effluent.

Adsorbents

HAOPs were prepared by neutralizing a 0.1 M solution of $Al_2(SO_4)_3 \cdot 18H_2O$ to pH 7.0 with NaOH and heating the resulting suspension in a closed container at 110 °C for 24 h [73]. The resulting suspension was cooled and refrigerated until use. Powdered activated carbon (Darco G-60, Fisher Scientific) was used as obtained. cPVDF was used based on

the idea of employing adsorbents of the same composition as the membranes [74]. A 2% w/v PVDF solution was prepared by dissolving 4 g PVDF powder in 200 ml N,N-dimethylformamide (DMF) and rapidly adding 300 mL of 0.1mM NaOH solution under moderate stirring resulting in the formation of a cloudy suspension. DMF was removed by dialyzing the suspension (12-14 kDa molecular weight cut-off, Spectrum™ Spectra/Por™) against ultrapure water for three days with 5-6 water changes until it was completely transparent at 270 nm (absorption maxima for DMF) and DOC < 0.2 mg/L (similar to ultrapure water) [74, 75]. The particle size distribution and electrophoretic mobility measured by dynamic/electrophoretic light scattering, respectively (Litesizer 500, Anton Paar) and the BET surface area measured via N_2 adsorption (Micometritics TriStar 3000) are summarized in **Table 1.**

Table 1 Important characteristics of adsorbents

Adsorbent	Particle size (μm)	Zeta potential at pH 7 (mV)	Specific surface area (m^2/g)
HAOPs	2.11 ± 0.05	+13.4 ± 0.04	110
cPVDF	0.22 ± 0.12	-33.4 ± 0.12	11.5
PAC	5 to >10	-6.05 ± 0.03	606

Adsorption pretreatment

The protocol for all three adsorbents employed two steps; contact with wastewater and removal after an appropriate contact time. The appropriate adsorbent dose was determined by first evaluating isotherms by adding a known amount of HAOP, cPVDF,

or PAC to raw water to achieve the target concentration and mixing vigorously until equilibrium was reached (**Supporting Information (SI) Figure A-1**). A 100 mg/L concentration of all three adsorbents achieved maximum EfOM (DOC) removal and therefore employed for MF pretreatment (**Figure 6d**). Before microfiltration of pretreated waters, the raw water with adsorbent particles after equilibration was vacuum filtered using coarse filters rated at 5-10 microns (VWR Grade 474). The resulting filtrate was additionally centrifuged for 10 minutes at 10,000g to remove any remaining smaller particles (see **SI Table A-1**) nearly "eliminating" carryover of the adsorbent to the MF membrane. This 2-step procedure prevented colloidal fouling by removing all adsorbent particles since our aim was to analyze changes in fouling behavior effected by EfOM removal. Importantly, centrifugation shifted the particle size distribution after pretreatment to significantly smaller values compared with the raw secondary wastewater effluent (see **Figure 9**). In contrast, prefiltration and centrifugation of the raw wastewater effluent without pretreatment reduced the size distribution only to a small degree (see filtered/centrifuged wastewater in **Figure 9**).

MF setup and procedure

A custom-made MF apparatus comprising two computer-controlled peristaltic pumps (Watson Marlow, 120U/D1), one each for filtration and backwash, four solenoid switching valves to control the flow and enabling automatic forward filtration and backwash cycles, two pressure transducers (PX303, Omega), a digital flow sensor (LS32-1500, Sensirion), and a temperature sensor (RTD, TJ120 CPSS 116G, Omega). A program

written in LabVIEW 14 (National Instruments) controlled instruments and continuously acquired data in the automatic mode.

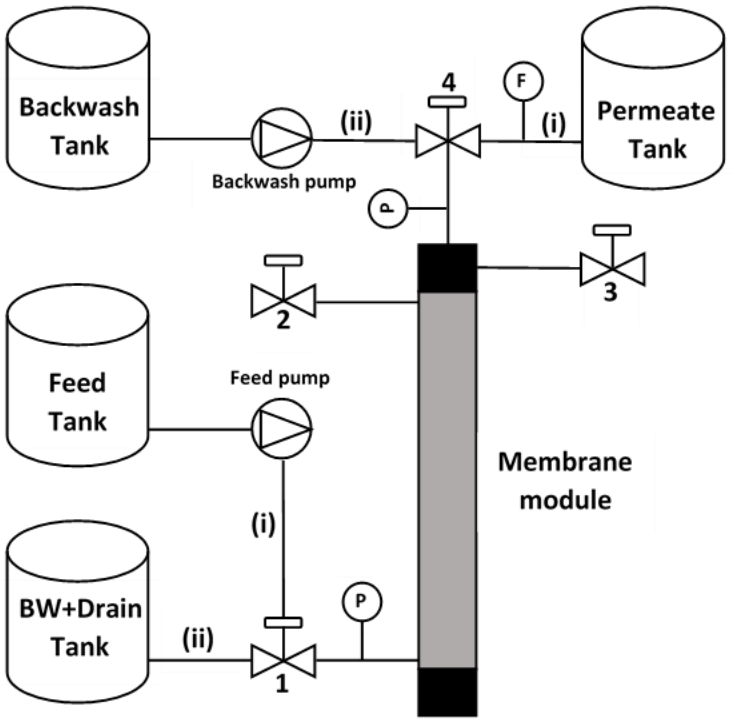

Figure 2 Schematic of the microfiltration apparatus

Each filtration/backwashing cycle comprised five steps (**Figure 2**). At the beginning of each cycle, the module was flushed with the feed water by opening valves 1(i) and 2. During the second step, filtration was performed at a constant flux of 60 L/m^{2}h as recommended by the manufacturer by opening valves 1(i) and 4(i); the feed was pumped from outside of the fibers and the permeate was collected from the fiber lumen. The feed pump was switched off after filtration for 40 minutes (i.e. backwashing interval). Next, the shell side (i.e. outside of the hollow fibers) was flushed by opening valves 4(ii) and 3 and filling it with ultrapure water for 90 seconds. Following this, backwashing was

performed at 60 L/m^{2}h for 1 minute by opening valves 4(ii) and 1(ii). Finally, by opening valves 2 and 1(ii), the module was gravity drained and emptied to remove the concentrate before starting the next cycle, ensuring similar initial conditions for the next cycle.

Blocking laws analysis

Dominant fouling mechanisms during each forward filtration cycle were identified using constant flux blocking laws [76]. Noisy pressure measurements were smoothed using robust local regression "rlowess" routine in MATLAB and then differentiated numerically to obtain the first derivative. However, this procedure was insufficient to obtain sufficiently accurate instantaneous second derivatives, which were estimated by using piecewise polynomials of order 4-7 for the first derivative and numerically differentiating it.

Membrane surface characterization

At the end of a filtration/regeneration experiment, all membrane fibers were carefully taken out of the module, one of which was cut into small pieces and dried for 24 h in a vacuum desiccator. The infrared spectra of membrane surfaces were obtained using a Nicolet iS10 spectrometer equipped with a mid-infrared Ever-Glo source, DTGS detector, KBr beam splitter, and Omnic 9.0 Software with a diamond iTX accessory to allow sampling in ATR mode. A background spectrum was also collected on a clean ATR window prior to each analysis. Samples were placed on the window and the IR spectrum was obtained by averaging 128 scans collected at 4 cm^{-1} resolution over 650–4000 cm^{-1}.

The spectra were recorded from top, middle, and bottom of each hollow fiber to obtain representative information on foulants.

Scanning electron microscope (SEM) images of virgin and fouled membrane surfaces were obtained using a Tescan Vega 3 instrument at 7000x magnification and 5 kV accelerating voltage after sputter coating a 10 nm gold layer on the vacuum dried samples. The streaming potential of the outer surface of the virgin and fouled membranes was measured against a background solution of 1 mM KCl in the pH range 3 to 9 with an electrokinetic analyzer fitted with an adjustable gap cell (SurPASS^{TM} 3, Anton Paar) [77] and converted to the zeta potential using the Helmholtz-Smoluchowski equation.

Results and Discussion

Forward MF of raw wastewater effluent

Figure 3a and **b** depict non-linear concave upward transmembrane pressure profiles for individual cycles, which were quantitatively explained by a power-law compressible cake filtration model [78]:

$$\Delta P = \Delta P_0 + \beta \Delta P^n v \quad (1)$$

where β is a pre-exponent term, n is the cake compressibility index designating variation of specific resistance with pressure [79], and v is the specific volume filtered. Importantly, the compressibility index for the entire duration of hollow fiber constant flux filtration was derived independently from separate constant pressure experiments using disc membranes ($n = 0.40 \pm 0.03$; **Figure 3a** inset) and not used as a fitting parameter. The constant pressure experiments were performed using a stainless-steel cell (SEPA ST,

Osmonics) also employing hydrophobic PVDF membranes (VVHP04700, Millipore). Excellent agreement was obtained ($R^2 > 0.99$) between **Equation 1** and pressure profiles for the one cycle in **Figure 3a** and all 9 cycles in **Figure 3b** using the independently measured compressibility index of 0.40 strongly suggesting that power-law compressible cake filtration was the dominant fouling mechanism during forward filtration of raw secondary wastewater effluent.

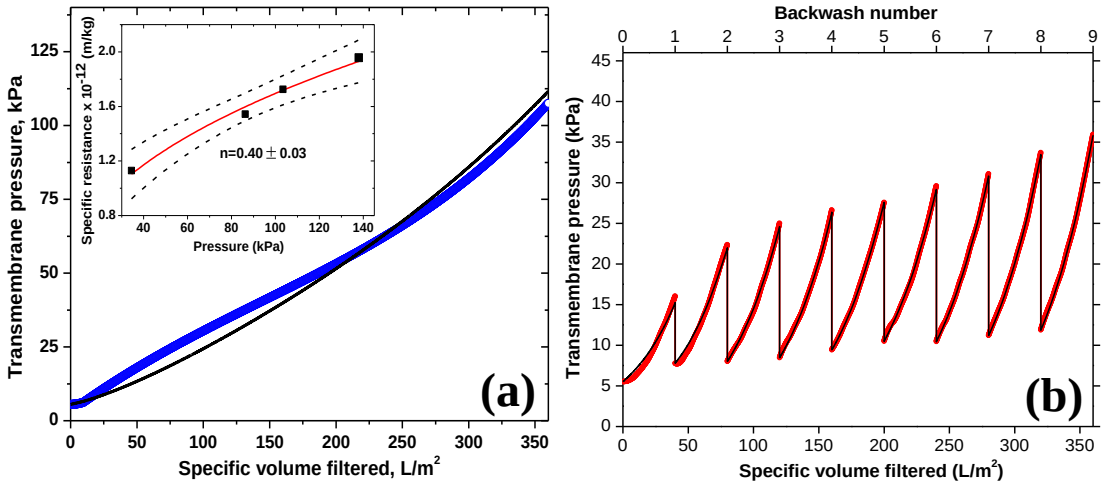

Figure 3 Instantaneous transmembrane pressure profile during MF of wastewater effluent without backwashing (top left panel blue color) and with backwashing every 40 minutes (top right panel red color). Predictions of compressible cake filtration theory (Equation 1, black) are also shown in both cases.

Irreversible fouling evolution during MF of raw wastewater effluent

As shown in the control experiment (**Figure 3a)**, transmembrane pressure increased to 107 kPa with no backwashing compared with only 35 kPa at the end of 9 cycles with backwashing every 40 minutes for the same volume filtered (**Figure 3b**) demonstrating long-term fouling control by periodic flow reversal [19, 21, 35]. Hydraulically irreversible fouling was evident with progressively increasing TMPs at the beginning of each forward filtration step; e.g. 5.5, 7.8, 8.0, and 8.4 kPa for the first 4-

cycles. The highest loss of membrane productivity was in the first cycle (42%) compared with only 3, 5, and 12 % for the next 3-cycles. Such a phenomenon can be seen in earlier publications e.g. [18, 20, 21, 29], and was attributed to the maximum exposure of the membrane surface and pores to foulants when first put in service and after chemical cleaning.

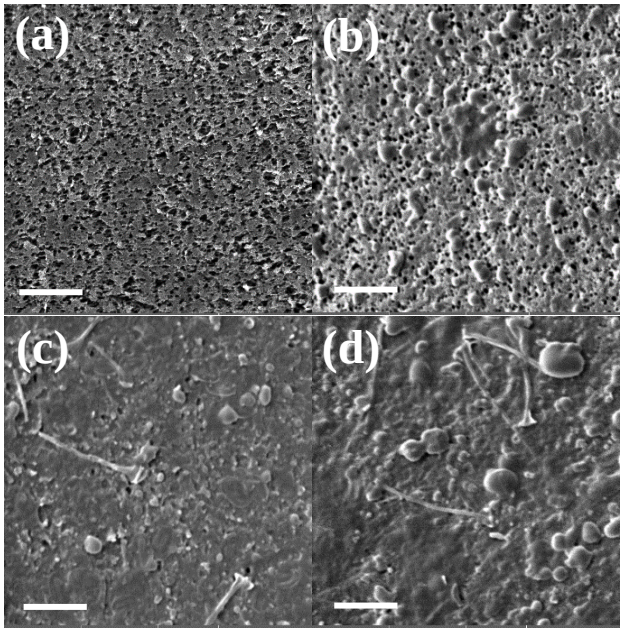

Figure 4 Electron micrographs of virgin membrane (a) and fouled membranes after 1, 7, and 9 backwash cycles (b), (c), and (d), respectively are shown on the bottom panels (5 µm scale bar).

Continually declining productivity even with backwashing demonstrates hydraulically irreversible foulant accumulation accentuating pressure buildup over long-term operation, eventually reaching 12 kPa for the start of the final (9^{th}) cycle corresponding to a 120% increase over the entire duration of filtration. Electron microscopy provided further evidence of progressive foulant accumulation with **Figure 4a** showing an interconnected network of pores, typical of commercial polymeric membranes. At the beginning of cycle 2, most of the surface is still visible (**Figure 4b**)

corresponding to a minimal amount of irreversibly deposited foulants. Additional filtration-backwashing cycling resulted in the accumulation of more and more foulants as shown in **Figure 4c** and **Figure 4d** after 7 and 9 cycles respectively. Surface deposition observed in these micrographs is consistent with the dominance of cake filtration inferred from **Equation 1** above.

Mechanism of progression of irreversible surface deposition

Attenuation of virgin membrane functionalities in ATR-FTIR spectra in **Figure 5** corroborated operational and visual evidences for progressive foulant buildup described in the section **Forward MF of raw wastewater effluent**. For example, CH_2 asymmetric and symmetric vibration of PVDF at 3027 and 2986 cm^{-1} [80] decreased by 8%, 38%, and 44% and 13%, 65%, and 81% after 1st, 7th, and 9th backwashes respectively. Intensifying peaks at 2963, 2926, 2875, and 2853 cm^{-1} (asymmetric CH_3, CH, and CH_3 and CH symmetric, respectively [81]) after each cycle suggests incomplete removal of hydrophobic foulants. This was particularly significant after the 1st cycle where peaks at 2963, 2926, 2875, and 2853 cm^{-1} increased by 71%, 74%, 134%, and 55% in area respectively. Subsequently, peak areas associated with hydrophobic end members increased relatively gradually over long-term operation; e.g. 94 and 127% increase at 2963 cm^{-1}, 92 and 149% increase at 2926 cm^{-1}, 152 and 190% increase at 2875 cm^{-1}, and 69 and 78% increase at 2853 cm^{-1} after the 7th and 9th cycles, respectively.

In contrast to hydrophobic moieties containing more CH groups that magnified during the *initial stages* of operation, more polar functionalities such as O-H/N-H peaks at 3700-3300 cm^{-1} [81] representing polysaccharides and proteins intensified significantly

over *later time stages*. For example, NH stretch at 3200 cm^{-1} increased 120% in area after 1st cycle but by a remarkable 1000% and 1500% after 7th and 9th cycles, respectively. Similarly, the area for OH stretch at 3350 cm^{-1} increased by 48.5% initially, but by 840% and 1800% after 7th and 9th cycles.

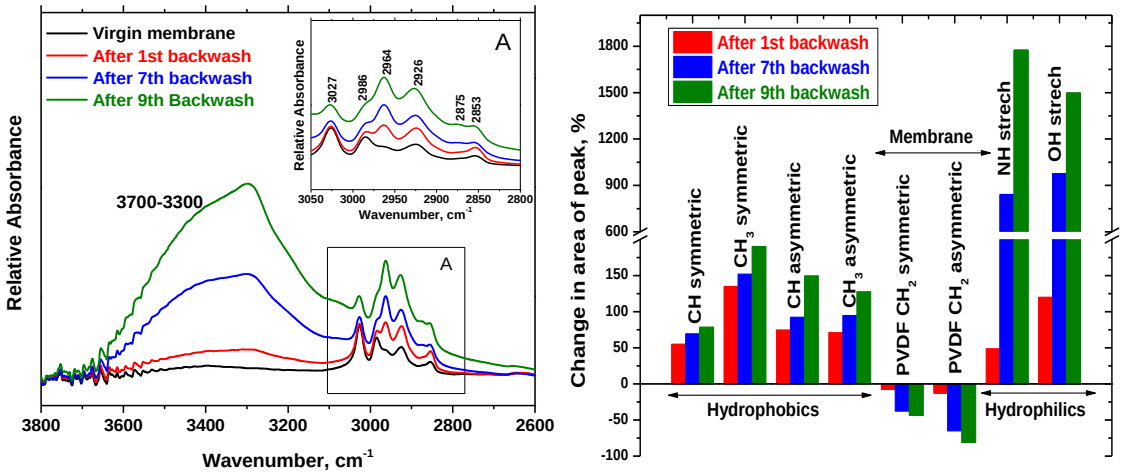

Figure 5 ATR-FTIR spectra of virgin (black) and irreversibly fouled membranes after 1 (red), 7 (blue) and 9 (green) backwashes (left panel). Changes in area of peaks of foulants and membrane with successive cycles (right panel).

Hence, physically irreversible loss in productivity followed a two-step mechanism initially by the preferential accumulation of relatively hydrophobic foulants directly on the membrane. This "conditions" the microfilter's surface ensuing the deposition of relatively more hydrophilic materials on the otherwise hydrophobic PVDF membrane leading to long-term fouling. Biphasic fouling progression deduced above wastewater reclamation has also been indirectly inferred for NOM fouling during drinking water treatment by interpreting differential transient removal of small hydrophobic organics and large hydrophilic organics [21, 35]. Importantly, such a two-step mechanism may discredit reductionist investigations with single model foulants in the feed water e.g. [24, 53] that

by definition cannot capture progressive accumulation of different materials at or near membrane surfaces. Indeed, synergistic interactions have been reported where significantly higher flux decline is caused by foulant mixtures compared to individual foulants, including EfOM isolates [30, 65], indicative of stepwise accumulation of disparate materials in the vicinity of membranes.

Additional information on EfOM components leading to (ir)reversible fouling and pressure increase during forward filtration was gleaned by comparing filter performance and feed water characteristics of the untreated and pretreated wastewater effluent (see **Adsorbents** and **Adsorption pretreatment** sections) as discussed next.

Fouling intricacies probed by pretreatment with different adsorbents

Fouling propensity and hydraulic reversibility are not direct functions of gross total EfOM content

Adsorbents were used to remove different amounts (and types) of organic matter to investigate EfOM effects on fouling. As expected, all forms of pretreatment significantly reduced fouling during each forward filtration cycle compared with filtration of untreated wastewater effluent as seen by comparing **Figure 6** with **Figure 3b**. The fouling behavior has been discussed in terms of dissolved EfOM since these have been shown to be the dominant foulant fractions [24] and there was no evidence of the presence of adsorbent particles after filtration-centrifugation (section **Adsorption pretreatment** and **SI Adsorption pretreatment**). The remaining dissolved EfOM after PAC, HAOP, and cPVDF pretreatment was 4.82 ± 0.12, 6.00 ± 0.14, and 8.68 ± 0.37 mg/L DOC,

respectively. Although DOC removal followed the trend PAC > HAOP > cPVDF (47%, 34%, and 4.5% respectively in **Figure 6d)**, fouling varied as PAC > cPVDF > HAOP (57%, 40%, and 30%, respectively for cycle 1 with similar results for all other forward filtration cycles, **SI Figure A-3**).

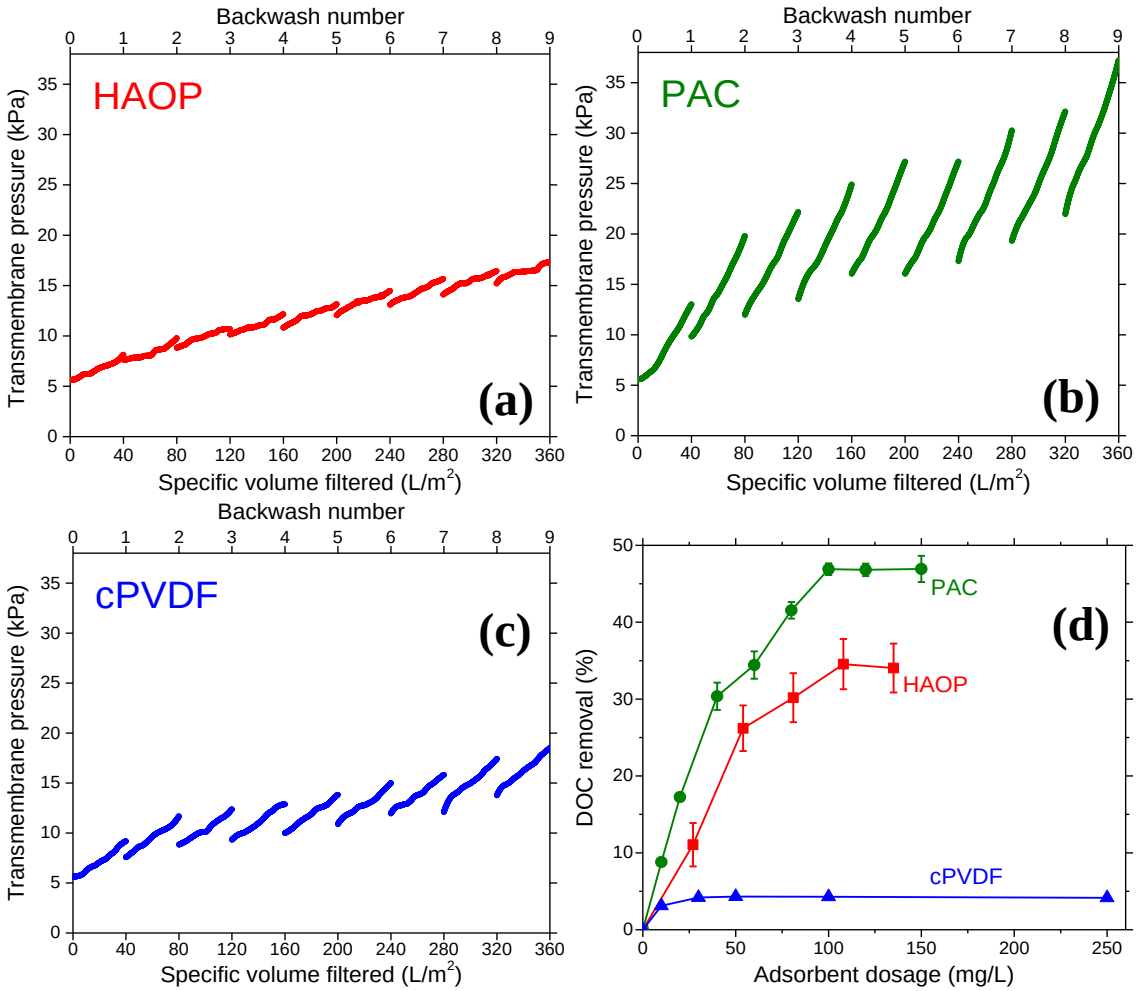

Figure 6 Instantaneous transmembrane pressure profiles over 9 successive filtration and hydraulic backwashing cycles for wastewater effluent following various pretreatments (a, b, and c). Corresponding DOC removal during adsorption pretreatment is summarized in the lower right panel (d).

This non-proportional relationship between EfOM and fouling behavior has also been shown in **SI Figure A-4**. Importantly, the same trend was also observed for

irreversible fouling control by backwashing wherein cPVDF and HAOP recovered pressure better than PAC (74% with cPVDF and HAOP compared to only 55% with PAC for cycle 1, **SI Figure A-3**). In other words, although PAC removed nearly 50% of influent DOC and cPVDF removed only < 5%, cPVDF controlled both reversible and irreversible fouling significantly better than PAC (**SI Figure A-3**). Hence, only a small fraction of EfOM was responsible for MF fouling and EfOM fouling propensity cannot be gleaned simply by monitoring gross DOC concentration in the feed water. Similar observations have been made with NOM in surface water [32, 82].

Besides, it can also be argued that the vast majority of EfOM moieties removed by PAC from the wastewater effluent (~50%) were non-foulants. Our results for secondary-treated wastewater MF are similar to an earlier report where coagulation pretreatment resulted in a higher flux compared with PAC, even though PAC removed significantly higher amounts of DOC [54, 68]. Additional evidence for PAC removing non-fouling organic fractions has also been presented for humic acid filtration [83]. In other words, PAC appears to remove bulk and otherwise "inert" DOC that would have simply deposited and interacted negligibly with the microfilter surface, which would have been easily removed by backwashing. Therefore, PAC pretreatment appears to increase the exposure of the "clean" membrane surface to specifically interacting (i.e. adsorbable) foulants leading to more pronounced hydraulically irreversible fouling, which has also been previously reported [84, 85]. Further, although HAOPs removed significantly more EfOM than cPVDF (**Figure 6d**), both pretreatments were equally effective in controlling irreversible fouling again suggesting that only a small and specific fraction of influent

organics are directly responsible for irreversible fouling, which is similar to NOM behavior during surface water MF/UF to generate potable water [16, 74, 86].

Based on these arguments, I can infer that the nature of the EfOM removed by different pretreatments had a profound effect on fouling behavior. These differences are interpreted in more detail next by analyzing the surface chemistry of fouled membranes.

Different fouling behavior but similar surface foulant chemistry

Figure 7a shows difference spectra of irreversibly fouled membranes after subtracting the spectrum of the wetted virgin membrane surface. Peak locations were nearly identical for the raw wastewater effluent and after the different pretreatments suggesting a largely similar nature of EfOM foulants in all cases even though fouling profiles were significantly dissimilar. The -C=O stretching peak at 1732 cm^{-1} is typical for carboxylic groups present in humic and fulvic acids [53]. Peaks at 1650 cm^{-1} and 1544 cm^{-1} are characteristic amide-I and amide-II peaks representing protein fingerprints [24, 29, 53]. Peaks at 1260 cm^{-1}, 1098 cm^{-1}, 1040 cm^{-1}, and 803 cm^{-1} correspond to ν_{as}-C-O-C, ν_{as}-C-O, ν_{s}-C-O-C- stretch, and ν_{s}-O-C=O respectively, characteristic of polysaccharides [24, 29, 87, 88]. Importantly, peak intensities in **Figure 7** varied generally as HAOP < PAC < cPVDF < raw wastewater, corresponding to the respective extent of surface deposition visualized qualitatively by microscopy in **Figure 10** and **Figure 4d**.

Further evidence of the similarities in foulants and their functional groups for various feed waters was provided by membrane surface zeta potential behavior. As seen in **Figure 7b**, the virgin membrane's surface was substantially negatively charged (-33 <

ζ < -20 mV) over the pH range ~3 – 9 [89]. Irreversible EfOM attachment during filtration of raw and pretreated secondary effluent increased the zeta potential to significantly less negative values (~ -20 < ζ < +3 mV) similar to [35, 68]. In all cases, protonation of surface functionalities at progressively acidic conditions increases zeta potential at lower pH. Relatively similar zeta potential values and trends for all fouled membranes points to the similar nature of irreversibly attached EfOM as inferred from **Figure 7a** and described in the previous paragraph.

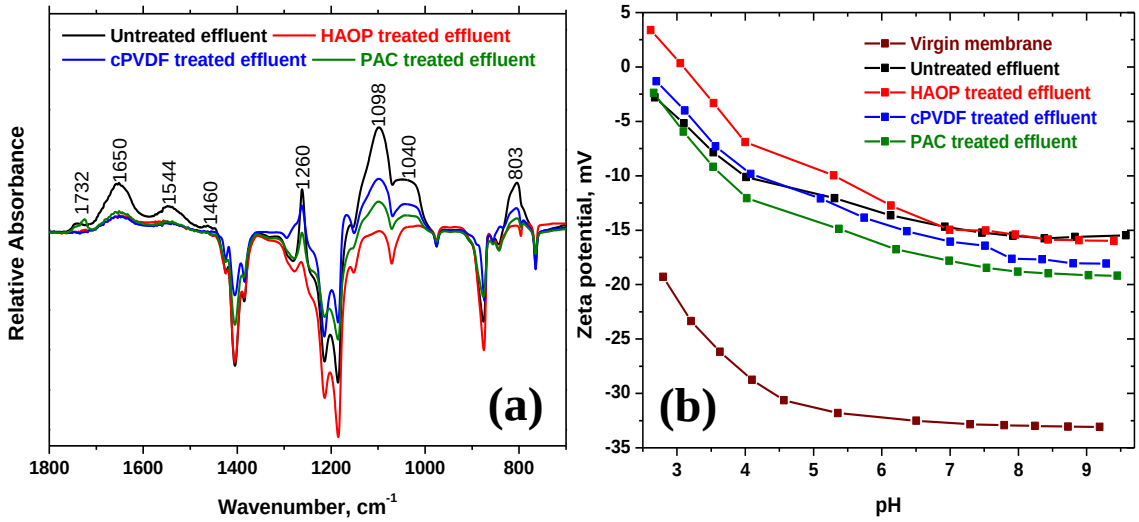

Figure 7 (a) Difference spectra of irreversibly fouled membranes following nine filtration/regeneration cycles and filtering 360 L/m^2 (red: after HAOP treatment, blue: after cPVDF treatment, green: after PAC treatment, and black: untreated raw wastewater effluent). (b) Variation of surface zeta potential as a function of solution pH with 1 mM KCl as background.

Hence, FTIR spectra point to constituents with similar functional groups dominating microfilter surfaces after multiple filtration/backwashing cycles for both raw and pretreated wastewater effluents with pretreatment only changing the cumulative amount of deposited foulants. Similarities in the chemical nature of surface foulants stand in stark contrast to substantial differences in fouling behavior reported in the previous

section. This is similar to an earlier report [24], where hydrophobic and hydrophilic base/neutrals EfOM were the dominant constituent on surfaces of hydraulically cleaned membranes even though they did not cause any fouling. Nevertheless, changes in the nature of foulants and consequent differences in fouling behavior argued in the previous section were not explicitly captured by IR spectra. This could be a consequence of low ATR-IR signal penetration into the entire depth of the fouling layer and the streaming potential being reflective of the overall surface chemistry. In other words, IR spectra and zeta potential were dominated by EfOM functional groups at the top few microns of the deposited foulant layer rather than in the vicinity or inside the pores [24].

It is worth noting that direct proof of internal pore fouling is difficult to obtain with researchers generally resorting to indirect, empirical/modeling lines of evidence indicating the same. For example, the importance of internal pore adsorption and blockage in irreversible fouling was operationally established by experimentally demonstrating that membranes with smallest pores fouled the least followed by ones with progressively larger nominal pores [16, 63, 90]. Similarly, the flux has been shown to reduce negligibly for membranes with smaller pores and attributed to the inability of nanocolloids and macromolecules in the feed water to enter its pore network and deposit internal to the membrane matrix [91, 92]. Evidence for internal pore fouling transitioning to surface fouling can also be obtained by blocking law analysis [93], which is pursued next.

Pore- and surface fouling during forward filtration of pretreated waters

Figure 8 summarizes statistical fits of constant flux blocking laws to experimental pressure profiles of all pretreated waters; note only filtration/backwashing cycles 1, 6, and

9 are shown for the sake of brevity. Standard blocking (exponent n → 4/3) dominated the first forward filtration cycle in all cases suggesting material deposition inside the pores was responsible for fouling during the initial stages of MF. This continued throughout the entire duration of experimentation for HAOP pretreatment (entire top row) but transitioned to intermediate blocking (n → 1) after 3 cycles for PAC (2nd row middle and right panels) and after just 1 cycle for cPVDF (bottom row middle and right panels).

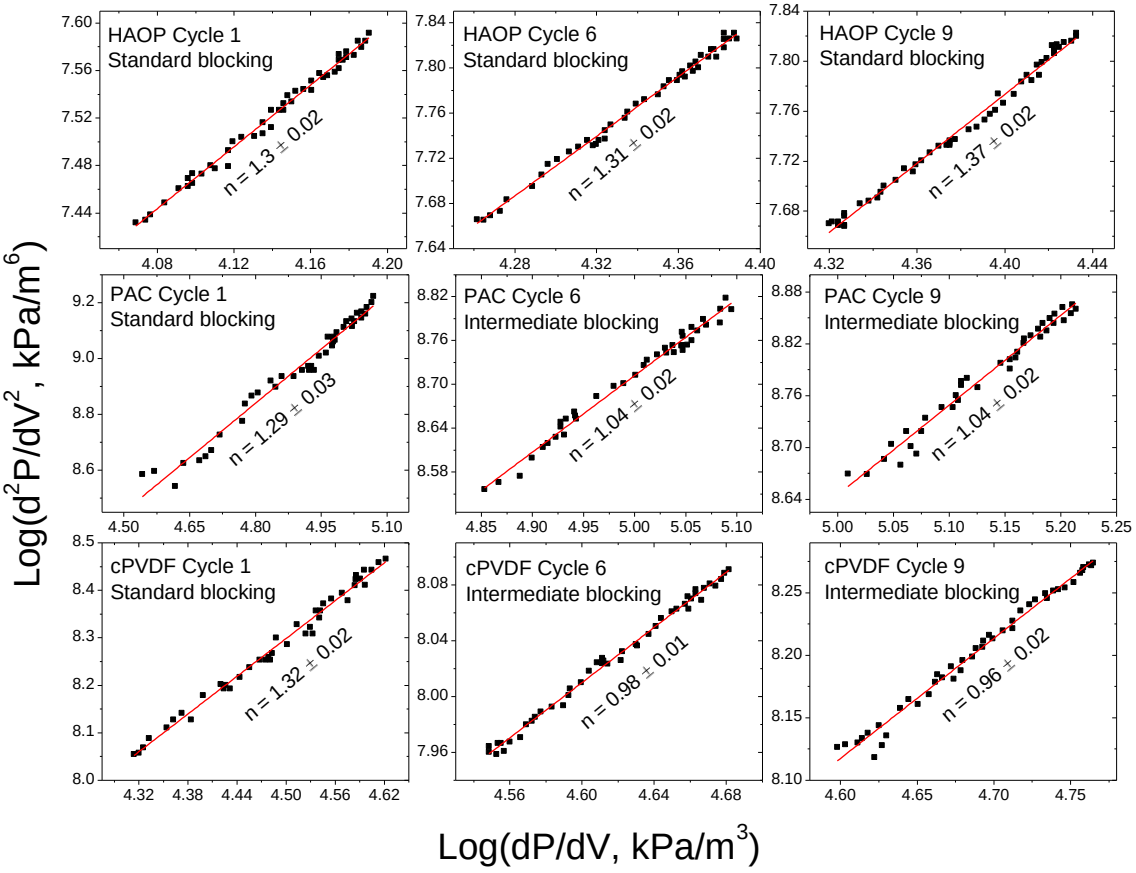

Figure 8 Evaluation of blocking law mechanisms during individual filtration cycles after different adsorption pretreatments. Only three cycles (1, 6, and 9) have been shown.

Particle size distributions (PSDs, **Figure 9**) of the four different feed water supported fouling mechanisms identified by blocking laws. Colloids larger than the

membrane nominal pore size (0.1 μm) dominated the wastewater effluent leading to straining and surface deposition during forward filtration in its case i.e. cake formation as described earlier in section **Forward MF of raw wastewater effluent** and **Figure 3a** & **b**. In contrast, HAOP pretreatment shifted PSDs < ~0.1 μm (**Figure 9**) allowing internal pore fouling, i.e. standard blocking throughout the entire experiment (entire top row in **Figure 8**) suggesting continued availability of sites inside the membrane's polymer matrix for EfOM deposition because fouling was low and backwashing was effective (**Figure 6**). PAC pretreatment also reduced particle sizes in the MF feed water to < ~0.1 μm, consistent with standard blocking during the initial filtration stages. However, fouling transitioned to intermediate blocking, i.e. surface deposition after the first 3 cycles (middle and right panels in middle row of **Figure 8**). This is attributed to the greater extent of fouling and less effective backwashes (**Figure 6**) with PAC pretreatment that would have saturated internal sorption sites relatively quickly transitioning to surface fouling. cPVDF pretreatment also resulted in standard blocking initially, developing to intermediate blocking after only one cycle potentially due to the second size peak at 1-4 μm causing surface deposition to dominate the latter filtration stages even though fouling was low throughout, i.e. internal sites continue to be available.

The size distribution of particles in wastewater after coarse filtration and centrifugation (see section **Adsorption pretreatment**) is also shown for comparison. As expected, it shifted to smaller values compared with the untreated wastewater, even though relatively large particles (> 0.1 μm) were detected in it as well as the cPVDF-pretreated wastewater after filtration and centrifugation. Note that although centrifugation

parameters were selected for "complete" removal of adsorbent particles, larger particles in **Figure 9** represent very low-density moieties possibly biopolymer aggregates and/or humic acid (hydro)gels [94-96].

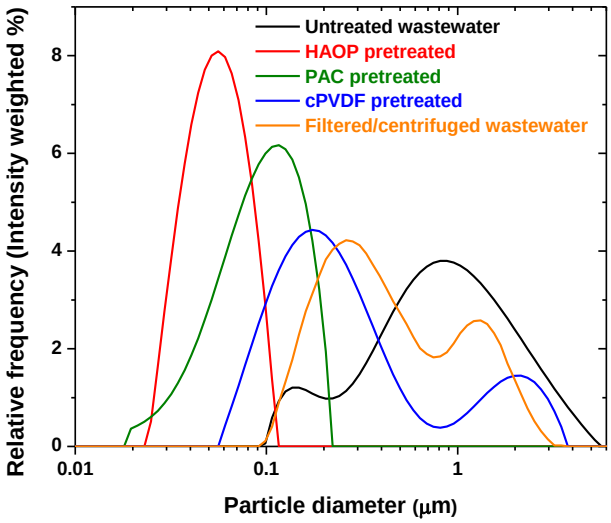

Figure 9 Particle size distributions of different feed waters showing a shift to smaller sizes with pretreatment.

Figure 10 shows electron micrographs of membrane surfaces at the conclusion of each pretreatment experiment that supports dominant fouling mechanisms identified above. **Figure 10a** shows a morphology similar to the virgin membrane (**Figure 4a**) with only a sparse surface coverage of foulants and many visible pores implying that deposition was largely inside the membrane matrix, i.e. standard blocking for the entire experiment as summarized in **Figure 8**. Significant surface deposits in conjunction with regions of open/unblocked pores were observed in the case of both cPVDF and PAC pretreatment (**Figure 10b** and **c)** consistent with intermediate blocking in **Figure 8.**

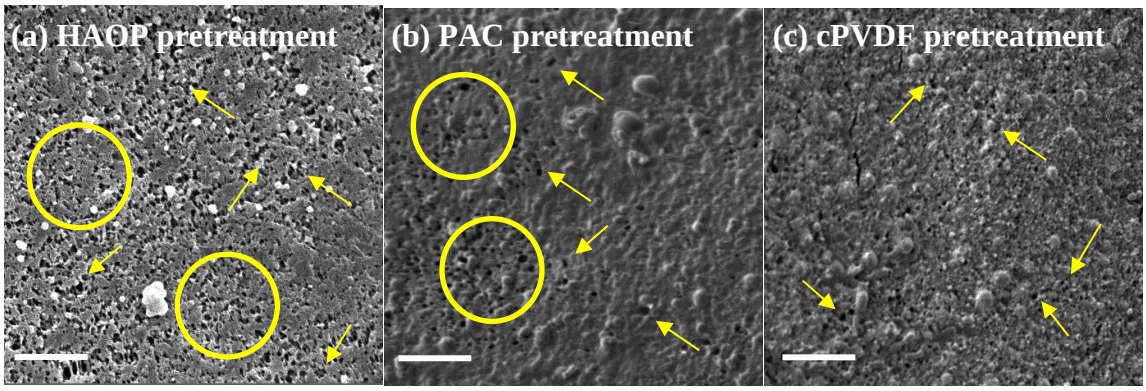

Figure 10 Electron micrographs of membranes after 9 filtration/backwashing cycles for different pretreatments showing distinct differences in fouling layer morphologies (5 µm scale bar). Arrows point to visible open pores and circles encompass open membrane surfaces. Figure 4 shows the virgin membrane and after filtration of untreated wastewater.

Several visible open pores and large areas of the open membrane even after 9 cycles in **Figure 10** lends further evidence of deposition inside the pores causing increased irreversible fouling in the case of all pretreatments, which was inferred earlier from standard blocking model fits and presence of sub 0.1 µm particles in the feed water. Adsorption of low molecular weight molecules [66, 97], intercalation of < 200 nm colloids [98], 0.02 – 0.5 µm "meso-particles" [99], and submicron colloids [18] on pore walls inside the membrane matrix have all been implicated in long-term hydraulically irreversible fouling. Since the untreated wastewater effluent formed a thick cake layer completely obscuring all pores (**Figure 4d)** resulting in the least extent of irreversible fouling over the long-term, it appears that the formation of a 'dynamic secondary membrane' decreases exposure of pores to foulants reducing irreversible fouling [91, 100]. To further confirm our hypothesis that particles entering membrane pores causing irreversible fouling, I monitored MF fouling during re-filtration of its own permeate as discussed next.

Re-filtration of MF permeate reduced reversible fouling but increased irreversible fouling

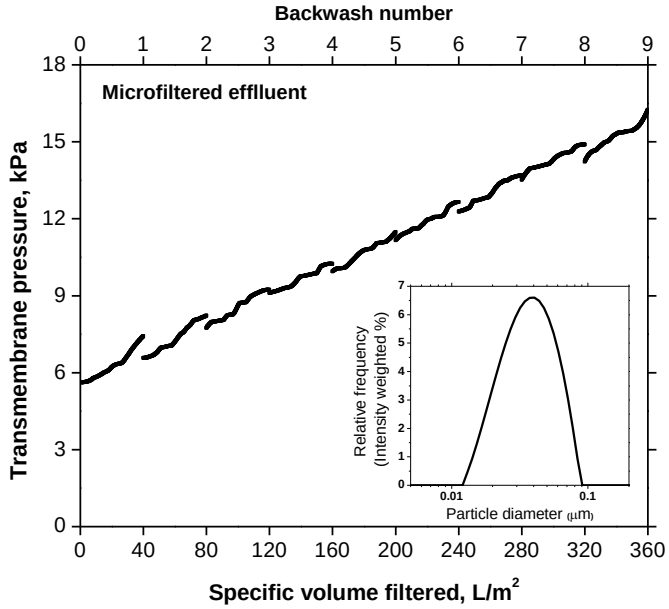

Figure 11 Instantaneous transmembrane pressure profiles over 9 successive filtration and hydraulic backwashing cycles for microfiltered wastewater effluent. The particle size distribution of the MF effluent is shown in the inset.

As summarized in **Figure 11**, hydraulic backwashing well-controlled overall fouling over multiple filtration/regeneration cycles during MF of its own permeate compared to that of the raw effluent. For example, at the end of the 1st cycle, reversible fouling contributed 78% to the total fouling (**Figure 3b**) whereas for MF permeate it only contributed 47% to the total fouling (**Figure 11**) with a similar trend for the successive 8 cycles. In contrast, the extent of irreversible fouling with MF effluent was more pronounced. For example, the pressure at the start of 9th cycle was 150% of the pressure at start of 1st cycle for MF permeate (**Figure 11**) compared with only 120% in the case of untreated effluent (**Figure 3b**). These results are consistent with irreversible fouling

caused by nanocolloids (sub 100 nm, **Figure 11** inset) that enter and specifically interact with membrane pores nominally rated at 100 nm in our case [35, 63] resulting in poor recovery by backwashing.

Conclusions

The progression of hydraulically irreversible surface deposition of EfOM was inferred to be initiated by the deposition of relatively hydrophobic species which conditioned the membrane surface for the further deposition of more hydrophilic species. This two-step mechanism is similar to NOM fouling of MF/UF [21, 35] during surface water treatment even though there are characteristic differences between EfOM in wastewater effluent and NOM in surface water [34, 72, 101, 102]. For example, EfOM contains additional bulk organic matter in the form of soluble microbial products, extracellular polymeric substances, and biodegradation products of anthropogenic organics, which result in the dissimilar performance of conventional water treatment processes with iron coagulation removing only ~40% EfOM but nearly 60% NOM [71]. In contrast, our results suggest that differences in organic matter characteristics may not be the most dominant factor in determining the cumulative extent of deposition and/or fouling behavior for MF/UF, but it may affect the kinetics of fouling.

The disparity between the magnitude of EfOM removal by adsorption pretreatment and the extent of reversible and irreversible fouling implies that only a specific organic fraction dominates MF/UF fouling [16, 74, 86]. Importantly, this demonstrates that total DOC concentration, which is commonly considered by practitioners as a fouling indicator,

should not be an accurate fouling predictor, which is confirmed by literature reports of feedwaters with higher DOC exhibiting lower fouling propensity [32, 82]. Further, our results point to the irreversible attachment of feed water constituents to the membrane surface is not the dominant reason for permeability loss, which is instead dominated by adhesion inside the pores internal to the membrane matrix. Hence, the hydrodynamic size of EfOM is an important determinant of fouling propensity and hydraulic reversibility.

In this study, I monitored multiple successive filtration/backwashing cycles using a popular commercially available hydrophobic membrane. Hence, our results need to be cautiously extrapolated to other membranes, since long-term fouling and regeneration by backwashing will strongly depend on their material of construction, which will control initial specific foulant-membrane interactions, in turn determining foulant-foulant interactions as filtration progresses.

CHAPTER III

PRE-CHLORINATION EFFECTS ON FOULING DURING MICROFILTRATION OF SECONDARY MUNICIPAL WASTEWATER EFFLUENT *

Introduction

Even though secondary-treated municipal wastewater effluents are almost always chlorinated prior to microfiltration (MF) and ultrafiltration (UF) to reduce biofouling during potable reuse [9, 48, 49], there is a lack of detailed information ascertaining the effects of pre-chlorination on low-pressure membrane fouling [103] with most previous work focusing only on non-disinfected feedwaters e.g. [52, 66]. On the other hand, aqueous phase chlorine reactions with dissolved organic matter (DOM) and associated alterations have been extensively studied in the context of drinking water treatment [104, 105] and known to modify DOM structure, functionality, and polarity (e.g., bond cleavage and increasing hydrophilicity arising from thiol oxidation to sulfonic acid). Additionally, the nature and extent of physicochemical DOM alterations have been reported to undergo a transitional change as a function of the applied NaClO dose, i.e. its behavioral trends change at a threshold chlorine concentration [50, 51]. For example, the effective size of model organic compounds (bovine serum albumin and dextran) and biopolymers increased at low chlorine concentrations whereas their size decreased at higher dosages

* Reprinted with permission from "Pre-chlorination effects on fouling during microfiltration of secondary municipal wastewater effluent", Gupta, K and S. Chellam, Journal of Membrane Science, 620, 118969, Copyright 2020 by Elsevier.

[50]. Low dosages also enhanced the tendency of proteins and humic acids to sorb onto a hydrophobic surface, which reversed at higher doses [51]. Additionally, changes in organics' size (in relation to membrane pore diameter) will influence pore blocking whereas changes in functionality and/or polarity will impact its specific interactions with membranes, both of which impact fouling kinetics and mechanisms [106-108]. Importantly, effluent organic matter (EfOM), which refers to DOM in municipal wastewater effluent is comprised of both DOM from surface water and soluble microbial products i.e. biopolymers [34]. Therefore, I hypothesized that analogous to DOM in surface water, EfOM will undergo dose-dependent transformations in its structure and functional groups upon chlorination that will influence its interaction with membrane surfaces thereby changing MF fouling behavior during wastewater reclamation.

To date, the vast majority of investigations of pre-chlorination for MF/UF pretreatment have been restricted to surface water [103], which to our knowledge have also not systematically analyzed the role of chlorine dose on fouling behavior. Further, results available to date are contradictory with chlorination reportedly increasing fouling in some cases [109, 110] and mitigating it in others [111, 112]. Fouling reduction has been attributed to lower bacterial and extracellular polymeric substances (EPS) loading and the formation of a more porous cake layer [112]. Paradoxically, the breakdown of large molecular weight components has been invoked as an explanation for both reduction [111] and aggravation of fouling [109]. Hence, consistent explanations for the empirically observed differences in fouling behavior upon chlorination are lacking.

In this manuscript, I pursue clues to physicochemical interactions [113] between chlorinated EfOM and a commercially available hollow fiber polyvinylidene fluoride (PVDF) microfilter to ascertain fouling trends during filtration and backwashing using the extended Derjaguin-Landau-Verwey-Overbeek (XDLVO) theory [114-117]. Our objective is to elucidate the impacts of chlorination-influenced changes in EfOM on physical and chemical interactions with a microfilter and associated hydraulically (ir)reversible fouling. To this end, experiments incorporating multiple filtration-backwashing cycles were performed with raw and chlorinated effluents over a range of concentrations. EfOM effective hydrodynamic size and its non-covalent (Lifshitz-van der Waals and Lewis acid-base) interactions with the membrane were systematically characterized before and after adding chlorine to gain a comprehensive understanding of the effects of pre-chlorination. Interfacial free energies of adhesion between the membrane surface and EfOM (raw and chlorinated) were estimated using XDLVO theory. The effects of chlorination-induced changes in EfOM physicochemical properties and consequent interactions were evaluated in terms of its sorption tendency and streaming potential as a measure of its fouling propensity. Additionally, fouling resulting from thermodynamic resistance of gel layer [118, 119] and due to the adsorption/deposition of foulants [120, 121] will be affected by changes in EfOM character. Therefore, constant flux blocking laws [76, 78] were also employed to capture fouling mechanisms as affected by chlorination.

Materials and methods

Source water

An effluent sample was collected from the 9.5 million gallons per day (MGD) conventional activated sludge Carter's Creek municipal wastewater treatment plant in College Station, Texas on February 21, 2019, after UV disinfection and just prior to discharge. This sample had a pH of 8.02 ± 0.12, turbidity of 2.1 ± 0.5 NTU, EfOM concentration of 7.75 ± 0.101 mg/L measured as dissolved organic carbon (DOC), UVA254 of 0.165 ± 0.007 cm-1, chemical oxygen demand (COD) of 21 ± 3.4 mg/L, and alkalinity of 160 ± 13 mg/L as CaCO3. The ammonia concentration was very low (close to the detection limit of 0.01 mg/L NH3-N) and the total N was 19.6 ± 2.3 mg N/L. Samples were filtered with 0.45 µm polyethersulfone disc filters (PES, Pall Corp.) within 24 h of collection, stored in the dark at 4 °C, and brought to room temperature immediately before use.

Chlorination of wastewater effluent samples

A 10,000-mg/L stock solution of NaClO was freshly prepared each time from household bleach solution for appropriate dosing, 1.5 to 15 mg/L of NaClO (free chlorine measured in the range 1.35 to 13.5 mg/L) to the wastewater effluent, which encompasses engineering practice and is comparable to other publications [48, 51, 109, 111]. Dosing was carried out in 1 L amber bottles with Teflon lined caps after a thorough cleaning to make them demand-free by immersing in a 0.1 % bleach solution overnight and drying in a muffle furnace at 250 °C for 4 hours. Bottles were well-mixed following chlorine

addition and stored in the dark for 24 hours, after which 150 mL of chlorinated effluent was taken for characterization and the remaining 850 mL was used for the MF experiments. In all cases, no residual free chlorine was detected at the end of 24-hours as in earlier studies [51, 122] and the pH remained at 8.0 ± 0.10 owing to its high buffering capacity.

Microfiltration

Membrane and filtration module

PVDF hollow fiber membranes with 1.29 mm outer diameter and 0.71 mm inner diameter (Aria™, Pall Corp.) nominally rated at 0.1 μm were prepared for each experiment by potting four 18.5 cm long fibers (active filtration area of 30 cm^2) in transparent 15 mm PVC tubes using epoxy resin. Outside-in MF was accomplished by closing fiber lumens at one end and leaving them open at the other end. Before experimentation, following manufacturer recommendations, modules were thoroughly rinsed with ultrapure water to remove the biocide preservative (NaN_3), followed by a 50% ethanol solution for pore wetting, and again rinsed multiple times with ultrapure water.

Filtration setup and experimental procedure

Each experiment at a predetermined NaClO dose (0, 1.5, 2.5, 5, 7.5, 10, and 15 mg/L) consisted of five forward filtration cycles with intermittent backwashing performed using a custom-made bench-scale apparatus [123]. Each cycle began with flushing the module with the feed water. The second step was constant flux filtration at 90 $L/m^2 \cdot h$ by pumping feed water to the shell side of the module and collecting permeate from the lumen

side. After forward filtration for 30 minutes (i.e. a specific volume of 45 L/m^2), the feed pump was switched off after which backwashing was performed also at 90 L/m^2·h for 3 minutes using ultrapure water. Finally, the module was gravity drained and emptied to remove the backwashing water and dislodged foulants before commencing the next cycle. This procedure was repeated five times for each NaClO dose, i.e. 5 forward filtration and backwashing cycles. At the end of every experiment, i.e. after 5-cycles, parameters determining the overall membrane performance such as the cumulative extent of irreversible fouling (R_{ir}^{Total}) and the average initial fouling rate $\left(\frac{dTMP}{dt}\right)_{avg}$ were calculated [12]:

$$R_{ir}^{Total} = R_5 - R_1 \qquad (2)$$

$$\left(\frac{dTMP}{dt}\right)_{avg} = \frac{\sum_{i=1}^{5}\left(\frac{dTMP}{dt}\right)_i}{5} \qquad (3)$$

where R_1 and R_5 are overall (membrane + foulant) Darcy resistances (m^{-1}) at the beginning of the 1st and 5th cycle, respectively and $\left(\frac{dTMP}{dt}\right)_i$ is the fouling rate (kPa/h) during the first five minutes of an individual filtration cycle *i*.

Quality assurance comprised of repeating entire 5-cycles of forward and reverse filtration at 0, 2.5, and 7.5 mg/L NaClO as shown in **SI Figure A-5** from which fouling parameters in **Equations 2** and **3** were calculated. These chlorine dosages were chosen because they represent different physicochemical conditions and fouling mechanisms (discussed later under **Results and discussion**) thereby increasing the stringency of our quality assurance protocols. Mann-Whitney U tests revealed no statistical differences between the instantaneous pressure values obtained from these duplicate experiments at

95% confidence. Additionally, the relative percentage difference values for the fouling parameters were low, ranging between 0.05 <R_1< 2%, 0.06 < R_5 < 2.7%, 1.4 < R_{ir}< 6.4%, and 1.5 < $\left(\frac{dTMP}{dt}\right)_{avg}$ < 8% demonstrating statistically consistent laboratory protocols. Hence, the hydraulic behavior of membranes and results obtained over the entire course of experimentation could be quantitatively compared validating our findings.

Colloidal PVDF (cPVDF) particles preparation and sorption tendency estimation

cPVDF particles having the same composition of the MF membrane were prepared [74, 75, 123] and used as a surrogate to estimate the sorption tendency of the wastewater effluent components towards the microfilter [74, 86]. The concentration and method for the preparation of cPVDF particles were based of our previous work [123]. Briefly, a 2% w/v PVDF solution in N,N-dimethylformamide (DMF) was rapidly added to 0.1 mM NaOH solution under moderate stirring, resulting in the formation of a cloudy suspension of cPVDF particles. DMF was removed by dialyzing the suspension (12-14 kDa molecular weight cut-off) against ultrapure water. The detailed steps in preparation are described in our recent paper [123]. The sorption tendency was estimated by measuring the % removal of EfOM as DOC and UVA_{254} after exposing the raw and pre-chlorinated effluents to 100 mg/L of cPVDF particles for 3 hours in duplicate.

Streaming potential to estimate EfOM sorption

Streaming potential measurements (SurPASS 3, Anton Paar) were also made to better understand changes in the sorption tendency of EfOM upon chlorination.

Adsorption kinetics of prefiltered raw and chlorinated wastewaters on the membrane surface was investigated by measuring the variation in streaming potential in the slow adsorption mode at constant pressure [124]. The measuring cell for flexible tubing was used and target pressure was maintained constant at 25 kPa by supplying nitrogen gas externally. Temporal variations of streaming potential were used to analyze the sorption tendency in terms of the extent (total change) and rate (slope of its linear portion at early times) of adsorption (see **Figure 15b** and **SI Figure A-6**). Employing streaming potential allows relatively *in situ* analysis by reducing interferences in estimating adsorption behavior and decreases the level of extrinsic modifications to either the membrane or the organics [125] as typically required by the atomic force microscope and the quartz crystal microbalance [51, 107].

Foulant-membrane physicochemical interaction energy

XDLVO theory

The free energy of adhesion per unit area, ΔG_{mlc}^{Tot}, between the membrane and the wastewater effluent components was estimated using the XDLVO theory as a fouling predictor [115, 116]. The cumulative interaction energy is the sum of the interfacial Lifshitz-van der Waals (LW) interaction, ΔG_{mlc}^{LW} and the interfacial Lewis acid-base (AB) interactions, ΔG_{mlc}^{AB}, **Equation 4**. While XDLVO theory also includes electrostatic interactions, owing to the complex nature of EfOM, only the non-electrostatic interaction energy between foulants and the membrane surface were considered in our analysis [115, 117].

$$\Delta G_{mlc}^{Tot} = \Delta G_{mlc}^{LW} + \Delta G_{mlc}^{AB} \quad (4)$$

The LW and AB adhesion energies per unit area (mJ/m^2) are given by **Equations 5** and **6**, respectively [126].

$$\Delta G_{mlc}^{LW} = 2\left(\sqrt{\gamma_l^{LW}} - \sqrt{\gamma_m^{LW}}\right)\left(\sqrt{\gamma_c^{LW}} - \sqrt{\gamma_l^{LW}}\right) \quad (5)$$

$$\Delta G_{mlc}^{AB} = 2\sqrt{\gamma_l^+}\left(\sqrt{\gamma_m^-} + \sqrt{\gamma_c^-} - \sqrt{\gamma_l^-}\right) + 2\sqrt{\gamma_l^-}\left(\sqrt{\gamma_m^+} + \sqrt{\gamma_c^+} - \sqrt{\gamma_l^+}\right) - 2\left(\sqrt{\gamma_m^+\gamma_c^-} + \sqrt{\gamma_m^-\gamma_c^+}\right) \quad (6)$$

where γ^{LW}, γ^+, and γ^- are the LW component of surface tension, electron-acceptor parameter of surface tension, and electron-donor parameter of surface tension, respectively. The subscripts m, l, and c represent membrane, liquid (water), and colloids (EfOM molecules), respectively. The free energy of cohesion between the EfOM molecules, ΔG_{clc}^{Tot} can be calculated according to **Equation 7**.

$$\Delta G_{clc}^{Tot} = -2\left(\sqrt{\gamma_c^{LW}} - \sqrt{\gamma_l^{LW}}\right)^2 - 4\left(\sqrt{\gamma_c^+\gamma_c^-} + \sqrt{\gamma_l^+\gamma_l^-} - \sqrt{\gamma_l^+\gamma_c^-} - \sqrt{\gamma_c^+\gamma_l^-}\right) \quad (7)$$

The surface tension components/parameters of the membrane and EfOM molecules can be determined by performing contact angle measurements using three probe liquids with known surface tension parameters and employing the Young-Dupré equation [114, 127], **Equation 8**:

$$(1 + \cos\theta)\left(\gamma_l^{LW} + 2\sqrt{\gamma_l^+\gamma_l^-}\right) = 2\left(\sqrt{\gamma_s^{LW}\gamma_l^{LW}} + \sqrt{\gamma_s^+\gamma_l^-} + \sqrt{\gamma_s^-\gamma_l^+}\right) \quad (8)$$

where, θ is the contact angle. The subscripts s and l correspond to solids (membrane and EfOM molecules) and the probe liquids, respectively. As recommended, two polar liquids

(ultrapure water and formamide) and one apolar liquid (diiodomethane) were used [127]. Formamide and diiodomethane were obtained from Fisher Scientific. Ultrapure water was obtained from a Thermo Scientific™ water purification system. **Table 2** lists the surface tension components/parameters for the probe liquids [127].

Table 2 Surface tension properties (mJ/m^2) of the probe liquids at 20 °C.

Probe liquid	γ_l^{LW}	γ_l^+	γ_l^-
Ultrapure water	21.8	25.5	25.5
Formamide	39.0	2.28	39.6
Diiodomethane	50.8	0.0	0.0

Contact angle

The sessile drop method was used to measure the contact angle (Dataphysics Optical Contact Angle Pro 15). Membrane samples were vacuum dried for 48 hours at room temperature prior to measurement. The pure water contact angle for the virgin membrane was 112.8° ± 0.14° exhibiting the relative hydrophobicity of PVDF membranes [128]. The contact angle of the dissolved EfOM was measured by adapting a previously reported technique [115]. First, approximately 50 mL of raw and chlorinated effluent samples were air-dried on inert glass supports by intermittent deposition (adding 0.5 – 1 mL at a time using a pipette) and drying over multiple days. The glass support was first cleaned thoroughly by initially immersing it in 90% ethanol for 30 minutes, rinsing with ultrapure water, and then dried. Before contact angle measurements, the air-dried samples were further vacuum dried for 48 hours to remove any water residues. The contact angle for the virgin membrane and the effluent samples measured with the three probe liquids are summarized in (**SI Table A-2)**.

Analysis of fouling behavior

Fouling mechanisms associated with constant flux MF of wastewater effluent were identified using the power-law compressible cake filtration model [78] and blocking laws [76]; **Equations 9** and **10**, respectively.

$$\Delta P = \Delta P_0 + \beta \Delta P^c v, \quad (9)$$

where β is a pre-exponent term, c is the cake compressibility index designating variation of the specific cake resistance with pressure [79], and v is the cumulative volume filtered.

$$\frac{d^2P}{dv^2} = k\left(\frac{dP}{dv}\right)^n, \quad (10)$$

where k and n are model parameters [76]. The fouling mechanism is expressed by the index n: n → 3/2 for complete blocking, n → 4/3 for standard blocking, and n → 1 for intermediate blocking. The slope of an arithmetic plot of log $(\frac{d^2P}{dv^2})$ versus log $(\frac{dP}{dv})$ was used to obtain the value of n and therefore the corresponding blocking law or fouling mechanism. For analysis using **Equation 10**, noisy experimental pressure measurements were smoothed using the robust local regression "rlowess" routine in MATLAB and then differentiated numerically to obtain the first derivative. Following this, piecewise interpolating polynomials of order 4-7 were fitted to the smoothed first derivative of each cycle. Finally, the smoothed and interpolated data were numerically differentiated to calculate the instantaneous second derivative accurately. Modeling is essential since MF/UF fouling mechanisms are altered upon pre-oxidation [111, 117] and other pretreatments [46, 123].

Analytical measurements

Dissolved organic carbon (DOC) was used to quantify EfOM concentrations and measured by a Total Organic Carbon analyzer (TOC-L, Shimadzu Corp.). The size distribution of "dissolved" EfOM after 0.45-micron filtration using PES discs was measured by dynamic light scattering (Litesizer 500, Anton Paar) [94]. UVA_{254}, silica (silicomolybdate HACH method 8185), proteins (mg/L bovine serum albumin (BSA) equivalents via the modified Lowry protein assay, ThermoFisher Scientific), and polysaccharides (mg/L glucose equivalents) [129] were measured on a HACH DR6000 UV-Vis spectrometer. Turbidity was measured using a HACH 2100N turbidimeter. COD was determined using the reactor digestion method [130] (HACH method 8000). The infrared spectra of the vacuum-dried membrane samples were collected using the Nicolet iS10 spectrometer equipped with mid-infrared Ever-Glo source, DTGS detector, KBr beam splitter, and Omnic 9.0 Software. A diamond iTX accessory was also installed to allow sampling in ATR mode. IR spectrum was obtained by averaging 128 scans collected at 4 cm^{-1} resolution over 650–4000 cm^{-1}.

Results and discussion

Effect of NaClO dose on fouling

As summarized in **Figure 12**, low NaClO dosages (1.5 and 2.5 mg/L) substantially worsened fouling, with even a 5 mg/L dose resulting in higher pressures compared with raw secondary effluent. Adding more NaClO progressively decreased fouling and concentrations ≥ 7.5 mg/L were necessary to reduce fouling below the unchlorinated raw

wastewater. For example, the pressure associated with 90 L/m^{2}h flux at the beginning of the 5th cycle was 9 kPa for the raw effluent, which increased by 50% to 13.5 kPa for a low dose of 2.5 mg/L but decreased by 22% to 7 kPa for 15 mg/L dosage. This transitional trend (i.e. existence of a threshold NaClO concentration below which performance was worse and above which performance was improved) was observed both for overall fouling during individual cycles as well for hydraulically irreversible fouling over multiple cycles.

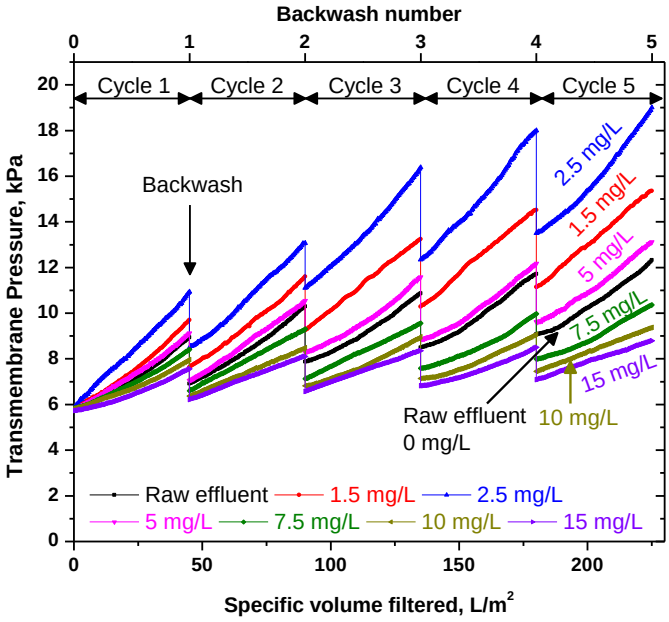

Figure 12 Transmembrane pressure profiles for raw (black) and pre-chlorinated secondary wastewater effluents. NaClO dosages ≤ 5 mg/L exacerbated fouling whereas dosages ≥ 7.5 mg/L effectively controlled it.

Lower pressures following NaClO addition (> 5 mg/L in this case) demonstrates that pre-chlorination can be an effective strategy to mitigate fouling if and only if sufficient concentrations are added. However, the biphasic trend in pressure behavior, i.e. worse fouling at low doses but reduced fouling at high doses suggests differences in EfOM character (e.g. molecular size [50] and polarity [51]) and associated interactions with the

membrane after it is exposed to free chlorine. A similar transitional irreversible fouling trend has been reported for ultrafiltration of ozonated secondary effluent [117] and chlorinated model foulant (lysozyme) solution [131]. In the subsequent sections, I analyze these chlorination-induced EfOM changes and discuss their mechanistic implications to fouling.

Gross EfOM characteristics (DOC, UVA_{254}, and biopolymers)

DOC and UVA_{254}

Chlorination had no influence on DOC concentration demonstrating that DOM was not mineralized in the range of dosages evaluated [104] (**Figure 13a**). UVA_{254} and specific ultraviolet absorbance (SUVA, UVA_{254} in m^{-1} divided by DOC in mg/L) monotonically decreased upon chlorination as shown in **Figure 13b** and **c,** symptomatic of chlorine attacks on activated aromatic rings, which constitute the predominant UV-absorbing chromophores in DOM [132-134].

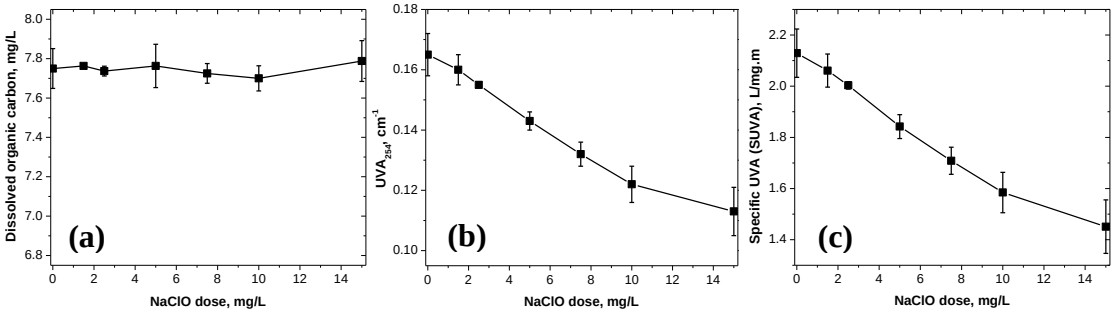

Figure 13 Changes in dissolved EfOM gross characteristics with NaClO addition.

Biopolymers

As summarized in **Figure 14**, protein concentrations remained constant up to a NaClO dosage of 2.5 mg/L after which it declined monotonically. Proteins react more

rapidly with chlorine in comparison to other biopolymers [104] losing their higher order (secondary and tertiary) structures due to oxidative modifications of amino acids [135, 136]. In other words, low dosages lead to structural modifications via unfolding [51, 135, 137]. Since the modified Lowry method targets the peptide bond [138], this assay shows constant protein levels at low (≤ 2.5 mg/L) NaClO dosages. However, higher chlorine dosages (≥ 5 mg/L in this case) fragment proteins and cleave peptide bonds measured by the Lowry assay as decreasing protein concentrations [139, 140]. NaClO dose-dependent behavior of proteins and its impact on fouling is further explored in section **Sorption tendency.** In contrast, polysaccharide concentrations monotonically declined with chlorine addition (**Figure 14**). Chlorine fragments polysaccharides and opens rings [141-143], which manifests as lower concentrations since the chosen assay (phenol sulfuric acid) targets its monomeric rings [129, 144].

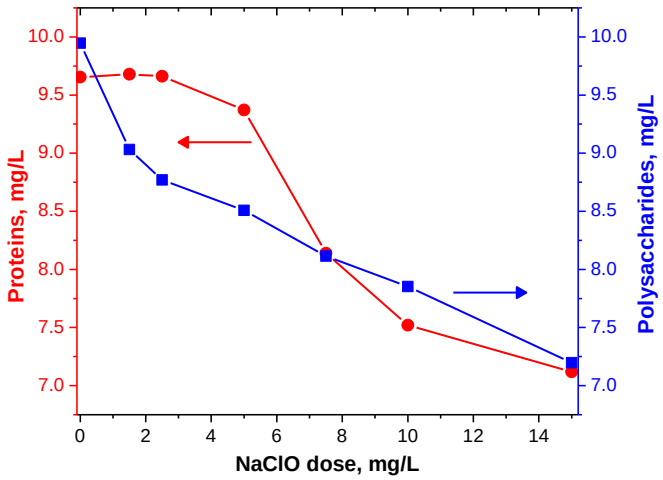

Figure 14 Biopolymers (proteins and polysaccharides) concentrations as a function of NaClO dose.

Figure 13 and **Figure 14** show that gross EfOM parameters either remained constant or decreased as progressively more NaClO was added (i.e. no transitional changes) and thus were inadequate to explain the dependence of pressure profiles on chlorine dose depicted in **Figure 12**. This implies that specific physicochemical changes (e.g. size and polarity [104, 105]), which would have impacted EfOM-membrane interactions [51] dominated fouling and are pursued next by measuring sorption tendency over the entire range of NaClO doses.

Sorption tendency

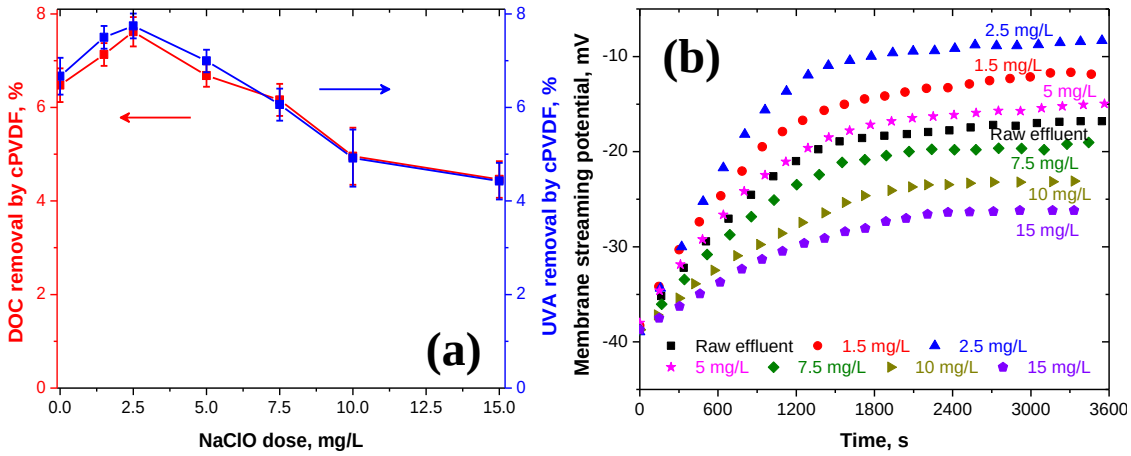

Figure 15 (a) Removal of EfOM (measured as DOC and UVA) by cPVDF adsorbent particles as a function of NaClO dose. (b) Streaming potential variation overtime during adsorption at different doses.

As summarized in **Figure 15a**, the magnitude of EfOM sorption (measured as DOC after removing cPVDF particles via centrifugation at 10000 g for 10 minutes) onto cPVDF particles was low and increased slightly initially from 6.7% for the raw effluent to 7.8% for a NaClO concentration of 2.5 mg/L and then decreased at higher NaClO doses eventually declining to 4.5% at the highest dose investigated. UVA_{254} trends were similar

validating chlorine-induced changes to the chemical nature of EfOM as previously reported for model proteins, humic acid, and natural organic matter isolates [51] and hypothesized in the **Introduction**.

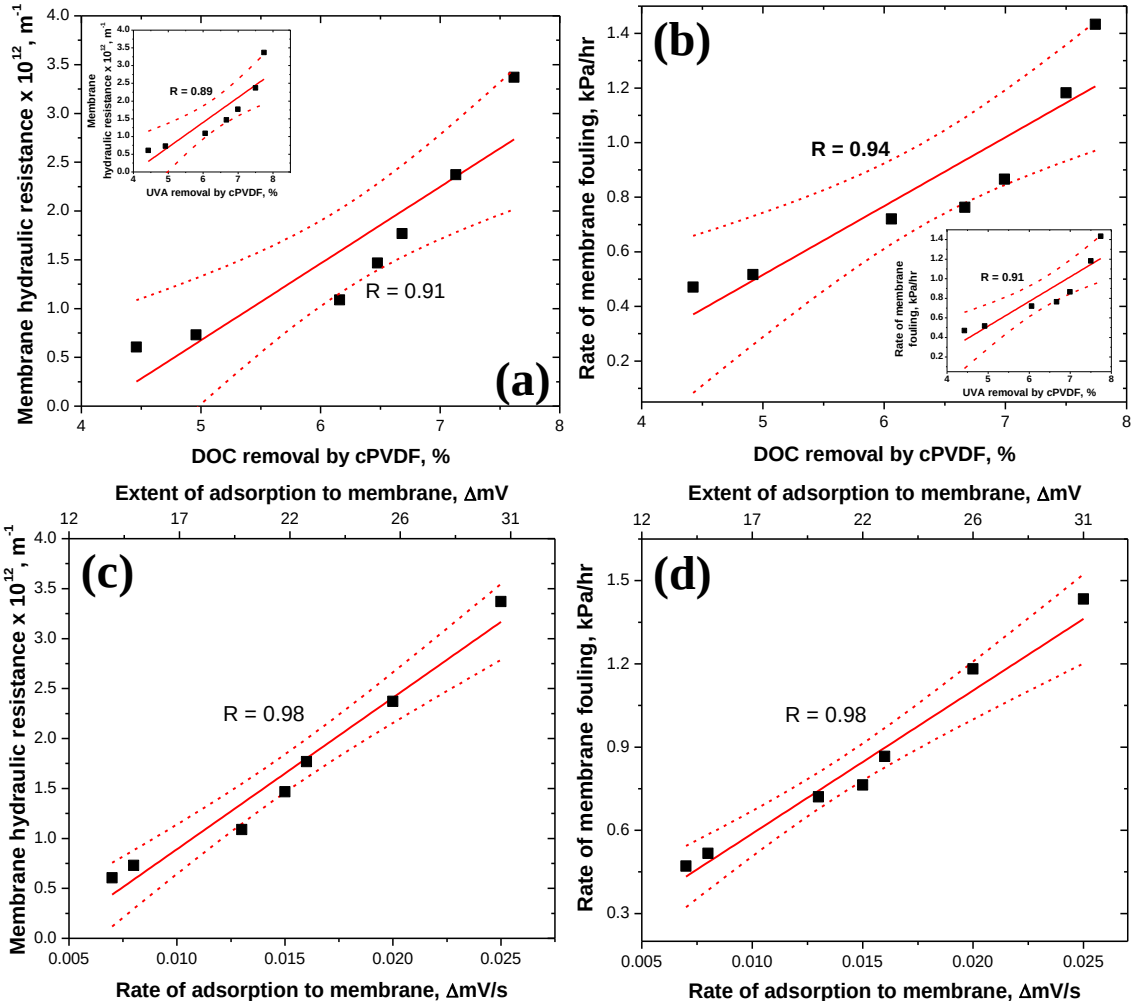

Figure 16 Correlations of fouling parameters with DOC and UVA removal by cPVDF (a, b) and rate & extent of sorption (c, d)

Although only a small amount of EfOM was sorbed on PVDF, it progressively increased membrane streaming potentials (i.e. making it less negative over time) in all cases following exposure to raw and pre-chlorinated wastewater effluent samples (**Figure 15b**) [123, 124]. Importantly, streaming potentials exhibited the same transitional dose-

dependent trend as EfOM uptake by cPVDF particles, i.e. increasing from raw effluent to a 2.5 mg/L NaClO dose and decreasing for higher concentrations. The extent and rate of EfOM adsorption on the membrane were estimated using these data (see **SI Figure A-6**) confirming their variation with disinfectant addition.

EfOM sorption tendency estimated in terms of DOC and UVA removal by cPVDF as well as the extent and the rate of adsorption were strongly and positively correlated (R > 0.9) with R_{ir}^{Total} and $\left(\frac{dTMP}{dt}\right)_{avg}$ (**Figure 16**). Hence, the sorption tendency strongly correlated with (ir)reversible fouling indices suggesting the important role of EfOM-membrane chemical interactions on MF.

Trends in the gross sorption tendency reported in **Figure 15** using aggregate parameters such as DOC, UVA, and streaming potential are governed by differences in reactivity of individual EfOM components such as biopolymers, humic-like materials, and low molecular weight amino acids and simple sugars with chlorine and associated transformation products [34, 101]. For example, proteins unfold and hydrophobic amino acids normally obscured in the protein core are exposed to the surface, reducing their polarity at low chlorine concentrations [51, 135, 137] thereby allowing them to sorb more on a hydrophobic surface such as PVDF [51, 131] consistent with the initial positive slope in **Figure 15a**. At higher chlorine doses, protein fragmentation accompanied by modification of amino acids to their carbonyl forms [139, 140] increases hydrophilicity correspondingly decreasing sorption tendency [51] contributing to the negative slope beyond 2.5 mg/L NaClO in **Figure 15a**. These predicted trends were confirmed by the intensified protein associated peaks; NH peak at 3300-3500 cm^{-1}, and amide I and amide

II bands between 1500-1700 cm^{-1} in ATR-FTIR spectra [145] of fouled membranes (**Figure 17**). As observed, protein-associated peaks were most intense at 2.5 mg/L NaClO dose and weakest at 15 mg/L NaClO dose.

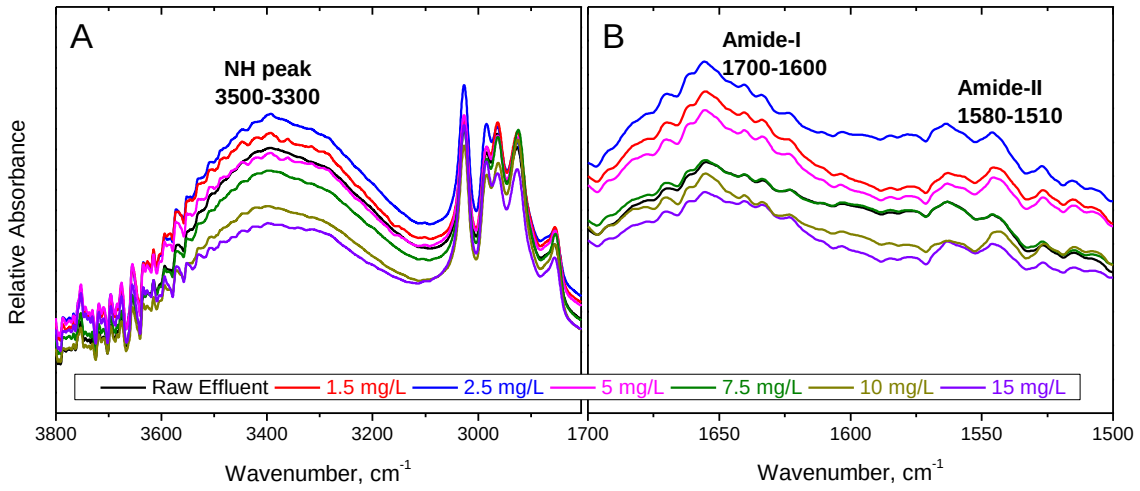

Figure 17 Intensity of protein associated peaks (A: 3300-3550 cm^{-1} and B: 1550-1700 cm^{-1}) were in the order 2.5 mg/L > 1.5 mg/L > 5 mg/L > Raw effluent > 7.5 mg/L > 10 mg/L > 15 mg/L trending closely with the sorption tendency (Figure 15) and free energy of adhesion.

Humic-like materials also undergo sequential reactions with chlorine reacting with phenolic moieties at low doses by electrophilic substitutions to form polychlorinated products [104] increasing their apparent hydrophobicity [146] and therefore their sorption tendency. High chlorine concentrations cleave the rings of these polychlorinated products to form polar compounds such as chlorinated low molecular weight aliphatics and non-chlorinated organic acids [147], reducing sorption tendency. In contrast, polysaccharides (and simple sugars) undergo depolymerization and ring opening, forming smaller and more polar fragments via oxidative modifications increasing hydrophilicity for all chlorine dosages [141-143]. Thus, EfOM sorption tendency trends reported in **Figure 15** appear to have been dominated by chlorine-induced transformations of proteins and humic-like

material at low dosages whereas all individual components including polysaccharides contributed at higher NaClO concentrations. Sorption behavior also quantitatively correlates with fouling trends reported in **Figure 12** (i.e. more fouling at NaClO dosages ≤ 2.5 mg/L but reduced fouling at higher chlorine concentrations) and fouling indices in **Figure 16**.

The free energy of EfOM adhesion on the membrane was estimated using XDLVO theory to further understand and validate these trends as well as the relationship between EfOM sorption and fouling as discussed next.

XDLVO estimates of free energy of interactions (cohesion and adhesion) and fouling behavior

The γ^{LW} of the virgin membrane was calculated to be 24.7 mJ/m^2. Consistent with the hydrophobic and apolar nature of PVDF [127] and a previous publication [113], its electron acceptor and electron donor components were calculated to be near zero (γ^+= 0 and γ^-= 0.06 mJ/m^2). It is noted that a range of XDLVO parameter values [115, 148] and contact angles [128] have been reported for commercial PVDF membranes owing to proprietary surface modifications employed by different manufacturers.

Estimated surface tension parameters for the EfOM molecules and the membrane (**XDLVO theory**) are summarized in **Table 3**. In all cases, i.e. with and without chlorination, EfOM molecules were calculated to have high electron donor monopolarity (high γ^- and negligible γ^+) similar to NOM, other EfOM samples, and model organic foulants [115, 117, 149]. Note that γ^{LW} and γ^- initially increased (NaClO ≤ 2.5 mg/L)

and the former monotonically decreased at higher dosages whereas the latter remained constant. In contrast, γ^+ decreased initially and then increased as the dose increased.

Table 3 Surface tension components and calculated free energy of cohesion and adhesion for EfOM fouled membranes.

NaClO dose (mg/L)	γ^{LW} (mJ/m^2)	γ^+ (mJ/m^2)	γ^- (mJ/m^2)	ΔG_{mlc}^{LW} (mJ/m^2)	ΔG_{mlc}^{AB} (mJ/m^2)	ΔG_{mlc}^{Tot} (mJ/m^2)	ΔG_{clc}^{Tot} (mJ/m^2)
0 (raw EfOM)	30.6	1.75	53.9	-0.52	-15.2	-15.7	32.7
1.5	32.8	0.82	58.5	-0.64	-19.4	-20.0	40.8
2.5	34.1	0.08	67.8	-0.71	-25.9	-26.6	57.9
5	31.2	1.71	57.0	-0.55	-15.4	-15.9	35.7
7.5	24.5	3.91	57.2	-0.17	-8.72	-8.89	30.7
10	22.4	4.97	57.9	-0.04	-6.22	-6.26	28.8
15	20.4	6.09	57.9	0.09	-3.84	-3.74	26.4

Also as shown in **Table 3**, the cumulative free energy of EfOM adhesion ΔG_{mlc}^{Tot} decreased sharply (became more negative) for low NaClO doses (≤ 2.5 mg/L) and then increased (became less negative) for concentrations ≥ 5 mg/L, similar to ozone oxidation of EfOM [117]. More negative adhesion free energies denote increasingly thermodynamically favorable EfOM adhesion to the membrane, which is manifested macroscopically as higher sorption tendency at NaClO concentrations ≤ 2.5 mg/L in **Figure 15**. This is consistent with the formation of more hydrophobic EfOM reaction products from protein and humic-like substances at low chlorine doses as described

earlier, which will preferentially adhere to the hydrophobic PVDF membrane thereby worsening fouling as shown in **Figure 12** (with opposite trends at higher concentrations). Importantly, free energies of adhesion were strongly and inversely correlated with fouling (R ~ -0.98) as shown in **Figure 18** validating the critical role of EfOM-membrane interactions in initiating fouling. Hence, XDLVO calculations provide additional evidence for oxidation and substitution reaction products and competing reaction pathways for modifying EfOM's macroscopic behavior following exposure to different amounts of chlorine.

Table 3 also summarizes free energies of cohesion between the EfOM molecules (ΔG_{clc}^{Tot}) at different chlorination conditions to obtain insights on foulant-foulant interactions that are important during the later stages of fouling [115]. Similar to adhesion, the cohesion free energy also showed a transitional trend as a function of NaClO dose, increasing from 32.7 mJ/m^2 for raw effluent (no chlorine) to a maximum of 57.9 mJ/m^2 at a NaClO dose of 2.5 mg/L and then gradually decreasing at higher doses eventually reaching 26.4 mJ/m^2 at the highest dosage (15 mg/L). As seen, $\Delta G_{clc}^{Tot}$was positive in all cases denoting unfavorable (repulsive) interactions between foulants that were previously deposited on the membrane and EfOM molecules that are newly approaching the membrane [150]. Continued fouling even when cohesion was repulsive suggests that the hydrodynamic permeation drag force dominated foulant-foulant chemical interactions over all 5-cycles of our experiments [115, 150] after EfOM adhered to the membrane at the early stages of filtration.

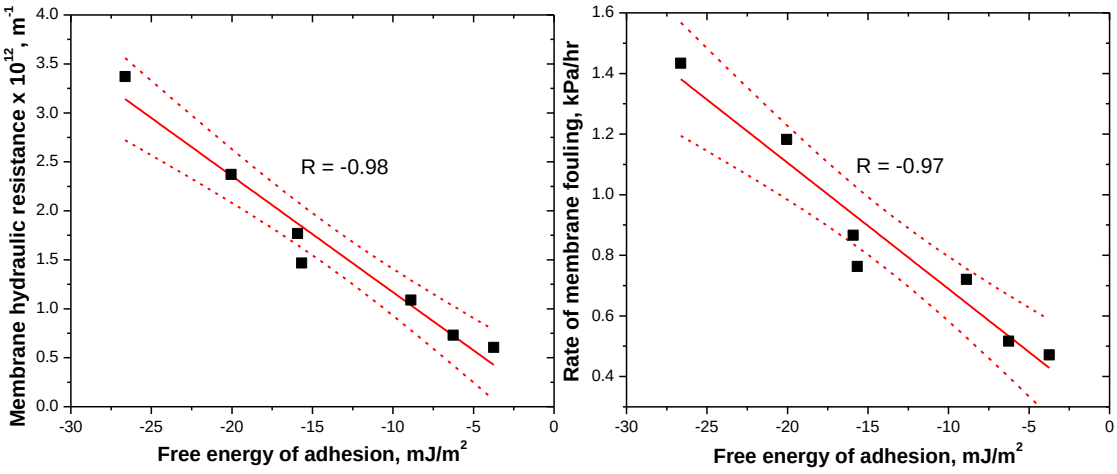

Figure 18 Correlation between the EfOM-membrane free energy of adhesion and fouling parameters

These results demonstrate that EfOM fouling is a complex manifestation of initial membrane-foulant and foulant-foulant interactions [150] superposed on module hydrodynamics. More positive free energy of cohesion has been associated with an increase in the hydrophilic nature of EfOM upon oxidation [117], which may also explain continued fouling at longer time-frames, associated with its accumulation on previously deposited foulant layers [21, 35, 123] once it is brought near the membrane surface by permeation drag.

In addition to specific chemical interactions discussed above, pressure profiles in individual filtration cycles and regeneration by backwashing are also governed by EfOM size relative to the pore, which is pursued next.

Pre-chlorination also changes physical fouling mechanisms

Cake filtration was the dominant fouling mechanism for the raw effluent with **Equation 9** fitting the pressure profile excellently ($R^2 > 0.99$) for each of the filtration

cycles (**SI Figure A-6**). This is consistent with dissolved EfOM size distribution in the raw secondary effluent shown in **Figure 21**, which was monomodally distributed with an average size of 250 nm that is significantly larger than the membrane nominal pore size of 100 nm, leading to sieving and surface deposition during forward filtration, i.e., cake formation. Importantly, values of the compressibility index and the pre-exponent were statistically invariant (c = 0.45±0.02 and β = 7.7±0.5 x 10^3 $kPa^{0.55}/m^3$, respectively) for each of the 5 filtration cycles validating the physical interpretation of cake formation and its power-law compaction. Also, the measured compressibility index is in the range of previously reported values for EfOM and model foulants [123, 151].

In contrast to the undisinfected (raw) wastewater, for all pre-chlorinated waters, fouling was initiated via standard blocking (**Figure 20**) representing internal pore fouling consistent with chlorine-induced cleavage of EfOM to sizes smaller than membrane pores as shown in **Figure 21**. As observed, NaClO dosages ≤ 5 mg/L resulted in a bimodal distribution, with the larger peak increasing from 136 nm to 200 nm and then decreasing to 84 nm when the dosage monotonically increased from 1.5 mg/L to 2.5 mg/L and then to 5 mg/L, respectively. In other words, a transitional change in EfOM size distribution was measured, similar to oxidative damages to model organics and effluent biopolymers [50]. This transitional increase was also captured in the average size of EfOM molecules (**Figure 21h**). For NaClO ≤ 5 mg/L, smaller EfOM macromolecules (i.e. the left-hand side peak in **Figure 21b**, **c**, and **d**) initially cause intrapore fouling as shown in **Figure 20**. As more and more wastewater was microfiltered, fouling transitioned to external fouling (intermediate blocking) either because all available sorption sites are occupied and/or

because EfOM molecules larger than the pores still exist (i.e. the right-hand side peak in **Figure 21b**, **c**, and **d**) depositing on the membrane surface [123]. The transition from intrapore to surface fouling occurred progressively earlier with each subsequent cycle for any given NaClO dosage (**SI Table A-3**), attributed to reduced available pore area for sorption in each subsequent cycle as more and more EfOM was filtered. Therefore, fouling transitioned from occurring inside the pores (standard blocking) to the membrane surface (intermediate blocking) at lesser volumes filtered. The fouling transformation pattern discussed has been shown schematically in **Figure 19**.

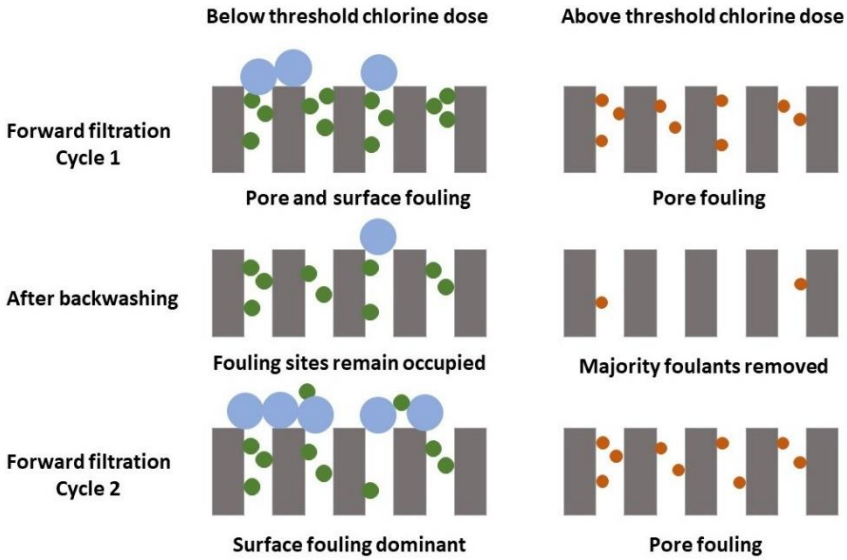

Figure 19 Schematic representation of the fouling transformation over two filtration and backwashing cycles. The schematics on the left correspond to chlorine doses below the threshold and the ones on the right apply to chlorine doses above the threshold. The blue and green circles represent the bimodal EfOM fragments produced at low chlorine doses, whereas the smaller orange circles represent the further smaller EfOM fragments produced at higher doses.

At NaClO ≥ 7.5 mg/L, EfOM fragments became even smaller and reverted to a monomodal distribution (**Figure 21e**, **f**, and **g**). At the highest NaClO concentration (15 mg/L), internal pore fouling persisted throughout the entire duration of the experiment, i.e. for all five filtration cycles consistent with the smallest EfOM size. Similar behavior

was observed for the next highest dose investigated (10 mg/L) that also resulted in very small EfOM fragments causing intrapore fouling in four of the five cycles. I also measured EfOM size in the permeates after filtration of raw and chlorinated effluent. Expectedly, the distribution only showed the presence of particles smaller than 0.1 microns (**SI Figure A-8**). However, since the concentration of individual particle sizes cannot be inferred from dynamic light scattering measurements owing to the complexity and variety of EfOM species [152], no additional conclusions could be drawn.

Importantly, the transition in the fouling mechanism occurred at lesser volume filtered at low chlorine doses relative to at higher chlorine doses (**SI Table A-3**). This is a consequence of increased fouling and reduced backwash efficiency at lower doses compared to that at higher doses, as discussed in section **Effect of NaClO dose on fouling**. Essentially, the increased fouling and reduced backwash efficiency due to stronger EfOM-membrane interactions at lower disinfectant doses decreased available pores in each subsequent cycle thus resulting in an earlier transition from internal pore fouling to surface fouling. In contrast, at higher doses (7.5 to 15 mg/L), sorption was lessened, controlling fouling and improving backwash efficiency, resulting in the continued availability of fouling sites during all filtration cycles, and therefore delaying the transition to surface fouling. These arguments related to EfOM size and specific interactions can also provide insights into similar transitions in fouling mechanisms reported earlier for untreated and UV/chlorine treated surface water [111].

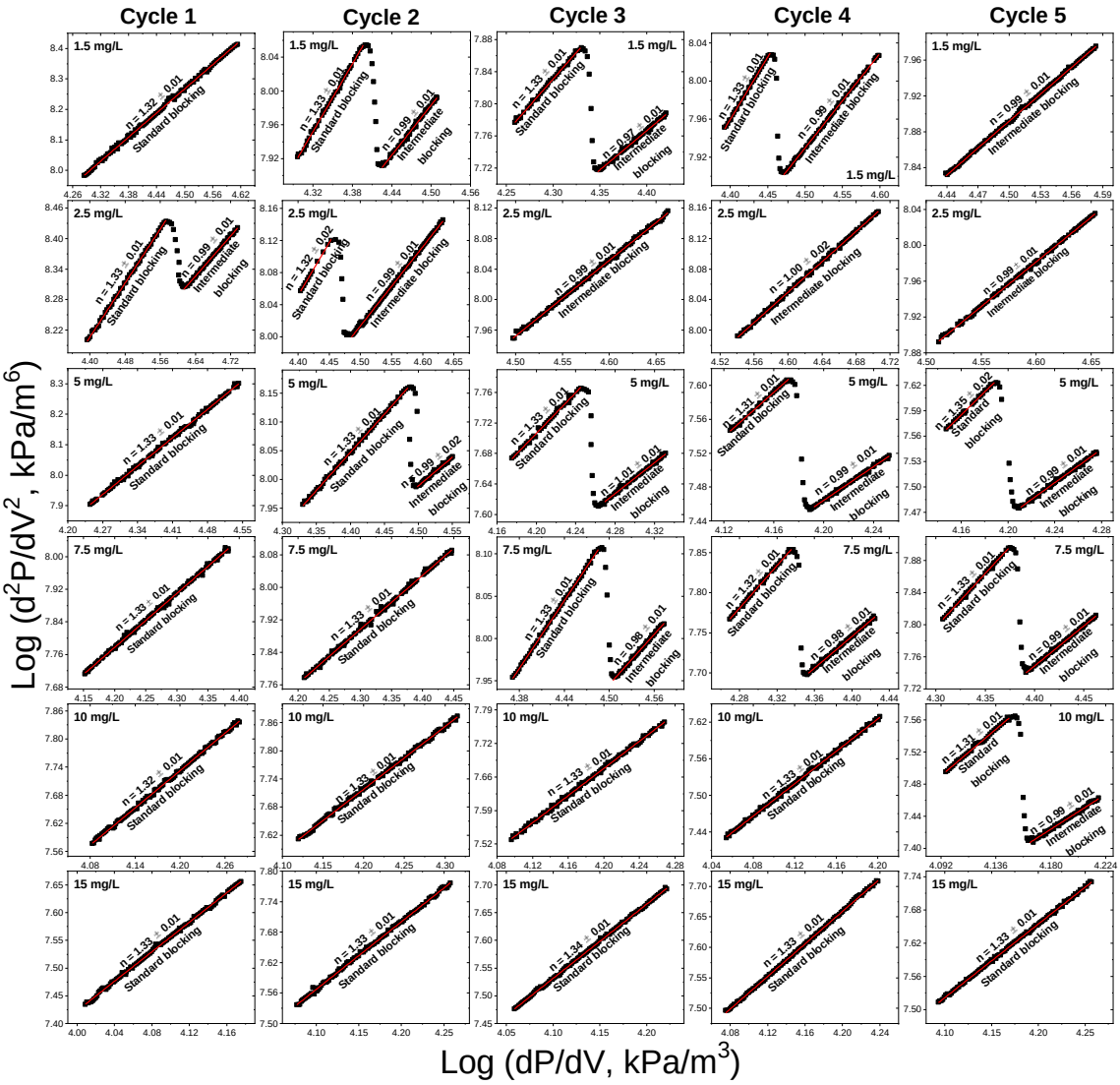

Figure 20 Constant flux blocking law analysis for pre-chlorinated wastewater. Each row corresponds to a fixed NaClO concentration; 1.5, 2.5, 5. 7.5, 10, and 15 mg/L from top to bottom.

Although chlorine fragments organic molecules at all dosages, larger-sized peaks in **Figure 21b**, **c**, and **d** are thought to arise via the formation of aggregates by either by cross-linking between cleaved fragments [51, 137] and/or loss of proteins' higher order structures that also promotes aggregation [51, 135, 137]. These changes in size distribution are consistent with long-chain (least oxidized) carbon molecules undergoing faster

reactions with disinfectants compared to medium-chain ones [133, 134], suggesting cleavage/degradation of larger, higher molecular weight molecules [111]. Such behavior potentially arises from variable reactivity and chlorination kinetics for the individual moieties constituting the complex concoction collectively referred to as EfOM [104, 105]. A similar argument has been invoked for natural organic matter (NOM) chlorination, specifically to the different types of local topochemistry of individual organics [132].

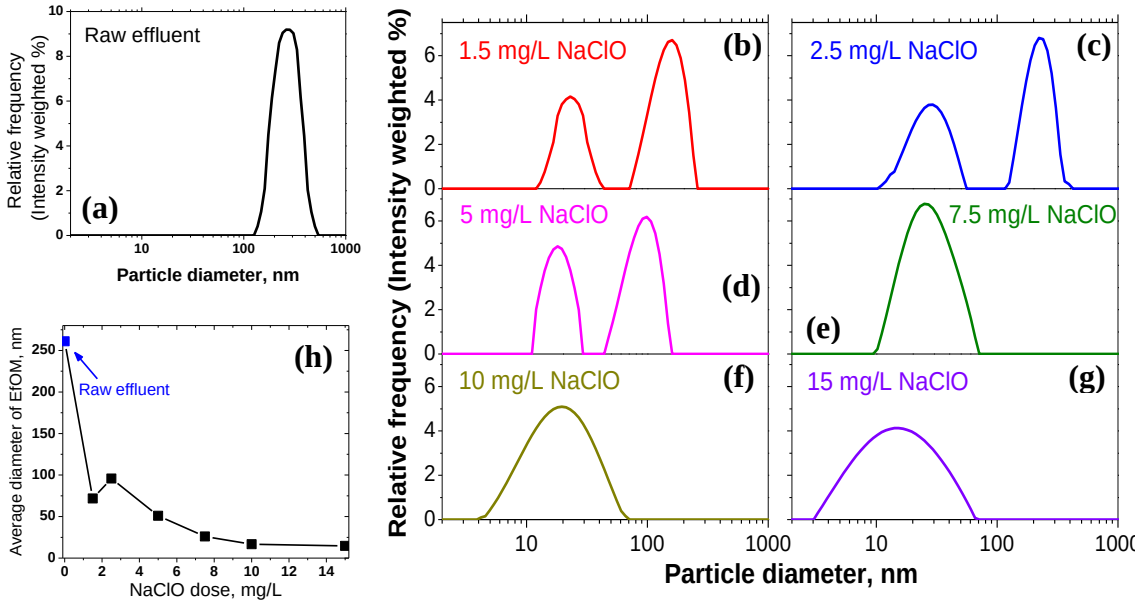

Figure 21 Dissolved EfOM size distribution of the (a) raw effluent and (b-g) after chlorination at different doses. (h) shows changes in the average size of EfOM as a function of NaClO dose.

Conclusions

The effectiveness of pre-chlorinating municipal wastewater effluent to control PVDF membrane fouling during potable reuse is strongly dose-dependent. Chlorine concentrations lower than a threshold value exacerbate fouling by creating more hydrophobic reaction products than the original EfOM which interact strongly with the PVDF membrane. This necessitates higher chlorine concentrations to generate more

hydrophilic EfOM that interacts less with the membrane consequently improving performance. Such transitional changes in fouling behavior stem from varying physicochemical alterations to EfOM when different amounts of chlorine are added. This includes oxidation and substitution reaction products and competing pathways that change foulant polarity coupled with macromolecular cleavage that creates smaller foulants. The smaller foulants, capable of lodging inside the membrane pores, are typically a dominant cause of irreversible fouling; however, decreased foulant-membrane interactions at the higher chlorine concentrations reduced the extent of the small size EfOM clogging the pores. Thus, the hydrophilization of EfOM at higher chlorine concentrations played an important role in fouling mitigation.

Fouling location (i.e. inside the pores or on the membrane surface) is determined by the relative size of EfOM and its fragments with respect to the pore. The location of foulant accumulation during continued filtration and backwashing is determined by sorption site availability; originating inside the pores eventually transitioning to the membrane surface. Finally, the close linkage between the applied chlorine dose and MF performance, the possibility that fouling can be worsened by adding inadequate amounts of disinfectant/oxidant, and variations in EfOM characteristics coupled with membrane surface properties, necessitate a careful evaluation of pre-chlorination under site-specific conditions.

CHAPTER IV

RELATION OF IRREVERSIBLE MICROFILTRATION FOULING TO THE MOLECULAR COMPOSITION OF DISSOLVED ORGANIC MATTER (DOM) ACROSS MULTIPLE WATER SOURCES

Introduction

The need for alternative or unconventional water sources has increased as a consequence of climate change, increasing population, and the subsequent growing water scarcity [153, 154]. Unconventional water sources, unlike conventional water sources like rivers, lakes, ponds, and freshwater wells, typically originate from the brackish surface and well water [155, 156] and wastewater treatment plant (WWTP) effluent [8]. The increased variety of sources also introduces a variety of constituents and species present in the feed water for treatment facilities. For example, dissolved organic matter (DOM) present in conventional sources is termed dissolved natural organic matter (dNOM) and is largely composed of biopolymers and humic substances [157, 158], whereas DOM in wastewater effluent is termed as dissolved effluent organic matter (dEfOM) [34, 158] and is composed of dNOM, soluble microbial products (SMPs), extracellular polymeric substances (EPS), and synthetic chemicals like pharmaceuticals, personal care products and surfactants [34, 72, 158]. This difference in DOM makeup has been shown to affect the performance of water treatment systems [71] and would expectedly affect low-pressure membrane systems (microfiltration (MF) and ultrafiltration (UF)) since DOM in the form of dNOM and dEfOM has been shown to be the major foulant [108, 157].

To date, many previous reports and results from our previous study [123] have shown typical water characterization parameters like dissolved organic carbon (DOC), turbidity, and UVA_{254} being unable to predict the UF/MF fouling during filtration of given feed water (conventional or unconventional). For example, the critical flux was lower for the Susquehanna River compared to the Mississippi River water even though the latter had higher DOC and turbidity [82]. Similarly, no clear correlation was observed between the DOC and UVA_{254} of three different sources of water and their respective fouling behavior [31]. On the same lines, [32] highlighted that general water quality indices of different surface waters like DOC, UVA_{254}, turbidity, and calcium concentration cannot explain the degree of fouling. Therefore, for a more robust and efficient design of treatment systems, it is imperative to improve our understanding of the characteristics of the DOM present across various sources and how these characters may affect membrane fouling.

Now, DOM characterization using tools like liquid chromatography with on-line organic carbon detection (LC-OCD) and fluorescence spectroscopy excitation-emission matrix (EEM) has been used to ascertain the nature of fouling causing components. For example, biopolymers were found to strongly correlate to the total fouling for three different sources of water; however, were not correlated to irreversible fouling [31]. Paradoxically, irreversible fouling was found to be strongly correlated to the biopolymer content of five different river water [32]. Additionally, while both these previous works observed no correlation between humic content and degree of fouling, another study reported humic substances significantly contributing to hydraulically irreversible fouling

[33]. Thus, the current state of knowledge on DOMs role in fouling certainly lacks conclusive and consistent understanding and I believe high-resolution mass spectroscopy can provide broader insights towards that goal. High-resolution mass spectroscopy has been successfully employed for the characterization of aquatic DOM and has resulted in developing molecular-level information critical in the progression of a variety of research themes, such as seasonal DOM variations in rainwater [159], assessing alterations in DOM makeup during various stages of water and wastewater treatment [105, 160-164], and investigation of the chemodiversity across sources [72, 165].

In this study, I employed orbitrap mass spectroscopy [160, 165, 166] to characterize the DOM of four different water samples. To incorporate the idea of the variability of water sources, the samples were collected from both unconventional and conventional sources (brackish surface water, two WWTP effluents, and one lake water). I analyzed and compared the fouling of microfilters over multiple filtration-backwashing cycles. The principal objective of our study was to investigate correlations between organic matter characteristics (DOM molecular fingerprints) and fouling behavior with the overarching goal to identify and develop clear predictors for the fouling propensity of different feed waters.

Materials and Methods

Source water

Four different feed water samples of varying origin were employed in this work. Brackish surface water (BSW) was collected from the Foss Reservoir in Custer County,

Oklahoma in November 2019. Municipal wastewater effluents, MWE1 and MWE2, from Carter's creek wastewater treatment plant and Texas A&M wastewater treatment plant in College Station, Texas, respectively were collected in December 2019. Surface water sample (SW) was collected from Lake Houston, Houston, Texas, in January 2020. Different water quality parameters measured have been listed in **Table 4**.

Table 4 Characteristics of different feed waters employed in this work

Water quality index	**SW**	**BSW**	**MWE1**	**MWE2**
DOC, mg/L	7.903±0.021	7.239±0.002	6.600±0.212	7.455±0.078
UVA_{254}	0.615±0.012	0.116±0.019	0.188±0.005	0.197±0.017
Turbidity, NTU	49±1.2	3.19±0.11	2.6±0.21	1.84±0.5
pH	7.7±0.14	8.27±0.03	8.15±0.02	8.42±0.11
Conductivity, µS/cm	212.4	2090	1241	1359
Alkalinity, mg/L $CaCO_3$	71.5±2.3	131.5±1.5	163±8	155±12
Hardness, mg/L $CaCO_3$	44.8±2.8	1620.7±10	50.2±4.8	70.0±1.8
Proteins, mg/L BSA	7.16	10.25	8.50	8.22
Polysaccharides, mg/L glucose	3.24	2.26	6.07	3.38

Membrane filtration: Setup and protocol

All filtration-fouling experiments were carried out using a custom-built bench-scale filtration setup. The filtration system was equipped with automatic backwash and control with continuous monitoring and recording of the transmembrane pressure (TMP) and flux. Constant flux was maintained using a peristaltic pump. Hydraulic backwashing

was performed using the permeate and was conducted using a separate backwashing pump flushing the fibers from inside to outside.

The filtration setup was equipped with mini hollow fiber membrane modules fabricated in the laboratory. A semi-clear PVC tubing (15 mm inner diameter, 22 cm long) was used as the membrane housing. The fibers were potted on both ends of the tube using epoxy, one end was sliced with a sharp razor to expose the membrane openings; this end served as the permeate collection and backwash feed side. Each experiment was performed with a new membrane module. The membrane module consisted of four 0.1-micron pore size polyvinylidene fluoride (PVDF) hollow fiber membranes having 1.293 mm O.D. and 0.711 mm I.D. (Aria™, Pall Corp., USA). The fibers after potting had an effective length of 18.5 cm each, resulting in a total active filtration area of 30 cm^2 for each module. At the start of each experiment, the membranes were thoroughly rinsed with ultrapure water and following manufacturer recommendations rinsed with 50% ethanol to wet the pores since the membranes were highly hydrophobic with pure water contact angle measured as 112.8 ± 0.14°. A final rinse with ultrapure water was performed before starting the filtration-fouling experiments. More details about the setup can be found elsewhere [123].

The fouling experiments for each feed water were performed for a total of 10 filtration-backwashing cycles. Forward filtration, outside to the inside of fibers, was carried out for 1 hour at a flux of 50 L/m^2h. Following this, backwashing was started, permeate was pushed from the inside of the fibers to the outside at flux 100 L/m^2h for

three minutes. After backwashing, the membrane module was gravity drained and filled with feed water before the start of the next filtration cycle.

Solid-phase extraction (SPE) of dissolved organic matter

DOM was extracted and concentrated using Agilent Bond Elut-PPL cartridges (500 mg, 6 mL) according to the method described previously [167]. Prior to extraction, the cartridges were rinsed with 6 ml of methanol (LC/MS grade, Fisher Chemical). The samples were filtered through 0.45 µm PES disc filters (Pall Corporation) and then acidified to pH 2±0.05 using concentrated HCl before extraction. Following this approximately 500 ml of each sample was flown through the cartridge using a peristaltic pump at a flow rate ≈ 25 ml/min. The cartridges were then rinsed with 12 ml of 0.01 M HCl and dried with high purity N_2 gas. DOM was eluted with 12 ml of methanol at a flow rate of 1 ml/min in pre-muffled (2 hours at 250 °C) glass ampoules and stored in the dark at -20 °C until used for analysis. The extraction procedure retained approximately 40-60% of DOC (see **SI Table A-4**) which is similar to previous reports employing SPE for both natural and wastewater derived samples [72, 160]. An extraction blank was also prepared by extracting ultrapure water with the same procedure and volumes as for the feed water samples. For MS analysis, methanol eluates were vacuum dried for 48 h and then re-dissolved in a 1:1 methanol:ultrapure water solution.

High-resolution mass spectroscopy and spectra analysis

Orbitrap MS

High-resolution mass spectrometry for the nontargeted analysis of organic matter was performed by Orbitrap MS (Q Exactive Focus, ThermoFisher Scientific). First, the Orbitrap MS was externally calibrated using the calibration solution (Pierce ESI Negative Ion Calibration Solution, ThermoFisher Scientific) covering m/z range of 265-1980. Samples were analyzed in flow injection mode using 100% methanol with 0.1% formic acid as mobile phase at a flow rate of 0.100 ml/min, with an injection loop capacity of 10 µL. The operational conditions for electron spray ionization (ESI) in negative mode were as follows: Sheath gas flow rate 7 arbitrary units, other gasses 0 arbitrary units, spray voltage 3.3 kV, capillary temperature 320 °C. Conditions for mass analysis in the orbitrap were: mass range 150-2000 m/z at a resolution of 70,000 at m/z 200, 1 microscan per scan, maximum injection time 50 µs, automatic gain control target 100,000. Also, the extraction blank was measured to check background peaks that were subtracted in mass spectrum analysis.

Formula assignment

Raw mass spectra were processed using the instrument software package Xcalibur Qual Browser (ThermoFisher Scientific). A peak list, including absolute and relative intensities, resolution, and noise levels, was generated from each mass spectrum using the inbuilt peak detection algorithm. From the processed spectra, the peaks with S/N > 3 were retained for further formula assignment [160, 168]. Elemental formula to each monoisotopic mass was assigned using Formularity software [169] which employs the

compound identification algorithm (CIA) [170]. Following parameters were employed for the formula assignment: Elements considered: $C_{0-\infty}$,$H_{0-\infty}$,$O_{0-\infty}$,N_{0-2}, and S_{0-2} [72, 160], mass error window for formula identification: 5 ppm, mass window allowed for identification by functional group relationship: 5 ppm. Additionally, lower count of heteroatoms (S+N) and lowest mass error were used to use resolve ambiguity in case of more than one formula matching the peak. The algorithm also uses the heuristic filtering of molecular formulas (7 golden rules) [171], Kendrick mass defect analysis [172], and cross-validation using the ^{13}C isotopomer analysis.

Calculations from spectra and assigned formulas

Elemental composition of the identified molecular formulas was converted to the following parameters for data analysis. Hydrogen to carbon ratio (H/C) and oxygen to carbon ratio (O/C) for the construction of van Krevelen diagrams to illustrate the major chemical classes of dNOM and dEfOM in the respective water samples [173] (see **SI Table A-5**). Double bond equivalency (DBE), a useful parameter in the characterization of the degree of unsaturation and aromaticity of a molecular formula, was calculated according to **Equation 11** [174]. Aromaticity index (AI), a conservative parameter for the identification of aromatic and condensed aromatic structures, was calculated according to **Equation 12** [175]. Besides, to classify the feed water samples and establish similarities and dissimilarities between them, hierarchical cluster analysis (HCA) was performed on the mass spectra of the samples [160, 176]. The relative abundances of the attributed peaks of each of the samples analyzed were selected as the variables. HCA has been carried out considering all the peaks in the individual spectrum and their relative abundances.

Additionally, in a further elaboration, HCA was also carried out considering only the molecular formulas common to all the water samples.

$$DBE = 1 + \frac{1}{2}(2C - H + N + P) \quad (11)$$

$$AI = \frac{1+C-O-S-0.5H}{C-O-S-N-P} \quad (12)$$

Results and discussion

Mass spectrometric analysis of DOM across water samples

Mass spectrum pattern and distribution of assigned formulas

A visual comparison of the mass spectra of the samples, **Figure 22**, shows that DOM in wastewater effluents was skewed towards low molecular weight (higher intensity peaks), whereas the surface water samples had a more natural distribution. Similar spectra distribution was reported in another study comparing dEfOM and SRNOM [72].

In total, 1473 to 1046 unique molecular formulas were identified in each sample. Three classes of molecular formulas were found to dominate the spectra of all the samples, namely CHO, CHON, and CHOS. The formulas classes identified here are similar to what has been reported previously in the literature [72, 160, 176]. The formulas containing only C, H, and O are the most abundant formula class, comprising 48 to 75% of all identified formulas. The dominance of CHO formulas agrees with previous studies on wastewater effluents and SRNOM [72, 160, 176]. Also, similar to previous reports, the wastewater effluent samples had a higher percentage (16 to 20%) of molecular formulas containing C, H, O, and S compared to surface waters (6 and 8%). These sulfur-containing molecular formulae originate from detergents, surfactants, amino acids, and pharmaceuticals [72,

176]. Effluent samples also showed a higher percentage of C, H, O, and N containing molecular formulae, 30 to 40% compared to 16 to 20%. N-containing compounds derived from proteins and amino sugars are common in wastewater [176].

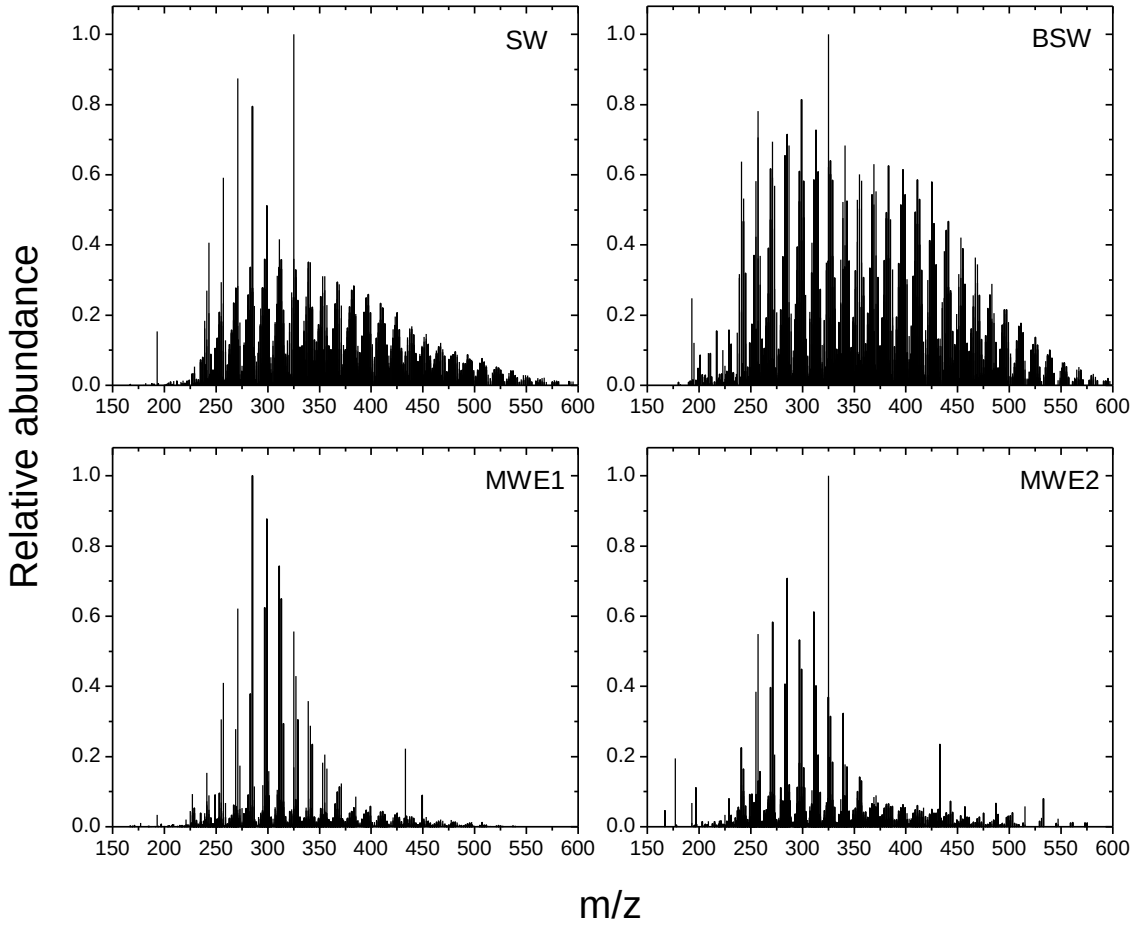

Figure 22 Negative ESI Orbitrap mass spectra of each of the samples showing the relative abundance of the identified peaks

Analysis of the averaged characteristics (DBE and AI) of the three molecular formula classes for each of the samples, **Table 5**, revealed important information about the characteristics of the organic matter. All the three molecular formula classes in the wastewater effluent samples were less unsaturated (lower DBE) compared to the same formula class in surface water samples. The difference in unsaturation was more apparent

in the case of CHOS, thus suggesting the different origin of sulfur-containing compounds in the effluents and surface water samples. In contrast, AI did not follow a similar trend across molecular formulas and sources. For CHO, the AI was similar for all sources, possibly indicative of the ubiquitous humic-like material [177]. For CHON and CHOS, the two wastewater effluents showed similar values and were lower than the surface waters; however, in the case of CHON, the brackish surface water had an AI only half that of the surface water and for CHOS the opposite was true. Thus, even across surface water samples, the organic matter character was different.

Table 5 The average ± standard deviation of the DBE and AI of the three formula classes identified for each water sample.

Source	CHO		CHON		CHOS	
water	DBE	AI	DBE	AI	DBE	AI
SW	9.16±3.29	0.09±0.15	8.56±3.10	0.67±1.12	7.14±3.41	0.25±0.62
BSW	8.99±3.38	0.07±0.15	8.80±2.79	0.38±0.60	7.46±3.22	0.52±1.09
MWE1	8.05±3.04	0.09±0.33	7.75±2.54	0.24±0.43	5.46±2.55	0.15±0.57
MWE2	8.30±3.35	0.10±0.41	8.04±3.95	0.22±0.35	5.72±2.34	0.19±0.69

Cluster plot obtained from the HCA, using each sample as an individual cluster, revealed two clear groupings, **Figure 23**. The two wastewater effluent samples (MWE1 and MWE2) and the two surface water samples (BSW and SW) were grouped. Importantly, the two clusters are positioned at a relatively larger distance, signifying significant differences between the dEfOM from wastewater effluent samples and the dNOM from surface water samples. Thus, rehashing the main basis of this study that across sources inherent differences between DOM character exists, which consequently will determine fouling behavior. The clustering of the samples in specific groups also

reveals inherent similarities between organic matter originating from similar types of sources. This is an important inference suggesting possible similar behavior of water from similar sources in different treatment techniques. Importantly, similar cluster results, **Figure 23b,** were observed by considering only the 8% peaks common to all samples, indicating that the HCA derived separation is not merely based on the presence/absence of specific peaks, but also on the relative abundance differences of the common molecular formulas.

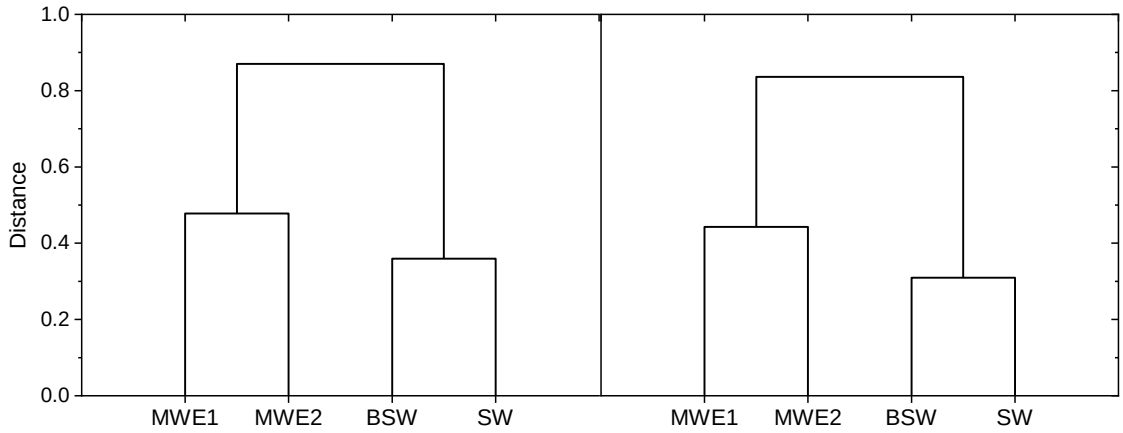

Figure 23 Cluster plots obtained from HCA (a) using all the peaks from the mass spectrum of each sample and (b) using 8% of the common peaks across spectra of all the samples.

Classification of DOM using van Krevelen diagrams

The van Krevelen diagram is an excellent tool for the visualization of chemical class distribution of organic matter [72, 161, 173, 176]. The resulting formulas from the spectrum of each sample were classified into 7 different chemical classes based on their respective H/C and O/C ratios (**Table A-5**) [176, 178, 179] and are shown in **Figure 24**. A note of caution needs to be added here, the element ratios employed represent a logical set of rules derived from chemical formulas of well-characterized molecules in the natural

products literature [72, 160, 161, 173, 176, 178]. Thus, some fallibility is inherent in the chemical class assignment [178].

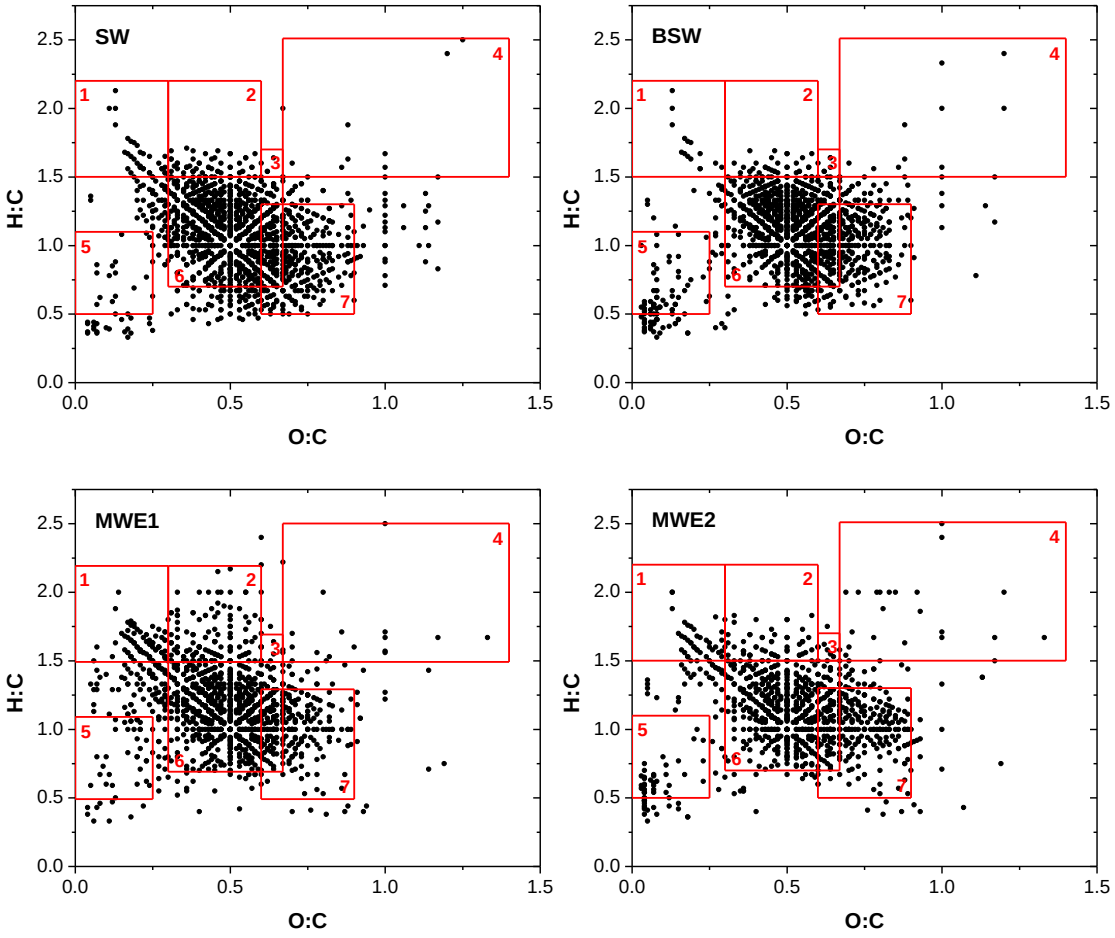

Figure 24 The van Krevelen diagrams for all the four samples showing their respective chemical class distribution. The numbered rectangles mark the regions associated with (1) lipids, (2) proteins, (3) aminosugars, (4) carbohydrates, (5) condensed hydrocarbons, (6) lignins, and (7) tannins

The percentage distribution of the chemical classes for each of the water samples is listed in **Table 6**. As is evident (see **Figure 24** and **Table 6**), the most dominant chemical class across all samples is lignin and tannin with percentage contribution ranging from 70 to 80%. Similar dominance of these chemical classes was reported by Maizel et al. [176] in the formula distribution of wastewater effluents. Additionally, although Gonsior et al.

[72] and Lv et al. [161] used a different classification scheme, similar dominance of these two chemical classes can also be inferred from the van Krevelen diagrams presented for SRNOM and peat leachate, respectively. Dominance across water sources observed here and previous works suggest the ubiquitous nature of these chemical classes. However, as I show later (see **Relationship of Fouling with water characteristics**), this dominant DOM class likely plays a negligible role in determining the fouling behavior of the different water samples.

Table 6 The percentages of the various chemical classes from the van Krevelen diagram for each sample.

Chemical Class	SW (%)	BSW (%)	MWE1 (%)	MWE2 (%)
Lipids	2.44	1.12	5.87	4.02
Proteins	4.68	3.67	10.62	6.50
Aminosugars	0.34	0.67	0.38	0.67
Carbohydrates	0.54	0.75	1.05	2.01
Condensed hydrocarbons	1.15	4.27	2.64	3.44
Lignin	50.85	50.94	47.52	43.50
Tannin	15.75	15.73	9.94	17.59
Lignin/Tannin	11.00	13.18	10.84	11.95
Others	13.24	9.66	11.14	10.33

Further, a comparison between the sources also reveals a greater percentage of biopolymers (proteins, lipids, and carbohydrates) in the wastewater effluent samples

(MWE1 and MWE2) than the surface water samples (SW and BSW). This greater percentage can be attributed to the dEfOM concoction comprising of SMP and EPS in addition to dNOM [23, 34, 158, 180]. Both SMP and EPS are composed of a complex mixture of components of microbial origin which include proteins, carbohydrates, polysaccharides, and lipids [158, 181-183]. This difference in the biopolymer content can play a major role in determining the fouling behavior of water samples since biopolymers have been identified to be the dominant foulants during long-term filtration of both surface water samples and wastewater effluents [21, 32, 123, 181].

The mass spectrum analysis revealed important insights about the DOM makeup across the four water samples establishing important similarities and dissimilarities. In the following sections, I discuss the fouling behavior of these water samples during microfiltration and assess the usefulness of these DOM makeup revelations as predictors or determiners of fouling behavior.

Microfiltration of different feed waters

The TMP profiles of the four water samples employed in this study are shown in **Figure 25**. As is seen, each of the feed water has a distinct TMP profile, thus clearly demonstrating the existence of characteristic dissimilarities among the water samples and how they subsequently interact with the membranes.

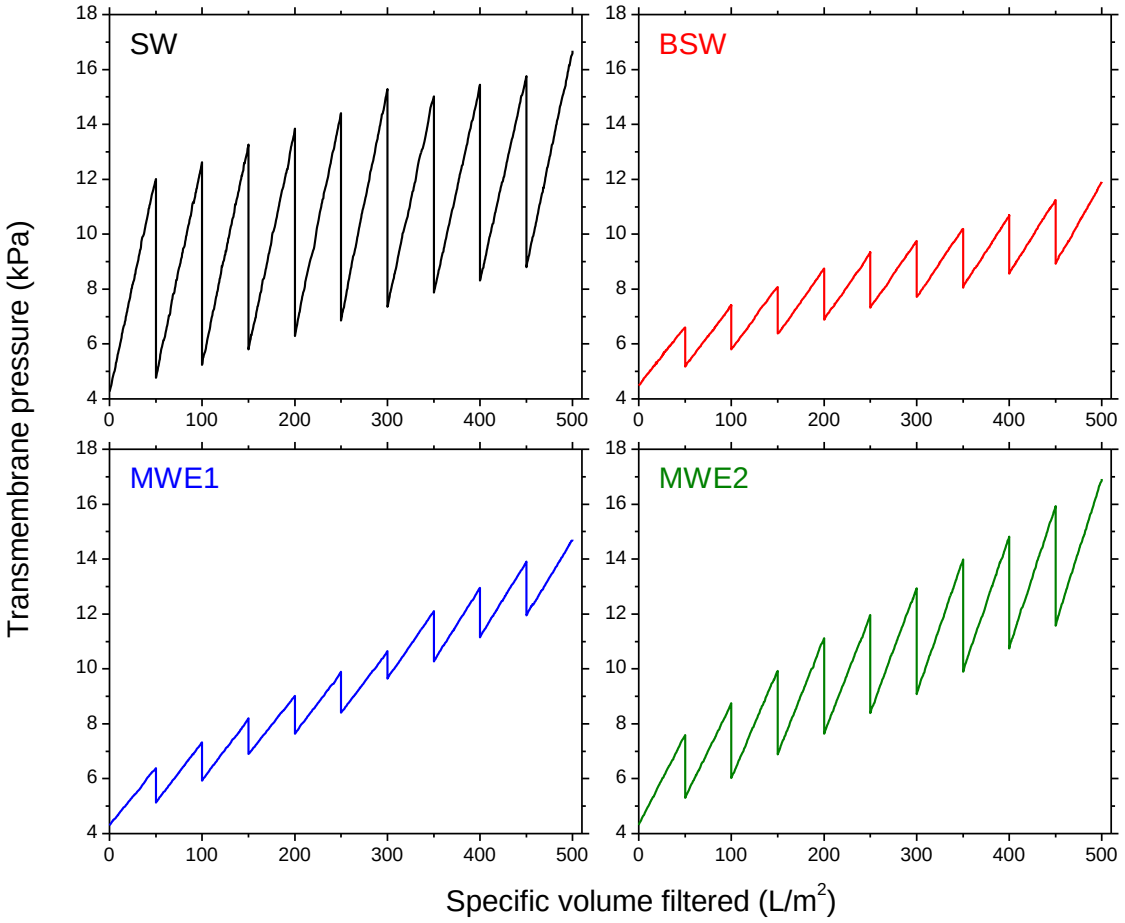

Figure 25 Transmembrane pressure profiles for the different feed waters employed in this study.

To better evaluate and compare the TMP profiles, fouling was quantitatively estimated as net irreversible resistance (R_{ir}) and the average rate of fouling ($Rate_{avg}$) [12], according to **Equations 13** and **14**.

$$R_{ir} = R^{10}_{initial} - R^{1}_{initial} \quad (13)$$

$$Rate_{avg} = \frac{\sum_{i=1}^{10}\left(\frac{dTMP}{dt}\right)_i}{10} \quad (14)$$

where, $R^{i}_{initial}$ is the hydraulic resistance at beginning of the ith cycle, R^{i}_{final} is the total

hydraulic resistance at the end of a cycle, and $\left(\frac{dTMP}{dt}\right)_i$ is the rate of fouling (kPa/h) in an individual filtration cycle i. A comparison among the four samples revealed that the two fouling parameters followed a different order. For R_{ir}, MWE1 > MWE2 > SW > BSW and for $Rate_{avg}$, SW > MWE2 > BSW > MWE1. This difference highlights that different species and phenomena influence the overall fouling [184].

In the following section, I have explored the relationship between the fouling caused by different feed waters and typical water characterization parameters along with DOM characteristics obtained from the analysis of their respective mass spectra (see **Mass spectrometric analysis of DOM across water samples**).

Relationship of Fouling with water characteristics

Rate of fouling during forward filtration

The increase in TMP i.e. the rate of fouling during forward filtration is a result of the deposition of particulate matter (typically reversible) and the deposition/attachment of DOM to the membrane pores and surface (hydraulically irreversible) [33, 108, 184]. The highest rate of fouling in the case of SW, therefore, can be attributed to its significantly high turbidity (49 ± 1.2 NTU) which would have resulted in relatively greater deposition of particulate matter during forward filtration, **Figure 25a**. However, the higher rate of fouling with MWE2 compared to BSW and MWE1 cannot directly be associated with the turbidity values of the respective feed waters (BSW = 3.19 ± 0.11 NTU, MWE1 = 2.6 ± 0.21, and MWE2 = 1.84 ± 0.5 NTU).

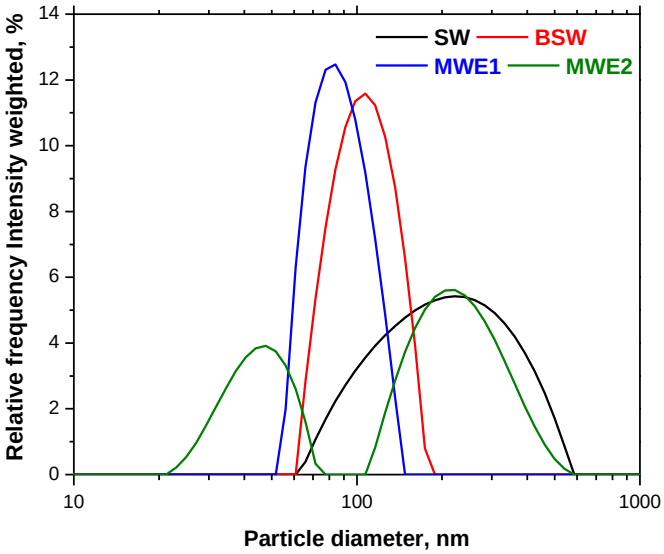

Figure 26 Size distribution of the DOM for different feed waters showing apparent differences.

In the case of DOM fouling by membranes, the interactions between the DOM and membranes determine the reversibility of fouling [149, 185], and the absolute size and the distribution affect the fouling during forward filtration, i.e., TMP increase [149]. Therefore, to account for the rate of fouling trends among BSW, MWE1, and MWE2 ($Rate_{avg}$, MWE2 > BSW > MWE1), I also looked at the size distribution of the DOM (after 0.45 micron filtration) in the different water sources, **Figure 26**. The size distribution measurements showed critical differences across samples which would have impacted the fouling. For example, for both BSW and MWE1 the size distribution was narrow with a single sharp peak. In comparison, MWE2, which showed the highest $Rate_{avg}$ amongst the three water samples, had a broader size distribution with two distinct peaks, i.e., was more polydisperse. Additionally, MWE2 also had a larger size DOM compared to BSW and MWE1. I would like to note here that although I have shown the size distribution data for SW, no commentary has been added since the rate of fouling in

the case of SW is dominantly influenced by its significantly high turbidity (49 ± 1.2 NTU).

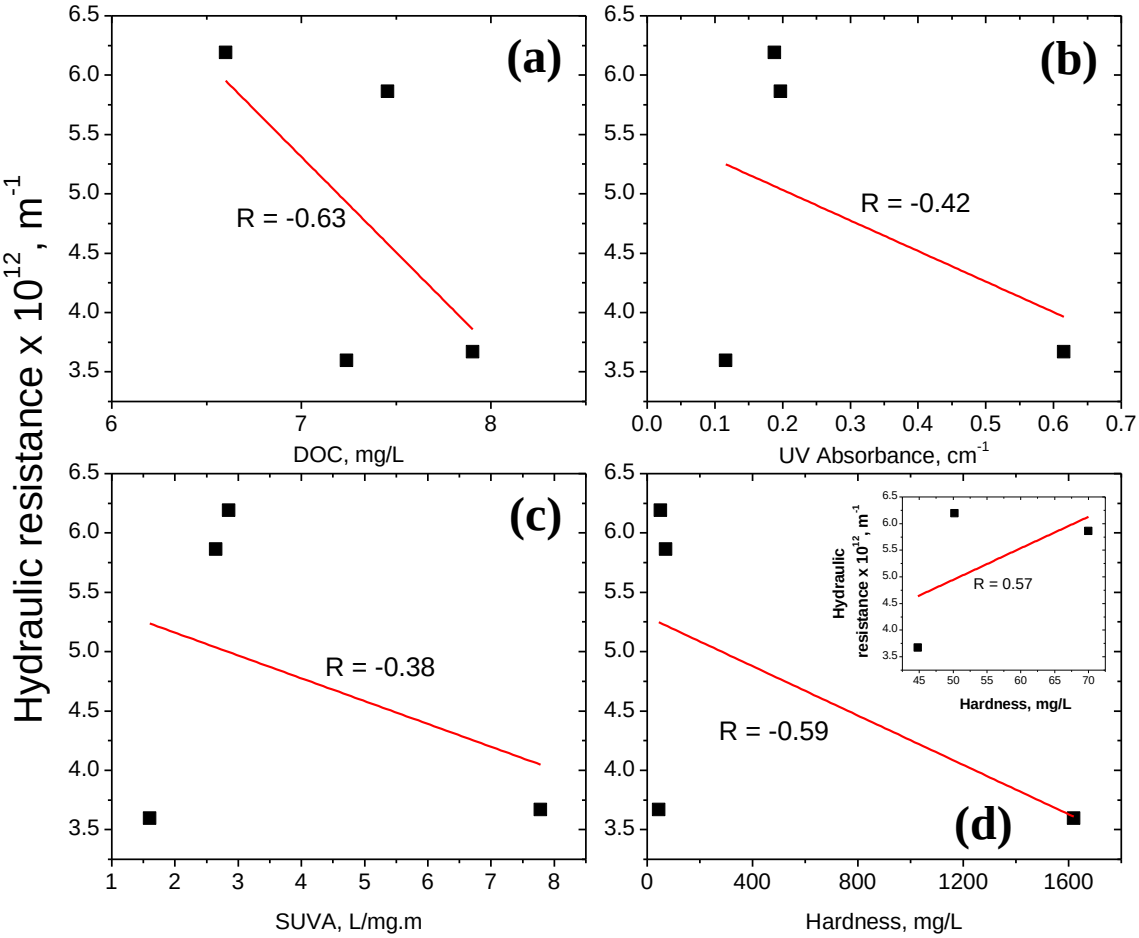

Figure 27 Relationships between hydraulically irreversible resistance and general water quality indexes.

The presence of larger size DOM species along with the greater polydispersity in the case of MWE2 compared to BSW and MWE1 can account for the $Rate_{avg}$ during the forward filtration. Essentially, each deposition of the larger size DOM (> 0.1 microns) would result in a possible complete blocking of pores compared to internal pore blocking by the smaller DOM (< 0.1 microns) and therefore, a more apparent increase in TMP in the former case [123]. Besides, a greater polydispersity also results in the formation of a more packed fouling layer and thereby greater hydraulic resistance and the consequent

higher $Rate_{avg}$ [186].

Irreversible fouling

Irreversible fouling is predominantly dependent on the specific interaction between organic foulants and the membrane [16, 123, 185]. However, broad DOM characterization parameters (DOC, UVA, and SUVA) are poor predictors of the fouling propensity of feed waters [31, 32, 82, 123]. Unsurprisingly, in this study weak ($R < 0.6$) and negative correlation between these parameters and the irreversible fouling was observed, **Figure 27a**, **b**, and **c**. Additionally, although the presence of divalent ions is suggested to be important for irreversible fouling [187, 188], a similar weak correlation existed between total hardness and irreversible fouling, even with the exclusion of BSW (outlier hardness), **Figure 27d**.

Next, I looked at the relationship between irreversible fouling and the percentage weighted concentration (mg/L DOC in SPE extract * fraction of a chemical class in the sample) (see **Classification of DOM using van Krevelen diagrams**) of the different chemical classes. The most abundant chemical class among all water samples, lignins and tannins, showed a strong but inverse correlation ($R = -0.94$). Two important inferences can be drawn from this correlation analysis, (i) only a small fraction of the DOM is actually responsible for the fouling, as has been reported previously for both dNOM and dEfOM [16, 123], and (ii) the presence of these DOM may beneficially inhibit the more detrimental DOM-membrane interactions and thereby restrict irreversible fouling. Additionally, as I show later, during filtration this abundant class of DOM undergoes the least rejection of all organic species identified (see **Permeate DOM analysis**), further

reinforcing the observed negative correlation.

Out of all the other chemical classes identified, only proteins and lipids classes showed a strong positive correlation with the irreversible fouling with R = 0.90 and 0.92 for proteins and lipids, respectively **Figure 28**. Additionally, the carbohydrates class showed a very weak positive correlation (R = 0.50). All other remaining chemical classes showed no correlation with R < 0.1 (see **SI Figure A-9**).

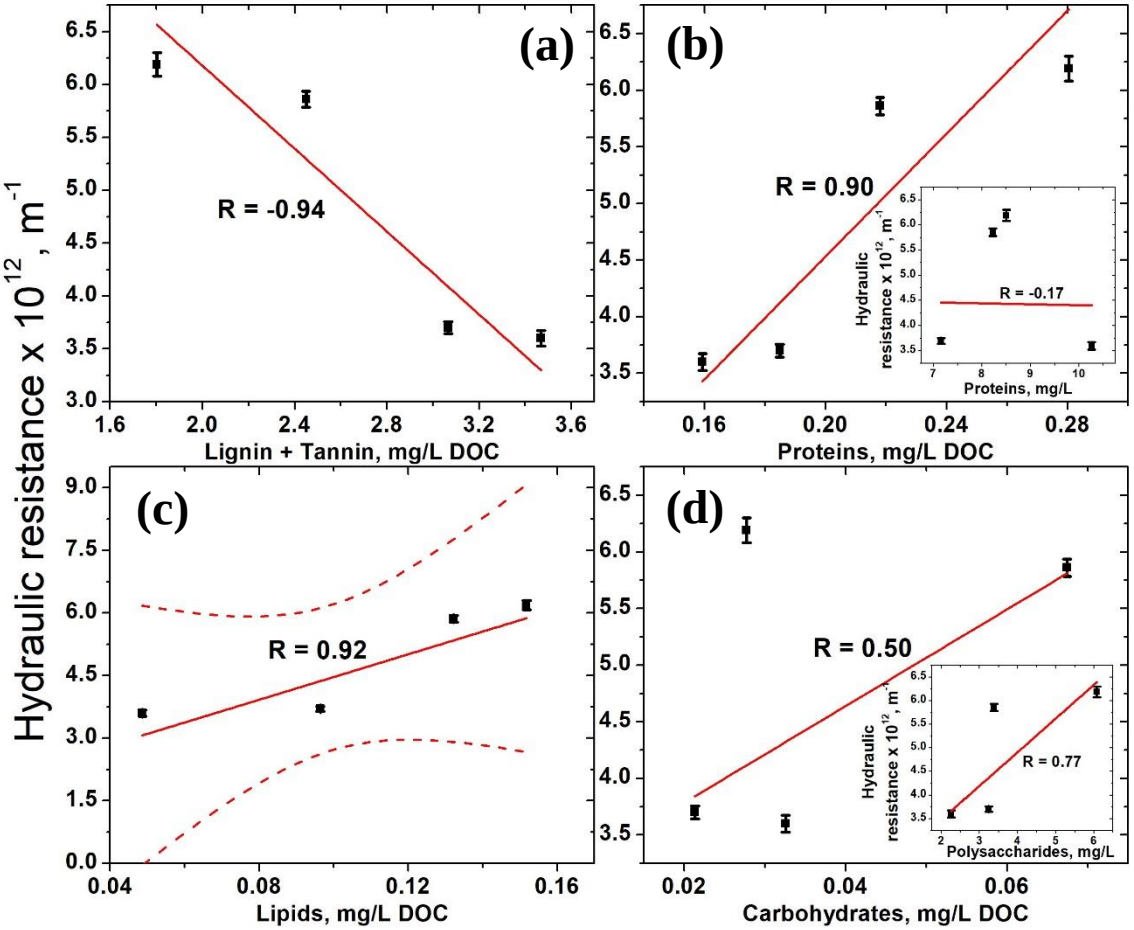

Figure 28 Relationships between hydraulically irreversible resistance and percentage weighted concentration of different chemical classes determined from high-resolution mass spectra. Relationships with colorimetric measurements are shown in inset (b) proteins and (d) polysaccharides.

The hydrophobic PVDF membrane is susceptible to loss in permeability due to the adsorption of proteins to the surface and inside the pores [128]. Additionally, relative protein abundance was observed in high fouling river waters; however, no quantitative assessments were made [32]. Thus, the protein correlation to irreversible fouling observed here is not unexpected and is supported by previously published reports. Similar to proteins, carbohydrates have also been reported as major foulants in multiple previous studies. Specifically, the organics that are included in the carbohydrate class, namely glycosides and polysaccharides [178], dominantly constitute the biopolymers fraction of dNOM and dEfOM [34], a fraction shown to be strongly correlated to fouling of UF and MF membranes in a variety of water sources [31, 32]. Therefore, the weak correlation observed here is an artifact of SPE, as carbohydrates are negligibly absorbed by PPL cartridges [189].

Interestingly, these correlations did not reflect in a similar form for protein and polysaccharide concentrations determined colorimetrically, **Figure 28b** and **d**. While for proteins no correlation ($R = -0.17$) was observed, the polysaccharide concentration showed a strong correlation ($R = 0.77$). This may be attributed to the fact that while bulk water and extracted DOM contain similar fractions, their relative proportions differ owing to the extraction process [190]. Additionally, these chemical class assignments are not definitive (i.e. a protein-like formula is not necessarily derived from proteins) [176, 178] and as mentioned prior are based on a set of rules (see **Classification of DOM using van Krevelen diagrams**). Nevertheless, they do provide a general insight into the compound classes.

The lipids chemical class showed a relatively stronger correlation to the irreversible fouling (R = 0.92 compared to R = 0.90 and 0.50 for proteins and carbohydrates, respectively). Although, both dNOM and dEfOM are known to contain lipids [156, 191, 192], they have not been typically identified as the foulant class during surface water or effluent filtration. This is possibly an artifact of the generally employed DOM characterization techniques of LC-OCD and EEMs, which classify organics into broad groups. For example, LC-OCD typically resolves DOM into five groups, namely biopolymers (proteins and polysaccharides), humic substances, microbial building blocks, low molecular weight (LMW) neutrals, and LMW acids [31, 32, 156]. Similarly, EEMs resolves DOM into four groups, namely proteins, microbial byproducts, humics, and fulvics [31, 156, 180]. As is evident, these popular techniques do not specifically identify lipids and hence inferences drawn based on these techniques cannot account for contributions of lipids like species to fouling. Thus, the relationship between lipid content and irreversible fouling demonstrated here is important learning.

The discussion about the role of lipids in fouling although lacking in current DOM fouling literature has received some attention in the past with few reports. For example, Al-Halbouni et al. suggested the role of hydrophobic interaction of lipids with PVDF membrane as a plausible explanation for fouling in a membrane bioreactor (MBR) [193]. Barry et al. examined the fouling of UF membranes by liposomes (synthetic vesicles composed of phospholipid bilayers) and speculated liposome-like material in secondary effluent being responsible for 20-60% of the fouling [191]. Park et al. observed during nanofiltration out of the three DOM fractions extracted from brackish surface water, the

fraction dominated by lipids and some portion of proteins resulted in maximum flux decline [156].

In the past, our research group has elaborated the mechanism of progression of irreversible fouling during microfiltration of lake water and wastewater effluent [21, 123]. Importantly, in both cases fouling was found to be initiated by the preferential deposition of relatively hydrophobic species (identified as containing CH groups by FTIR spectroscopy). While in these previous reports no categorical identity was established, results here indicate that these CH containing hydrophobic organics were likely belonging to the lipids chemical class. As previously noted, hydrophobic interactions between lipids and membrane material have been implicated in the fouling of MBRs [193-195]. It is important to reiterate that the chemical classes here are representative, and the lipids class represents a concoction of species including fatty acids, aliphatic hydrocarbons, terpenes, and sterols [178], all of which contain long CH chains [196].

While interesting relationships were observed by the simultaneous analysis of DOM character and fouling, I wanted to explore the correlation vs. causation argument. Essentially questioning whether the observed correlations can be utilized to legitimately deduce a cause-and-effect relationship. For this purpose, DOM mass spectra of the microfilter permeate were obtained and analyzed similarly to feed water DOM spectra. I have discussed the results of our analysis in the next section.

Permeate DOM analysis

I analyzed the mass spectra of the permeate DOM (**SI Figure A-10**) for all the four

feed water samples and obtained the chemical class distribution, **SI Figure A-11** and **Table 7**. Permeate DOM characterization provided insights about the nature of DOM being rejected during the filtration. The change in the composition of the DOM after filtration was estimated as the difference in the percentage of the individual classes between the feed and the permeate waters (Δ = % in permeate - % in feed), **Figure 29**. As can be seen, out of the identified classes, lipids, carbohydrates, and condensed hydrocarbon classes underwent a reduction in their respective percentage contribution, whereas proteins, lignins + tannins, and aminosugars classes showed an increase in their percentage contribution.

Table 7 The percentages of the various chemical classes from the van Krevelen diagrams for the permeate of each feed water sample.

Chemical Class	SW (%)	BSW (%)	MWE1 (%)	MWE2 (%)
Lipids	1.17	0.61	2.97	1.03
Proteins	4.96	5.84	10.84	8.56
Aminosugars	0.41	0.68	0.70	0.93
Carbohydrates	0.29	0.53	0.61	1.34
Condensed hydrocarbons	0.93	1.59	0.61	2.78
Lignin	52.86	57.59	51.57	52.78
Tannin	17.29	13.73	11.19	13.30
Lignin/Tannin	11.80	11.99	11.89	10.72
Others	10.28	7.44	9.62	8.56

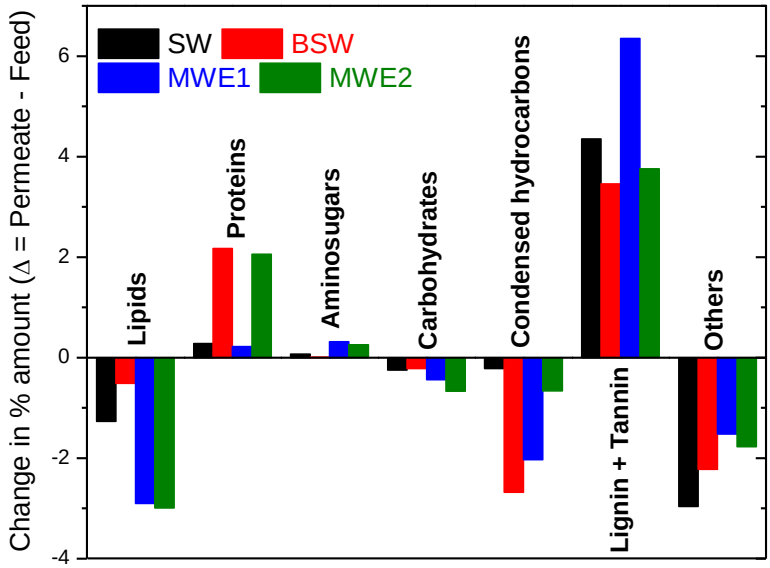

Figure 29 Change in the percentage of different chemical classes after filtration

The change in the DOM composition after filtration gives interesting insights into the possible fouling components. Essentially, while the rejected DOM class is likely to play a major role in the fouling, the permeated DOM conversely not so much. The decrease and increase in the percentage contribution of different chemical classes imply that the specific DOM species were rejected more than others and vice versa. In this context, the highest increase was observed for the lignin + tannin class (Δ = ~4-6), which is also the most dominant class in all the feed (70 to 80%, see **Table 6**) and permeate (75 to 85%, see **Table 7**) samples. Thus, it is fair to argue that organic species belonging to this class were negligibly rejected and possibly minimally contribute to fouling (inversely related to irreversible fouling, see **Figure 28a**). The aminosugars class also showed an increase but since both its percentage contribution, in feed and permeate, and the corresponding change is relatively small for all water sources (0.3 to 0.6% in the feed, 0.4 to 0.9% in permeate, and Δ = 0.01 to 0.3), any comment on the involvement of this chemical class in fouling

would be highly speculative. The next chemical class to show an increase in percentage contribution was proteins, which have been identified as a major class of foulants [23, 32, 108], and as shown earlier their percentage weighted concentration across sources are strongly correlated to the irreversible fouling (see **Figure 28b**). Thus, this increase of percentage contribution in the permeate endorses the question, whether the correlation can legitimately be inferred as causation.

I believe, a definitive answer to this question requires a more elaborate design of experiment accompanied with a suite of organic matter characterization tools like high resolution nuclear magnetic resonance, gas chromatography-MS, time of flight MS (TOFMS), and high-resolution MS [159]. Such an analysis was beyond the scope of this study. Nevertheless, previous reports of high susceptibility of protein adsorption to membranes [128] suggest the correlation may very well be causation. The increased percentage contribution in the permeate may be an artifact of the complex concoction forming the protein class. This is further suggested by the fairly variable quantitative increase in percentage contribution (Δ = ~0.2 to 2.2), among the four feed water samples, **Figure 29**.

For the chemical classes showing a decline in percentage contribution, the argument for their higher rejection and possible involvement in fouling certainly holds. Out of the three classes undergoing reduction, as noted before, the lipids and the carbohydrate class showed a correlation to the fouling (**Figure 28c** and **d**). Although no such correlation was observed for the condensed hydrocarbon class, the organic moieties comprising this chemical class (primarily aromatic compounds [179]), present in both

dNOM and dEfOM, have been shown to lead to greater flux decline [29, 188] and also undergo higher rejection [197].

Conclusions

The non-targeted analysis of DOM yielded important insights into the similarities and dissimilarities across a variety of water sources. While the study demonstrated differences in the composition of dNOM and dEfOM, it also showed characteristic differences can exist within dNOM and dEfOM from different sources. Further detailed analysis of the mass spectra of the DOM using van Krevelen diagrams provided molecular level characterization and classification. The classification served as an important tool in understanding the possible role of different chemical classes in MF fouling. Correlation analysis between percentage weighted concentration of different chemical classes in the feed waters and their respective irreversible fouling extent revealed the important roles of proteins and lipids in the irreversible fouling of microfilters. However, the role of proteins was put into contention upon analysis of the permeate samples. Therefore, although the presented analysis shone a spotlight on a previously overlooked fraction of organic matter (lipids), it also raised questions for possible future work. Nevertheless, this approach will prove useful in expanding our understanding of membrane fouling by DOM.

Additionally, some constraints influenced the results in this study and should be considered during the extrapolation of these results and possible future work. The DOM characterized in this study is 40 to 60% of the total, thus the extraction method introduces an inherent bias [198, 199]. Besides, the instrumentation employed also introduces specific limitations, for example, the type of electrospray ionization affects the type of

organics revealed in the spectra. While some organic species are more amenable to positive mode ionization, others are more amenable to negative mode ionization [176]. Hence, our results should be treated as partial insights in the complex domain of DOM and MF/UF fouling.

CHAPTER V

AGING OF POLYVINYLIDENE FLUORIDE (PVDF) MICROFILTRATION MEMBRANES OVER MULTIPLE FOULING AND CHEMICAL CLEANING CYCLES DURING WASTEWATER EFFLUENT FILTRATION

Introduction

With increasing water scarcity, there is a growing demand for water reuse as part of improved urban water management strategies [5]. The Texas State Water plan 2017 estimated that by 2070 around 13% of all new drinking water facilities will be based on water reuse [69]. The United Nations world water development report 2017 argued for improved wastewater management (reuse and resource recovery) to achieve the Sustainable Development Goal targets [7]. An integral component of water reuse treatment trains is low-pressure membrane filtration, i.e., microfiltration (MF) and ultrafiltration (UF) [10, 200]. These membranes over the duration of operation undergo performance deterioration (aging) warranting replacement [36]. Thus, for more predictable long-term operation and capital planning, I need to develop a better understanding of the aging of membranes during water reuse. However, only a few water reuse facilities have been operating for long enough times to provide adequate information about the aging of these membranes. For example, the world's largest indirect potable reuse facility in Orange County, California, began operation only in 2008 [48].

Now, multiple previous studies have investigated the accelerated aging of the membranes as affected by the degradation of membrane material upon exposure to a high

dose of chemical cleaning agents [36, 201-203]. However, the operational aging of membranes over long-term operation is due to the prolonged exposure to chemical cleaning agents and by the irreversible attachment of foulants [38]. Therefore, this experimental design cannot account for the role of irreversibly bound foulants [204]. A recent study looking at MF membrane samples at different stages in their operational lifetime (1-8 years) from drinking water facilities demonstrated that typically employed aging protocol of short-term exposure of membranes to a high concentration of cleaning agents (generally NaClO) is not representative of long-term operational aging [41]. The critical role of irreversibly attached foulants was also highlighted in another autopsy study of membranes from several drinking water facilities [40]. They observed that membranes that underwent less frequent chemical cleaning aged significantly faster.

To date, very few studies have employed multiple fouling cleaning cycles experimental design to assess the aging of membranes as affected by both irreversible fouling and membrane material degradation. A membrane aging review published in 2016 [38] featured only four articles [205-208] that employed such a design. Importantly, out of these four, three [205-207] used model foulants, and one employed a pilot-scale membrane bioreactor [208]. The authors of the review [38], also highlighted the need for heightened attention towards the role of irreversibly attached foulants. Recently, another study compared the multiple fouling cleaning cycles protocol to high-dosage exposure aging and concluded that the former was a better surrogate for full-scale aging [204]; however, with either protocol they did not observe the long-term irreversible loss in permeability, associated with full-scale membrane aging [40].

In this study, the primary objective was to assess the combined impact of prolonged fouling and cleaning on the performance and intrinsic character of commercial polyvinylidene fluoride (PVDF) hollow fiber MF membranes during water reuse. To this effect, I analyzed the aging of membranes by carrying out multiple fouling and chemical cleaning cycles in a submerged membrane laboratory setup filtering wastewater effluent. Additionally, I membrane aging due to chemical cleaning was simulated by exposure of the pristine membrane to chemical cleaning agents under the same chemical cleaning conditions as employed in the fouling-cleaning cycles experimental design. The two experimental designs were compared to clearly distinguish between the two laboratory aging protocols and subsequently delineate the roles of chemical degradation and irreversible fouling in membrane aging. The aged membranes were characterized using membrane performance parameters (fouling propensity and pure water permeability), surface functionality (Fourier transform infrared (FTIR) spectroscopy, zeta potential, and contact angle), and mechanical strength (membrane integrity test and dynamic mechanical analysis (DMA)). I expect that our results will help to understand membrane aging in water reuse and provide insights for future research simulating membrane aging.

Materials and Methods

Source water for fouling-cleaning experiments

Wastewater effluent samples were collected during the period of September-December 2019 from the 4 million gallons per day (MGD) conventional activated sludge Texas A&M wastewater treatment plant, College Station, Texas after UV disinfection and

just before discharge. Collected water samples were stored in the dark at 4 °C and brought to room temperature overnight before the filtration experiments. The collected samples varied moderately in the water quality characteristics with pH = 8.2 - 8.6, dissolved organic carbon = 7.05 - 9.10 mg/L, chemical oxygen demand = 14 - 30 mg/L, UVA at 254 nm = 0.15 - 0.20 cm^{-1}, turbidity = 1.8 - 2.6 NTU, conductivity = 1100 - 1350 µS/cm, and alkalinity = 140 - 160 mg/L as $CaCO_3$.

Membrane aging experimental design and setup

Three different types of membrane aging protocols were employed, referred to as Type A, B, and C. Each protocol used identical membrane modules. The module consisted of 12 PVDF hollow fiber membranes (nominal pore size of 0.1 µm, 1.293 mm O.D., and 0.711 mm I.D.) provided by Pall Corp., USA. The effective length of each fiber after potting in epoxy resin was 24.5 cm, giving an active membrane surface area of 100 cm^2 for each module. Type A was a long-term fouling and cleaning protocol, Type B was a long-term adsorptive fouling and cleaning protocol, and Type C was a chemical cleaning agent exposure protocol. The three protocols are detailed below:

Type A. A bench-scale submerged membrane filtration system (**Figure 30**) was operated at a constant filtration and backwashing flux of 40 $L/m^2.h$ in a cycle of 1-hour filtration and 3-minute backwashing. Filtration was performed with disinfected wastewater effluent, and the permeate was used for backwashing. The transmembrane pressure (TMP) was continuously recorded using a compound pressure gauge (A2VAC/30PSI, Ashcroft), and the flux was maintained using a peristaltic pump (7528-

20, Cole Parmer). The pump's flow direction was changed to accomplish filtration and backwashing. Pump control and TMP data acquisition were performed automatically by a program written in LabVIEW 2019 (National Instruments, USA). The feed water level in the membrane vessel was maintained via continuous recirculation using an additional peristaltic pump.

The entire process of multiple filtration-backwashing (fouling) and cleaning cycles was run for around 150 days, equating to ≈100 days of filtration. During the 150 days, the filtration was stopped when the transmembrane pressure reached 60-70 kPa (pre-decided set pressure), and the membrane module was chemically cleaned (see **Cleaning in Place (CIP) Protocol**). After each cumulative ≈25 days of filtration, three membrane fibers were harvested from the module following the CIP. After each harvesting, the module was repaired and returned to the membrane vessel, with flow rates decreased to maintain the set flux of 40 $L/m^2.h$ during filtration and backwashing. The TMP profile for the filtration during the duration of the aging protocol is shown in **Figure 31**.

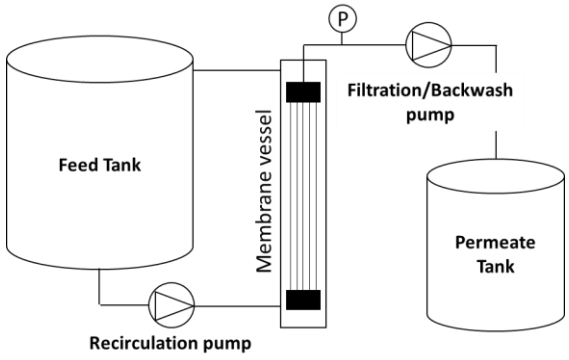

Figure 30 Schematic of the submerged membrane filtration system

Type B. Membrane module was submerged in wastewater effluent (no filtration

and backwashing) and followed the cleaning and harvesting cycles of the module in Type A. The effluent in the membrane vessel was continuously stirred and replaced every three days. The harvested samples from this aging protocol represented membranes aged by the progressive adsorption of specifically interacting foulants (responsible for irreversible fouling [209]) to the membrane and exposure of the membrane to cleaning agents during CIP.

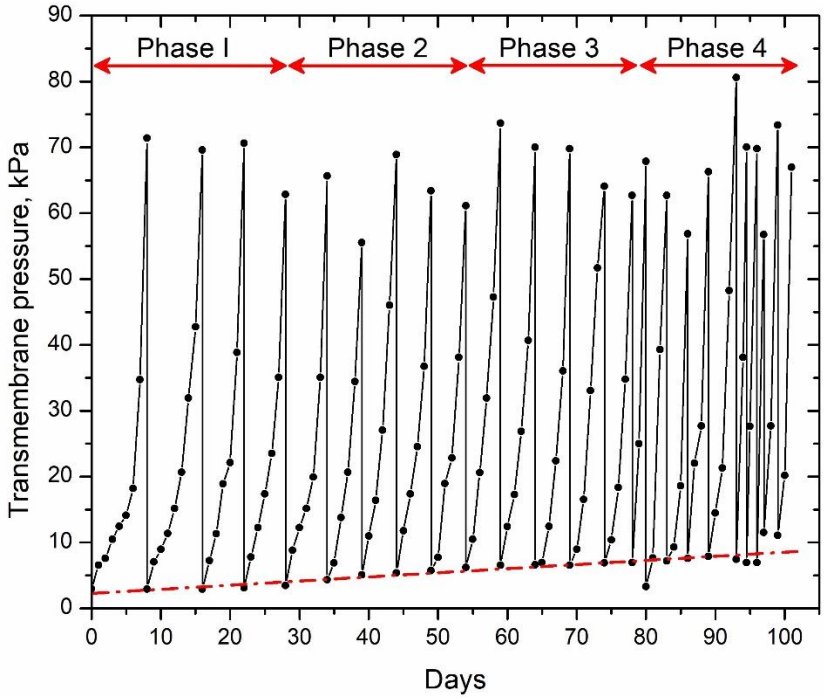

Figure 31 Transmembrane pressure profile for the entire duration of the fouling cleaning protocol (Type A). The red arrows mark the duration of each phase after which aged membranes were harvested. The red dashed line at the bottom shows the increasing trend of initial TMP after each CIP.

Type C. Membrane module remained submerged in ultrapure water and followed the cleaning and harvesting cycles of the modules in Type A and B. The harvested samples represented membranes aged by the prolonged exposure of pristine membranes to the chemical cleaning agents. This protocol is similar to the predominant accelerated

membrane aging experiment design [36, 201-203]. However, unlike typically practiced design of small duration high dosage exposure, the dosage and duration were as used during CIP.

From each module, four harvestings of three membrane fibers were performed. Each set of harvested samples are named Phase 1 (1^{st} harvest), Phase 2 (2^{nd} harvest), Phase 3 (3^{rd} harvest), and Phase 4 (4^{th} harvest) for all three membrane aging protocols.

Cleaning in Place (CIP) Protocol

The CIP was performed, as recommended by the manufacturer, in two steps employing a caustic bleach solution (1% NaOH + 0.2% NaClO (1800 ± 10 mg/L free chlorine), pH = 12.75 ± 0.01) and a dilute citric acid solution (2% anhydrous Citric acid in ultrapure water, pH = 2.05 ± 0.02). In the first step, membrane modules were submerged in continuously stirred fresh caustic bleach baths for 30 minutes and 4 hours successively. In the second step, membrane modules were submerged in continuously stirred citric acid baths for 30 minutes and 1 hour successively. The first and second successive immersions for both cleaning agents represent the flushing and recirculation cycles, respectively in typically practiced CIP. After each step, the membrane modules were immersed in a stirred ultrapure water bath to remove traces of cleaning agents.

Membrane performance parameters

Single fiber membrane modules (test modules) were prepared for evaluating the change in the performance of membranes with progressive aging. A 12 cm length of

membrane fiber (virgin and aged) was potted in nylon tube fittings with epoxy ensuring that the fiber opening was not blocked. The bottom end of the fiber was sealed with epoxy resin. Each test module, after potting, had a length of 10 cm, giving an active area of 4 cm^2. The test modules were used to estimate the following membrane performance parameters:

Pure water Permeability. Test modules were submerged in ultrapure water, and the TMP (kPa) was recorded at five different fluxes (40-130 L/m^2h). The slope of the plot of flux vs. TMP gave the membrane hydraulic permeability (L_p) ($L/m^2h.kPa$) as defined by Darcy's law ($J = L_p \Delta P$) [12].

Fouling propensity and reversibility. A critical factor determining the overall effectiveness of the membrane system is the extent of fouling [12]. Therefore, I estimated the effect of aging on the membrane performance in terms of fouling propensity and hydraulic reversibility of fouling. The test module was submerged in wastewater effluent, and filtration was carried out at a flux of 40 L/m^2h to produce 100 ml of permeate. The factor of increase in pressure during the filtration ($TMP_{final}/TMP_{initial}$) was calculated as a measure of the fouling propensity. To estimate the reversibility of fouling, the test module after wastewater effluent filtration was backwashed at 40 L/m^2h with ultrapure water for 5 minutes, and the pure water permeability was determined as described earlier.

Membrane characterization

Mechanical strength

Membrane integrity. The pressure decay test was carried out to test the integrity of the membranes [210]. Wetted test modules were placed in a sealed air pressurized cell (140 kPa). The pressure source was then closed off, and the pressure reduction was continuously recorded using a pressure transducer. The pressure declined linearly, and the rate of decline was estimated as a measure of the integrity of the membrane. The pressure decline rate for virgin membrane was used as a reference to estimate any changes in the integrity of the aged membranes.

Dynamic mechanical analysis (DMA). To characterize the membranes, DMA was carried out using the TA instruments DMAQ850 [211, 212]. Oscillatory strain sweeps were applied to each sample at a frequency of 1 Hz until breakage. The membrane fiber was held in place using the fiber/film clamps from TA instruments. The measurements were performed at room temperature (23 ± 1 °C). In the stress–strain measurement, an oscillatory strain is applied to the exposed samples in tensile mode and the resultant stress is measured. Young's modulus and dynamic storage modulus were estimated as measures of mechanical strength.

Surface functionality of the membranes

Membrane surface zeta potential (ZP). ZP of the membrane surface was estimated using an electrokinetic analyzer (SurPASS 3, Anton Paar). The measurements were carried out using freshly prepared 1mM KCl as background electrolyte in pH scan mode

(pH~ 2-10) using an automatic titrator. More details about the measurement and the method can be found elsewhere [123].

Fourier transform infrared (FTIR) spectroscopy. Infrared spectra of membrane surfaces were obtained using a Nicolet iS10 spectrometer equipped with a mid-infrared Ever-Glo source, DTGS detector, KBr beam splitter, and Omnic 9.0 Software with a diamond iTX accessory to allow sampling in attenuated total reflection (ATR) mode. A background spectrum was also collected on a clean ATR window prior to each analysis. Samples were placed on the window, and the IR spectrum was obtained by averaging 128 scans collected at 4 cm^{-1}.

Contact angle. The air-water contact angle of the surface of vacuum-dried virgin and aged membranes were measured using the Biolin Attension Tensiometer (Biolin Scientific). The measurements were made using the sessile drop method, a 0.5 µL droplet of ultrapure water was placed on the membrane surface, and five to ten frames were imaged at a rate of 1 frame per second. The images were processed using ImageJ, and the contact angle was estimated using the DropSnake plugin [213]. Two to three measurements were made for each sample, and the averages have been reported.

Results and discussion

Effect of aging on membrane performance

Pure water permeability

Pure water permeability of aged membranes from Type A protocol decreased with each phase (Phase 1 > Phase 2 > Phase 3 > Phase 4), **Figure 32**. The decline can be

attributed to the progressive attachment of chemically irreversible foulants over the duration of the experiment, evinced by FTIR spectroscopy (see **Surface functional groups**). Importantly, this shows that chemically irreversible fouling leads to the loss in the performance of membranes over long-term operation [40, 41, 214]. The decline in permeability observed here was also apparent from the gradual increase in initial TMP values (after chemical cleaning), as shown in the pressure profile for the Type A aging protocol, red dashed line in **Figure 31**. In contrast, while chemically irreversible foulants were observed in the case of Type B membranes, **Figure 34**, no change in permeability of the membranes from module Type B was observed. This implies that foulant attachment via adsorption was dominantly on the surface and not inside the pores and therefore, permeability remained unaltered.

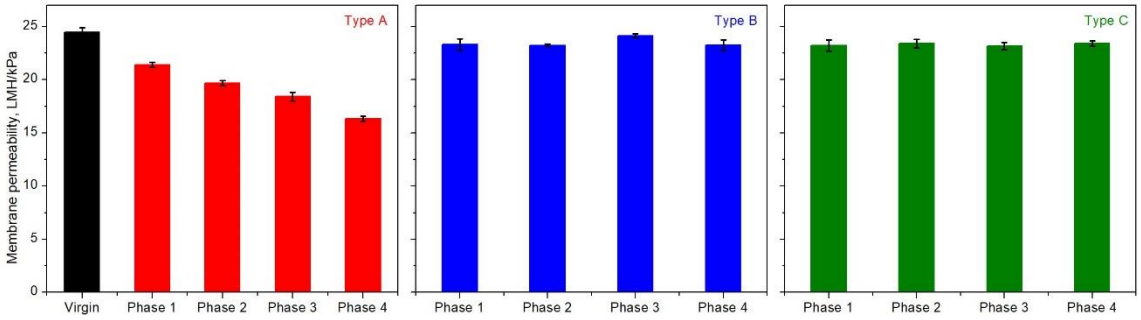

Figure 32 Pure water permeability (LMH/kPa) for the membranes harvested from the three modules (Type A, Type B, and Type C). The black line represents the pure water permeability of the virgin membrane.

Importantly, Type C membranes also did not show any change in permeability across all four phases. This is contrary to previous investigations that have consistently shown an increase in permeability of PVDF membranes upon long-duration exposure to high doses of sodium hypochlorite and sodium hydroxide [204, 211, 215, 216]. Critically, all these previous studies used blended PVDF membranes (PVDF dosed with hydrophilic

additives like Polyvinylpyrrolidone (PVP) and poly(methyl methacrylate) (PMMA) [128, 217]) as opposed to the non-blended PVDF membranes (not containing any hydrophilic additives) used in this work. Ravereau et al. demonstrated that upon exposure to high doses of sodium hypochlorite, while blended PVDF membranes showed an increase in permeability, non-blended PVDF membranes did not undergo any changes [201]. However, the authors conceded the possibility of undetected structural changes. As I discuss later under **Surface functional groups**, minimal oxidative degradation of PVDF was detected. Thus, it can be inferred that although the chemical cleaning agents' dose and the exposure duration employed in this study did cause some material damage, membrane permeability remained unaffected.

The contrastingly different behavior of Type A and Type C membranes underscores the drawback of high-dosage short duration exposure studies. A typical chemical cleaning agent exposure experimental design to study the aging of non-blended PVDF membranes will result in false inferences about their true operational aging. Based on these results, I can conclude that the truer aging of the membranes is dominantly due to the continued accumulation of chemically irreversible foulants. However, I will add a caveat to this conclusion. For relatively less chemically resistant membranes like blended PVDF membranes [201], the aging will likely be a function of both chemical degradation and the continued accumulation of chemically irreversible foulants [204]. Research comparing the two membrane types in similar experimental design could prove useful; however, it was beyond the scope of this work.

Membrane fouling potential and fouling reversibility

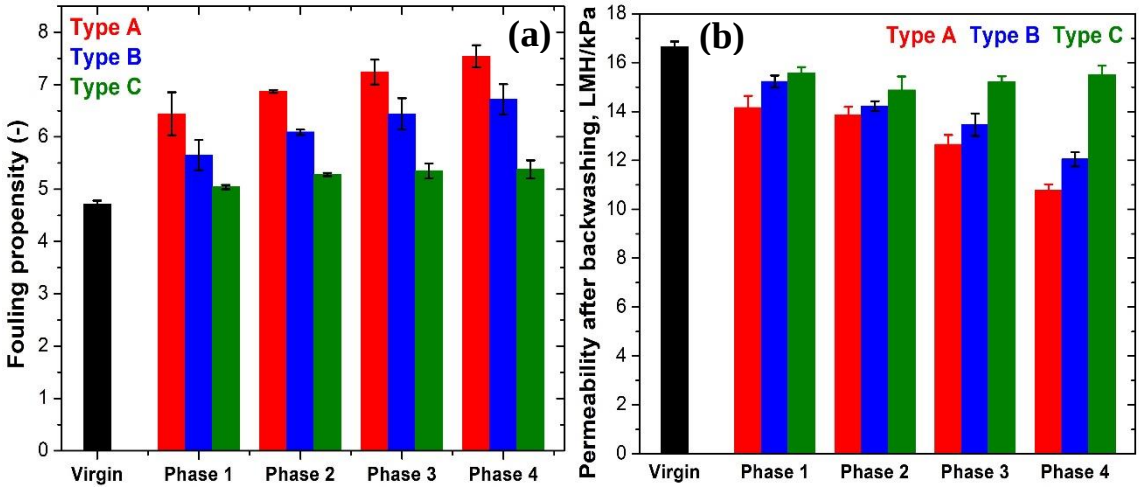

Figure 33 (a) Fouling propensity and (b) fouling reversibility (measured as permeability after hydraulic backwash) for the membranes from the three modules (Type A, Type B, and Type C). The black line represents the fouling propensity and permeability value for the virgin membrane.

Fouling potential for aged membranes from all the three protocols increased with each phase, **Figure 33a**. This increase in fouling potential can be attributed to the transition of surface character to more hydrophilic and less negative (see **Figure 35** and **Figure 36**). Phuntsho et al. argued that the reduced zeta potential (less negative) of aged membranes led to reduced repulsive forces between membranes and foulants and therefore increased fouling [42]. Robinson et al. also demonstrated with model foulants that the fouling propensity increased with the age of the membranes [41]. Additionally, for Type A membranes the decreased water permeability, **Figure 32**, will also contribute to the increased fouling potential. The increased fouling potential in Type A membranes was also evinced from the TMP profile (**Figure 31**), with the set pressure for CIP achieved earlier than the preceding cycle, more apparent in the later phases. The decline in permeability in the case of Type A membranes in conjunction with relatively larger

changes in the surface character (see **Effect of aging on the surface functionality of membranes**) led to Type A membranes showing the highest fouling potential, followed by Type B and Type C membranes, with Type C membranes undergoing minimal change.

The pure water permeability after backwashing, the measure of fouling reversibility, was maximally recovered for virgin membranes, **Figure 33b**. For the aged membrane samples, the recovery decreased with each phase; however, this decline was most significant in the case of Type A membranes. Type B membranes showed broadly similar behavior whereas Type C membranes showed only minimal changes only in the early phases. The reduced fouling reversibility in the case of Type A membranes was also evident from the TMP profile of long term experiments, **Figure 31**. As is seen, the initial TMP values at the beginning of each cycle after cleaning underwent a gradual increase over the duration of the experiment, marked by the red dashed line.

The reduced fouling reversibility implies that the progressive aging resulted in the increased tendency of the foulants to irreversibly adhere to the modified membrane surface and pores. This is possibly due to the progressive hydrophilization of the membrane surface (decline in water contact angle, see **Figure 36**). In MF and UF, irreversible fouling proceeds by the initial deposition of relatively hydrophobic species, which conditions the membrane for the deposition of the more hydrophilic species, e.g., polysaccharides and proteins [21, 35, 123]. Therefore, the newly available hydrophilic functional groups (irreversibly attached foulants and chemically modified PVDF, see **Figure 34** and **Surface functional groups**) circumvent the 1st step of hydrophobic sorption and result in faster and easier attachment of the hydrophilic foulant species. The decrease in fouling

reversibility among the three membrane types corresponds closely with the increase in the hydrophilicity of membranes (decreasing contact angle, **Figure 36**), thus, confirming our supposition.

The permeability and fouling behavior showcases the important role of irreversibly attached foulants in the progressive aging of the membranes and how it serves essentially as a feedback loop further amplifying its effect over time. Thus, proving that long-term irreversible fouling is detrimental to the long-term performance of the membranes.

As numerously referenced in this section, the progressive aging of the membranes was a result of modifications to the membrane character. In the next section, I analyze and discuss these changes in terms of the surface functionality of the aged membranes.

Effect of aging on the surface functionality of membranes

Surface functional groups

FTIR spectra revealed distinct changes in the surface functional chemistry of the aged membranes compared to the virgin membrane, **Figure 34**. For Type A membranes, the spectra in the functional group (4000-1500 cm^{-1}) and fingerprint (1500-650 cm^{-1}) regions showed the appearance of new peaks characteristic of foulant functional groups. More polar functionalities such as O-H/N-H peaks at 3700-3300 cm^{-1}, representing polysaccharides and proteins [81]. The -C=O stretching peak at 1735 cm^{-1}, typical for carboxylic groups present in humic and fulvic acids [53]. The peak at 1650 cm^{-1}, characteristic of amide-I peaks representing protein fingerprints [24, 29, 53]. Peaks at 1104 cm^{-1}, 1065 cm^{-1}, 1016 cm^{-1}, and 802 cm^{-1} correspond to ν_{as}-C-O-C, ν_{as}-C-O, ν_{s}-C-

O-C- stretch, and ν_s-O-C=O respectively, characteristic of polysaccharides [24, 29, 87, 88]. Although of lower intensity, similar functional group region peaks (O-H/N-H and -C=O) were also observed in the spectra of Type B membranes. However, only one of the fingerprint region peak at 1650 cm^{-1} (amide-I) appeared, hinting at the preferential adsorption of proteins to PVDF membranes [29].

The CH peaks (3027, 2964, 2928, and 2849 cm^{-1}) in the functional group region, characteristic of the CH chains present in both PVDF and long CH chain containing foulants [81], also showed different trends in peak intensities between Type A and Type B membranes.

For Type A membranes, the virgin membrane peak at 3027 cm^{-1} was attenuated in all four phases. However, the other three peaks at 2964, 2928, and 2849 cm^{-1}, were attenuated in the first two phases and then increased in intensity in the later phases. The attenuation is due to the obfuscation of membrane-associated peaks by foulants. The later increase in the intensity of other peaks suggests that the CH chain containing foulants slowly accumulated. This slow accumulation is also evident with the increasing intensity of these peaks going from Phase 1 to Phase 2, even though attenuated in comparison to the virgin membrane. In contrast, for Type B membranes, the CH peaks continued to increase in intensity with each phase, suggesting the progressive and preferential adsorption of relatively hydrophobic species, which are known to adsorb to the PVDF membrane [21, 123]. The differences in the spectra of the two membrane types (foulant peak intensities: Type A > Type B, absence of foulant peaks in Type B, and the difference in the trend of some foulant peak intensities) suggests that although irreversible fouling is

typically associated with adsorption by specific interactions of foulants and membranes, the hydrodynamic permeation drag force during filtration influence deposition [150], and thereby aid the interactions leading to irreversible fouling [218].

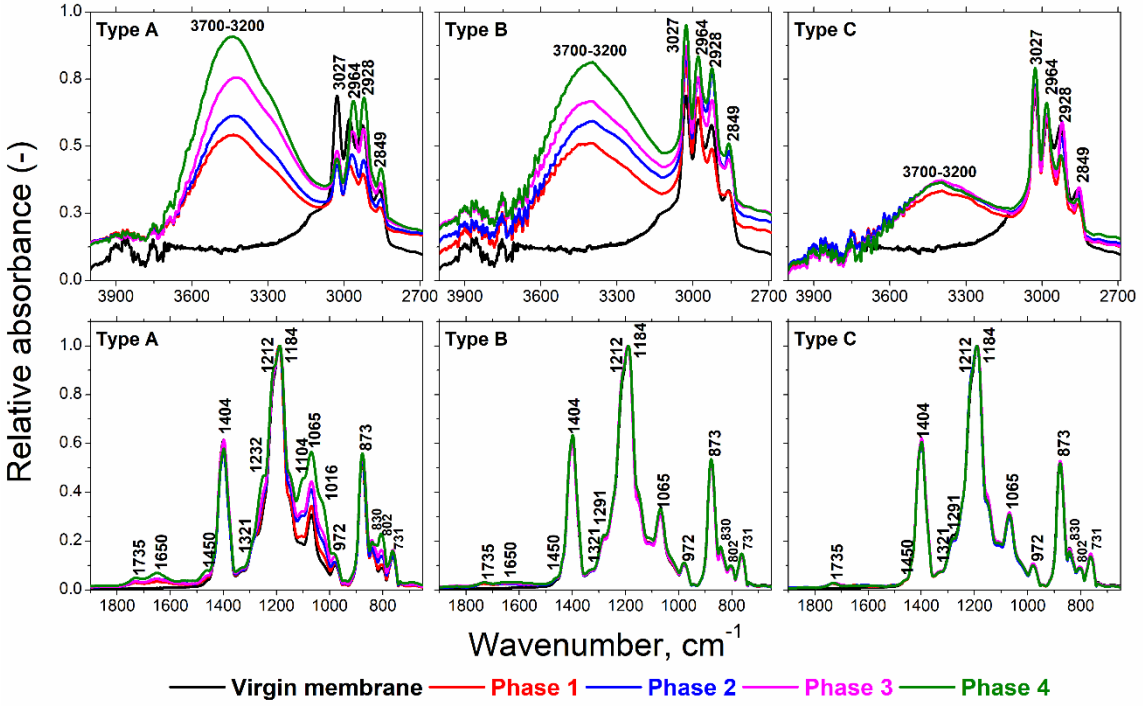

Figure 34 FTIR spectra of the aged membranes. Top panel: 4000-2700 cm^{-1}. Bottom panel: 1900-650 cm^{-1}.

In contrast to Type A and Type B, the spectra of Type C membranes did not reveal any changes in the fingerprint region. Additionally, in the functional group region CH related peaks also did not undergo any changes; however, O-H (3700-3300 cm^{-1}) and -C=O (1735 cm^{-1}) associated peaks appeared. The appearance of these peaks suggests the possible oxidation of PVDF [219]. This is an interesting observation since PVDF membranes with no additives are robust against concentrations of NaClO employed in our experiments and have been shown not to undergo oxidation [201, 216]. However, these studies used caustic sodium hypochlorite solution (pH ~ 11), whereas, in our work, the

CIP was performed using sodium hypochlorite under strongly alkaline conditions (0.25 M NaOH). This is important since similar NaOH concentrations have been shown to degrade PVDF material [215, 220]. Essentially under these conditions, the following two-step mechanism for the oxidation of PVDF exists [219, 221] : (i) double bond formation as a result of dehydrofluorination in strongly alkaline conditions [215, 216, 220, 222], and (ii) oxidation of the double bonds by the hypochlorite leading to oxidized functional groups of O-H and -C=O [219].

Apart from the identity of new and attenuated functional groups on the aged membrane surface, a comparison of the FTIR spectra of the aged membranes from different phases also revealed progressive aging. This was demonstrated by the evident increase in the intensity of the new functional groups in the spectra of Type A and Type B membranes going from Phase 1 to Phase 4. The increase in the intensity of foulant associated functional groups indicates the progressive accumulation of chemically irreversible foulants, which play a role in the gradual loss in performance of the membranes, i.e., aging. However, for Type C membranes, while the increase was evident going from virgin to Phase 1, only marginal to no increase was observed for the later phases. The plateauing behavior implies that after the initial reaction during Phase 1 aging, in subsequent phases only minimal or no reactions occurred; therefore, no further change in the PVDF oxidation products' peak intensity was detected. Thus, demonstrating the chemical robustness of the PVDF material [201].

Membrane Surface charge

The ZP of the virgin and aged membrane surfaces as a function of pH is shown in

Figure 35. The virgin PVDF membranes had a negative ZP across the whole range of pH examined. PVDF does not carry charged functional groups [223], and the negative charge can be attributed to the preferential adsorption of hydroxide ions [224, 225]. The three membrane sample types showed distinct ZP trends. For type A membranes, there was a definite shift towards a less negative ZP going from Phase 1 to Phase 4. This can be attributed to the progressively increasing irreversibly attached foulants [42, 123], as evinced by the FTIR spectra, **Figure 34**.

In contrast, Type C membranes became more negative at higher pH and less negative at lower pH. The change in ZP is due to the newly formed functional groups (O-H and -C=O, **Figure 34**) [223]. At higher pH the newly formed acidic functional groups are deprotonated and thereby render the membranes more negative, while at lower pH (<5), since for typical carboxylic acids the pKa values fall within 4-5 [226], they are protonated, and the ZP gradually shifts to less negative. However, the membranes from different phases did not show any distinctive differences. This indicates that the oxidative material degradation only happened during the initial phases, aligning with the behavior observed in the FTIR spectra (see **Surface functional groups**).

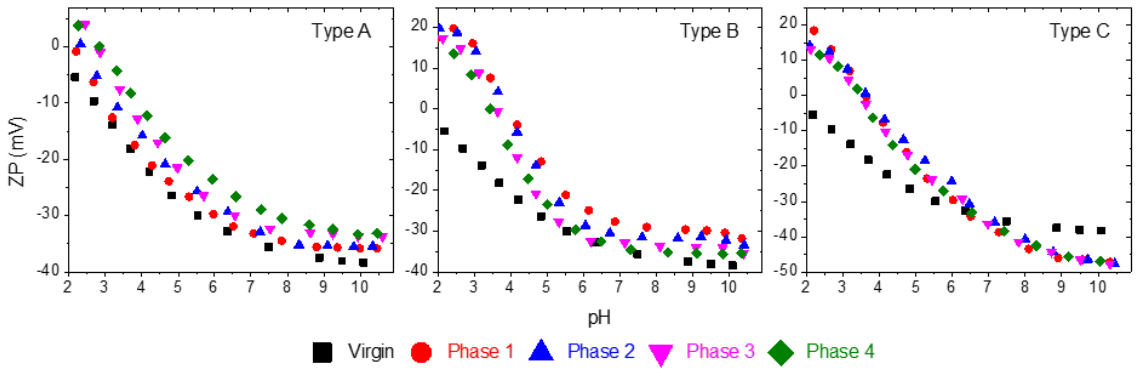

Figure 35 Variation of surface zeta potential of the virgin membrane and aged membrane samples as a function of solution pH with 1 mM KCl as background.

Type B membranes also showed a distinct behavior; while the ZP values were less negative throughout as in the case of type A membranes, there was a more substantial deviation at lower pH values (pH < 5), similar to type C membranes. This suggests that the aging of type B membranes was likely influenced by both irreversibly adsorbed foulants and the PVDF oxidative degradations. Based on this observation, it can be argued that PVDF oxidative degradations may also have happened in Type A membranes, but their presence in the FTIR spectra was likely obfuscated by the foulant associated peaks, and consequently surface character was dominantly influenced by the irreversibly attached foulants.

Contact angle

The appearance of new hydrophilic functional groups on the aged membrane surfaces as evinced by FTIR spectroscopy also resulted in a decrease in contact angle values, **Figure 36**, indicating an increase in the membrane hydrophilicity. The decline was most significant in the case of Type A membranes, followed by Type B and Type C membranes, with Type C showing relatively minimal plateauing changes. The trend of change across the three different types of membranes closely follows the trends in the intensity of new functional groups in the FTIR spectra of the membranes. Additionally, the contact angle also underwent a progressive decline from Phase 1 to Phase 4, thus reaffirming the progressive change in membrane surface characteristics.

The changes in the functionality of the membranes observed here, as they aged, affected the performance of the membranes as was discussed under **Effect of aging on membrane performance**. Importantly, similar to membrane performance, there are

distinct differences between the Type A and Type C protocols in terms of the alterations in surface functionality. Thus, further establishing that typical exposure-based aging experimental designs may result in erroneous inferences regarding the full-scale aging of membranes.

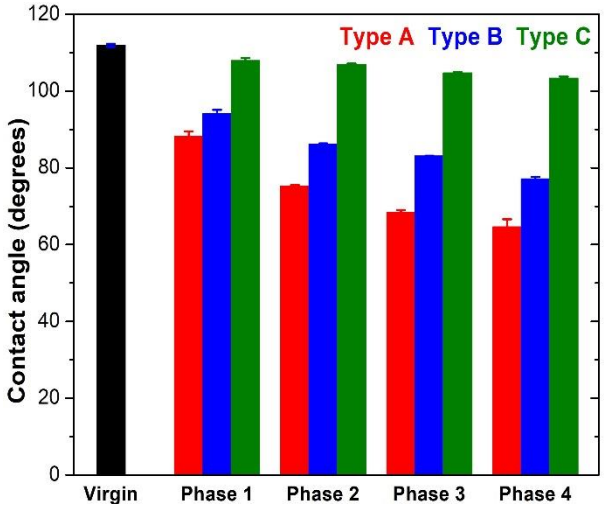

Figure 36 Contact angle of PVDF membranes, virgin and aged (Type A, Type B, and Type C) under different aging conditions.

Apart from the change in membrane surface character, the aging of the membranes can also affect the mechanical properties of the membranes [36, 38]. These alterations can be detrimental since a loss in mechanical properties can lead to membrane breach and therefore, compromise water quality [227, 228]. In the following section, I discuss the possible impacts of progressive aging on the mechanical properties of membranes.

Effect of aging on the mechanical properties of membranes

Membrane integrity

None of the membranes from any of the module types showed any change in integrity, **Figure 37**. Therefore, chemical agent exposure and fouling in the duration of

our experiments lead to no apparent change in the bulk mechanical properties of the membrane. However, a more detailed assessment of the mechanical properties of the membranes was obtained by DMA and has been discussed in the next section.

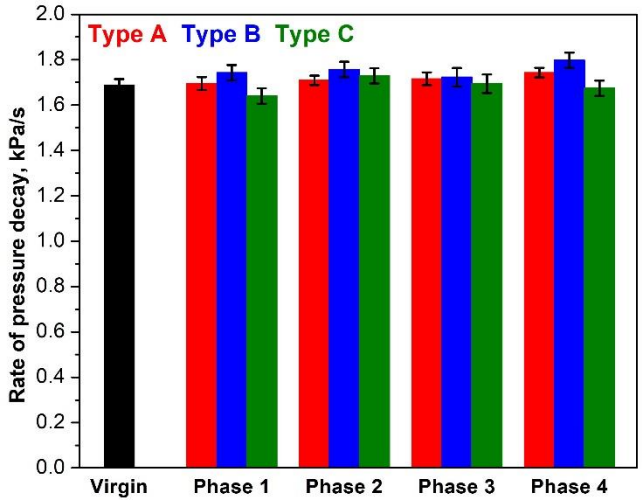

Figure 37 Rate of pressure decay during a pressure decay test for the integrity of the membranes from the three modules (Type A, Type B, and Type C). The black line represents the rate of pressure decay for the virgin membrane.

Dynamic mechanical analysis

The DMA test carried out were used to obtain stress-strain curves for each sample, where the slope of the line at low strains represents Young's modulus. The point where the slope changes marks the transition from linear viscoelastic response to a non-linear response. Apart from the stress-strain curves the oscillatory nature of the test allows us to probe both the elastic and viscous components of the polymer and obtain the complex modulus E* = E' + iE", where E' is the storage modulus (elastic component) and E" is the loss modulus (viscous component). Storage modulus is the measure of the elastic character (tensile strength) of the material and loss modulus is the measure of viscous character (dampening ability) of the material [229]. The ratio of E" to E' is termed as loss tangent

or tan δ, which ranges from zero for an ideal elastic solid to infinity for an ideal liquid. In our membrane samples, the tan δ values were close to zero (data not shown) suggesting the dominance of the solid-like character or the elastic character. Accordingly, no change in the loss modulus was observed in any of the membrane samples across different aging protocols [212]. Therefore, only Young's modulus from the stress vs. strain curves and the dynamic storage modulus of the virgin and aged membranes are reported and discussed, **Figure 38** and **Figure 39**.

As can be seen, both Young's modulus and storage modulus, for Type C membranes, did not undergo any significant changes under the conditions employed in this study (for example, Young's modulus for virgin membrane = 0.659 MPa, and Type C membranes = 0.630 to 0.664 MPa, in no definite order). This implies that although surface characterization revealed some oxidative degradation of the PVDF membrane, these changes were either only surface level or not consequential to the bulk properties of the membranes [230]. In contrast, there was an apparent decline in Young's modulus of both Type A and Type B membranes (decreased from 0.659 MPa for the virgin membrane to 0.522 and 0.544 MPa for Phase 4 Type A and Type B membranes, respectively). Similarly, a gradual decline in dynamic storage modulus with each phase was observed for both Type A and Type B membranes, **Figure 39Error! Reference source not found.**. Thus, the irreversibly attached foulants seem to play a more critical role than the degradation brought about by chemical cleaning agents. Besides, correlating the observations here with the results from membrane integrity tests, it can be concluded that the pressure decay test, although practical, is not a measure of the gradual changes that

membranes continue to undergo, losing mechanical strength due to long term fouling. Thus, there is certainly a need for an in-situ measure to predict a possible membrane breach [41].

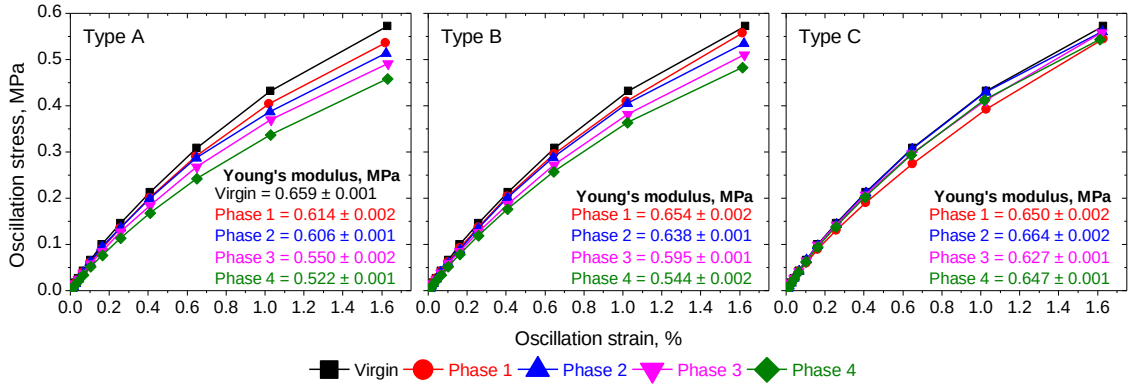

Figure 38 Stress vs. Strain curves for the different membrane samples (virgin and aged). Young's modulus (MPa) estimated from the slope of the linear portion of each curve is shown in the bottom panel.

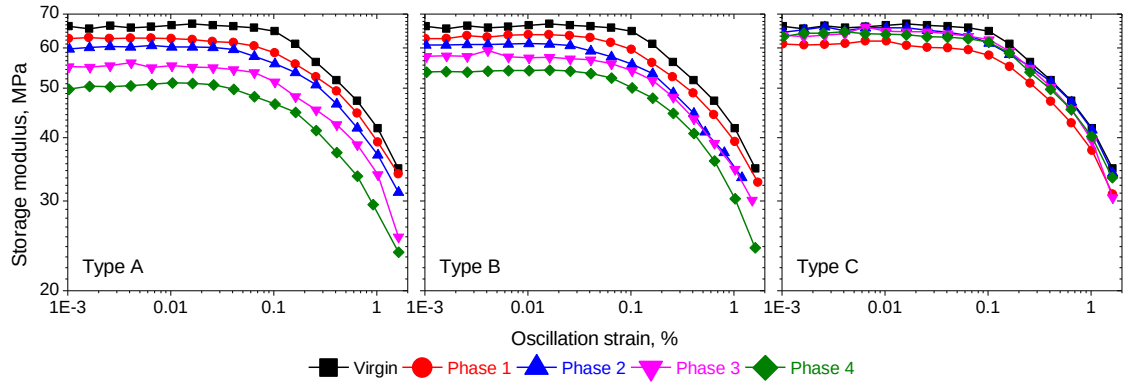

Figure 39 Dynamic storage modulus of virgin and aged membrane fibers as a function of applied oscillatory strain.

Since the focus of this work is to highlight the role of irreversible foulants in the long-term aging of membranes, the critical role of irreversible foulants is an important observation that typical chemical exposure aging studies will fail to provide [207]. Importantly, our observations are in-line with an autopsy study [40], which showed that the membrane samples with maximum loss in tensile strength were from a facility that did

not employ enhanced flux maintenance (a type of chemically enhanced backwash) and performed less frequent cleanings. Similarly, another autopsy study showed that loss in membrane permeability and loss in mechanical properties became apparent around the same age of the membranes (>5 years in operation) [41].

There have been only limited reports regarding the effect of irreversibly attached foulants on the mechanical properties of membranes [231]. For example, Powell et al. showed that fouled RO membranes had a lower young's modulus than virgin membranes [232]. In another report, Hajibabnia et al. showed that fouled and cleaned PVDF UF membranes had higher tensile strength than membranes exposed to cleaning agents without fouling [207]. In contrast, Zondervan et al. [210] observed that the rupture point of fouled polyethersulfone UF membranes was almost half of the value for virgin membranes, while it remained unchanged for membranes exposed to sodium hypochlorite. Importantly, none of these previous works commented on the possible mechanisms leading to the observed changes. Although Hajibabania et al. suggested that the fouling layer provided mechanical stability to the membranes, they did not provide any mechanistic reasoning to support their suggestion.

Now, the mechanical properties of semi-crystalline polymers like PVDF [128], depending on the magnitude of secondary intermolecular bonds that inhibit relative chain motion [233]. Thus, I propose that the irreversibly attached foulants disturb these weak intermolecular forces within the membrane material and thereby result in reduced mechanical strength. This proposed mechanism can explain the progressive decline in mechanical strength (Young's modulus and storage modulus) going from phase 1 to phase

4 in the case of both Type A and Type B membranes; more decline was observed with increased irreversibly attached foulants (see **section Surface functional groups**). Additionally, the relatively lower accumulation of foulants in the case of Type B membranes compared to Type A membranes led to a lesser decline in the case of former membranes. This observation further accentuates the validity of the proposed mechanism. While further elucidation of the proposed mechanism was beyond the scope of this work, it would be a fruitful area for further work.

Our observations directly contradict the results presented by Hajibabania et al. [207], even though both studies employ PVDF membranes. However, Hajibabania et al. used blended PVDF membranes, whereas the PVDF membranes in our work are not blended. This is a crucial distinction, as shown previously by Ravereau et al. in their long-term exposure study [201]. While non-blended PVDF membranes maintained their initial values for mechanical strength, blended PVDF membranes showed significant changes. Gao et al. [211] argued that the removal of additives from blended PVDF membranes results in the PVDF macromolecular chains cross-linking to generate new chemical bonds and thereby, improved mechanical strength. For example, blended PVDF membranes with PMMA as additive showed lower maximum stress compared to pure PVDF membranes [217]. This argument ties well with our proposed mechanism for loss in mechanical properties due to irreversible fouling. Essentially, the hydrophilic additives disrupt the secondary intermolecular bonds, like the irreversible foulants in our study, and their removal by chemical cleaning results in improved mechanical strength.

Conclusions

A comparison of three different membrane aging protocols (cyclical fouling and cleaning, cyclical adsorptive fouling and cleaning, and cyclical exposure to cleaning agents) were carried out using typically employed CIP conditions.

The cyclical exposure to cleaning agents resulted in minimal material changes (alterations in the membrane surface functionality) via oxidative degradation of PVDF material and did not affect the membrane performance and mechanical strength. In contrast, cyclical fouling and cleaning protocol resulted in a progressive decline in the membrane performance as well as the material properties (surface and bulk). Thus, the progressive accumulation of chemically irreversible foulants through cyclical fouling was responsible for the aging of the membranes. The presence and identity of these foulants were confirmed by FTIR spectroscopy (proteins, polysaccharides, and humic-like material). The critical role these foulants play in the aging of the membranes was further established by a comparison of samples from the cyclical fouling & cleaning and cyclical adsorptive fouling & cleaning protocols. The former having a more substantial presence of irreversible foulants, underwent a relatively more quantitative decline in mechanical strength and worsened membrane performance.

The study demonstrated the chemical stability of the PVDF membranes, and conclusively established the role of chemically irreversible foulants as the most significant contributor to the operational aging of membranes. Utilities observing a sustained decline in clean membrane permeability should actively employ enhanced cleaning protocols taking advantage of the chemical robustness of these membranes to prevent possible

membrane breaches due to loss in mechanical strength from the continued accumulation of foulants.

CHAPTER VI

PEERING THE MECHANISM OF IRREVERSIBLE FOULING THROUGH THE SCOPE OF BACKWASH WATER COMPOSITION

Introduction

Irreversible fouling of low-pressure membranes, ultrafiltration (UF) and microfiltration (MF), is detrimental to the long-term performance of these membranes. Justifiably, understanding the mechanisms involved in irreversible fouling is key to developing strategies for the control and mitigation of fouling and the consequent productivity. Irreversible fouling in MF and UF is predominantly associated with the irreversible attachment of organic matter with the polymeric membranes [123, 234]. Two mechanisms have been invoked to explain the attachment or membrane-foulant interactions: (i) direct attachment of specifically interacting organic matter to the membrane, and (ii) bridging by polyvalent cations between the organic matter functional groups and the membrane. For example, hydrophobic organic species attaching to the membrane surface and pores have been reported as initiators for irreversible fouling during surface water and wastewater effluent filtration [21, 35, 123]. Similarly, bridging between the negatively charged membrane and the organic species by divalent (e.g. Ca^{2+}) and trivalent (e.g. Al^{3+}) cations has been reported as possibly responsible for irreversible fouling [21, 235]. Critically, the relative contributions of the two mechanisms remains an unanswered question. This lacking in our understanding impedes the development of targeted strategies for fouling reversibility.

Now, backwashing, the reversal of flow direction for the removal of foulants, is an established industry practice for fouling reversal [18]. Typically, MF or UF permeate is used for backwashing; however, recently chemically enhanced backwashing (CEB) has also gained traction [19]. CEB as the name implies is backwashing enhanced by the addition of chemicals (e.g. NaClO, NaOH). The idea is that the added chemicals can alter the organic matter character and thus, more efficiently disrupt membrane-foulant interactions and thereby better fouling reversibility. Some reports have also argued the use of deionized (DI) water to control UF/MF fouling [236, 237]. The argument being that the DI water during backwashing will change the localized ionic environment of the fouling layer and thus disrupt foulant-ion-membrane bridges responsible for irreversible fouling. These arguments for CEB and DI water backwashing efficacy again invoke the question of the relative contributions of the two mechanisms for irreversible attachment of foulants. Essentially, the efficacy of any added chemical or the absence of it is dependent on the mechanisms of membrane-foulant interactions.

Interestingly, while CEB has slowly seen widespread usage in the water treatment industry [59, 238, 239], most of the previous research has been limited to the investigation of the applicability and efficacy of CEB, and mechanism evaluation has received very little to no attention [19]. For example, there is no report on how the most common CEB chemical, NaClO, brings about fouling mitigation. Some studies have reported possible reactions of organic foulants upon reaction with hypochlorite [240]. However, paradoxically a recent study analyzing NaClO cleaning observed better performance at high pH of 11 compared to the low pH of 5 (stronger oxidation capacity) [241]. In another

investigation comparing different cleaning agents against a variety of organic foulant layers, NaClO and NaOH performed equitably against a single organic foulant layer, and the latter performed better against mixed organics foulant layer [15].

In contrast to CEB, the mechanism during DI water backwashing has been explored; however, with inconsistent results [9]. For example, Li et al. observed that ultrapure water backwashing was more efficient compared to backwashing with water containing either monovalent (Na^+) or divalent cations (Ca^{2+}) [11, 12]. They concluded that the reduction in charge screening effect during ultrapure water backwashing resulted in increased repulsion forces between NOM and membrane and thereby better performance. In contrast, Chang et al. observed that backwashing efficiency by ultrapure water reduced with the addition of Ca^{2+} ions, whereas the addition of Na^+ ions or other monovalent ions (e.g. K^+, NH^{4+}) resulted in increased backwash efficiency [13, 14]. They argued that ion-exchange during monovalent salt backwashing destroyed organic matter-membrane complexes and thus, resulted in improved efficiency. Interestingly, NaCl backwashing was reported as equally effective to NaOH and NaClO backwashing of UF membranes fouled by model foulants (individual and mixtures) [15]; however, the authors did not comment about the possible mechanisms.

The inconsistencies across past research further highlight our point that there is a need to develop a better understanding of the mechanisms contributing to irreversible fouling. The primary objective of this study was to elucidate the mechanism of irreversible fouling of microfiltration membranes. To this effect, MF fouling experiments with filtration and backwashing were performed using wastewater effluent and model foulants

mixture. Importantly, it can be argued that the relative efficacy of different added chemicals or the different backwash water compositions can also give insights into the mechanisms responsible for the irreversible attachment of foulants to the membrane surface and pores. This forms the basis of the experimental design employed in the presented work. To this end, in this study, a range of cleaning agents (salts, alkalis, acids, and oxidizers) along with ultrapure water were employed for backwashing of fouled MF membranes.

Materials and Methods

Source water

Wastewater effluent

An effluent sample was collected from the 4 million gallons per day (MGD) conventional activated sludge Texas A&M municipal wastewater treatment plant in College Station, Texas on September 21, 2020, after UV disinfection and just prior to discharge. This sample had a pH of 8.3 ± 0.12, turbidity of 3.2 ± 0.5 NTU, EfOM concentration of 8.493 ± 0.342 mg/L measured as dissolved organic carbon (DOC), UVA_{254} of 0.308 ± 0.006 cm^{-1}, chemical oxygen demand (COD) of 22.1 ± 2.7 mg/L, hardness of 60 ± 5 mg/L as $CaCO_3$ and alkalinity of 180 ± 13 mg/L as $CaCO_3$. The ammonia concentration was very low (close to the detection limit of 0.01 mg/L NH_3-N) and the total N was 23.6 ± 1.9 mg N/L. Samples were filtered with 0.45 µm polyethersulfone disc filters (PES, Pall Corp.) within 24 h of collection, stored in the dark at 4 °C, and brought to room temperature immediately before use.

Model foulant solution

A synthetic feed water solution was prepared using model foulants (5 mg/L bovine serum albumin (BSA), 5 mg/L sodium alginate (SA), and 5 mg/L humic acid (HA) + 8 mM NaCl + 1.5 mM $CaCl_2$ + 1 mM $NaHCO_3$), the model foulants represented the major classes of organics found in surface water and wastewater effluent, namely proteins, polysaccharides, and humic substances [34, 157]. The synthesized feed water solution had a dissolved organic carbon (DOC) concentration of 3.804 ± 0.247 mg/L, UVA_{254} of 0.045 ± 0.002 cm^{-1}, chemical oxygen demand (COD) of 11.1 ± 1.4 mg/L, the conductivity of 500 ± 12 µS/cm, and the pH was adjusted to 8.2 ± 0.1 using 1 M HCl.

BSA, SA, and HA were received in powder form, and stock solutions (1 g/L) of each model foulant were prepared by dissolving each of the foulants in ultrapure water. BSA and SA were used as is without any purification. HA was purified according to methods published earlier [107, 242]: HA was dissolved in deionized water and precipitated at pH 1.0 by the addition of concentrated HCl and was finally separated by centrifugation at 4000 g for 20 min. The precipitate was then rinsed twice with 1 M HCl. Next, the precipitate was dissolved in ultrapure water and the sequence of operations of sedimentation, centrifugation, and rinsing was performed twice. Finally, the pellet containing purified HA was rinsed with ultrapure water and was oven-dried at 40 ± 1 °C for 72 hours. The dried pellet was pulverized using a glass mortar and pestle. Prior to each fouling experiment, 1 L fresh feed water solution was prepared by adding appropriate amounts of each stock solution and salt crystals to ultrapure water.

Backwash water

Five different types of chemical agents were tested as backwash water. The agents included, monovalent salt solution (10 and 20 mM NaCl), divalent salt solution (1.5 and 4.5 mM $CalCl_2$), acid (0.01 N HCl, pH 2 ± 0.1), alkali (0.01 N NaOH, pH 12 ± 0.1), and oxidizer (500 ± 10 mg/L NaClO as free chlorine, pH 10 ± 0.1). Additionally, ultrapure water (18 MΩ-cm, pH 5.6 ± 0.1) backwashing served as a reference. Fresh backwash water solutions were prepared using ultrapure water for each experiment.

Membrane filtration setup and experimental procedure

A bench-scale filtration setup equipped with a programmable peristaltic pump (Watson Marlow, USA) and compound pressure transducer (Ashcroft, USA) was used for all the filtration and backwashing experiments. Automatic control and data acquisition were performed using a program written in LabVIEW 2019 (National Instruments). The setup employed a membrane module comprised of a single polyvinylidene fluoride (PVDF) hollow fiber MF membrane having a nominal pore size of 0.1 µm, 1.29 mm OD, and 0.71 mm ID (Pall Corp., USA). A 12 cm length of virgin membrane fiber was potted in nylon tube fittings with epoxy ensuring that the fiber opening was not blocked. The bottom end of the fiber was sealed with epoxy resin. The total effective length after potting was 10 cm, giving an active filtration area of 4.08 cm^2.

During filtration, the membrane module was submerged in the feed water and outside-in filtration was carried out in suction mode at a constant flux (100 L/m^2h and 50 L/m^2h for wastewater effluent and model foulants solution, respectively) for 3 hours. A

lower filtration flux (50 L/m^2h) was used for model foulants solution since excessive fouling was observed at the higher flux of 100 L/m^2h. A longer filtration duration of 3 hours was chosen to ensure a significant deposition of foulants on the membrane surface. Following which the module was taken out from the membrane vessel and backwashing was performed at 100 L/m^2h for 30 minutes by reversing the direction of the peristaltic pump. The backwash effluent was continuously collected in 50 ml centrifuge tubes for characterization. Two such cycles of filtration and backwashing were performed during each experiment. A new membrane module was utilized for each experiment. Prior to use, the membranes were wetted by immersing in 50% ethanol for 30 minutes, followed by immersion and rinse with ultrapure water to remove residual ethanol.

Quality assurance comprised of repeating ≈ 50% of the experiments as shown in **SI Figure A-12**. Mann-Whitney U tests revealed no statistical differences between the instantaneous pressure values obtained from these duplicate experiments at 95% confidence. Hence, the results obtained over the entirety of experimentation could be quantitatively compared, validating our findings.

Backwash performance evaluation

The backwash performance of different backwashing water was evaluated in terms of percentage transmembrane pressure (TMP) recovery after the 1^{st} backwash. The recovery which indicated the extent of fouling reversibility was calculated using **Equation 15**:

$$\% \text{ TMP recovery} = TMP_1/TMP_2 \times 100 \qquad (15)$$

where, TMP_1 = TMP at the beginning of the first filtration cycle, and TMP_2 = TMP at the beginning of the second filtration cycle after backwashing.

Analytical measurements

Dissolved organic carbon (DOC) was measured by a Total Organic Carbon analyzer (TOC-L, Shimadzu Corp.). COD was determined using the reactor digestion method [130] (HACH method 8000). The infrared spectra of the vacuum-dried membrane samples were collected using the Nicolet iS10 spectrometer equipped with mid-infrared Ever-Glo source, DTGS detector, KBr beam splitter, and Omnic 9.0 Software. A diamond iTX accessory was also installed to allow sampling in ATR mode. IR spectrum was obtained by averaging 128 scans collected at 4 cm^{-1} resolution over 650–4000 cm^{-1}.

Results and Discussion

Effect of backwash water composition (salts, acid, base, and oxidizer)

Ultrapure water and salt solutions

Figure 40a shows the TMP profiles during filtration of wastewater effluent and backwashing using ultrapure water and salt solutions. Comparison of fouling reversal after backwashing in terms of % TMP recovery after 1st backwash, **Figure 40b**, shows that backwashing with ultrapure water performed better than salt solutions. However, the difference quantitatively was only 5-10% across all the salt concentrations and types employed. Interestingly, negligible quantitative differences in percentage recovery were observed between lower concentration salt solutions and their higher concentration

counterparts. Additionally, the recoveries with monovalent salt (Na^+) and divalent salt (Ca^{2+}) were also similar with Ca^{2+} performing slightly worse, but statistically insignificant (< 5% difference in the extent of recovery). The trends in recoveries with ultrapure water and salt solutions observed here are similar to results previously reported with surface water ultrafiltration [235, 243].

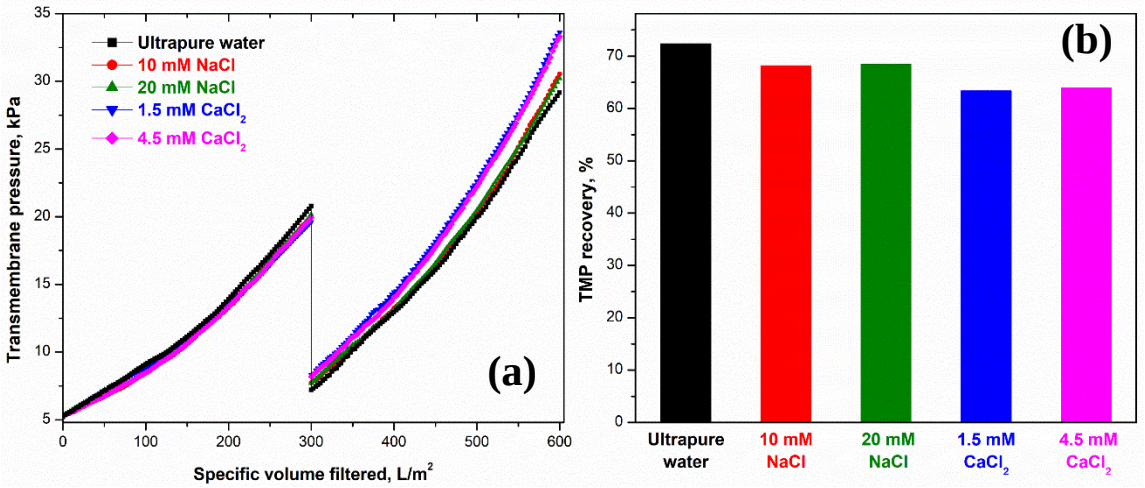

Figure 40 (a) TMP profiles during wastewater effluent filtration with ultrapure water and salt solution backwashing, and (b) % TMP recoveries achieved after 1st backwash.

The nominally better performance of ultrapure water compared to the salt solutions is typically associated with the dilution of the foulant layer ionic environment resulting in breakage of cation influenced membrane-foulant bridging [236]. However, the minimal adverse effect of the presence of salts (Na^+ or Ca^{2+}) in the backwash water evident from the observed similar performance across ultrapure water and salt solution backwashing suggests a minimal role of the bridging phenomena. No significant difference in performance between low and high salt concentrations further accentuates the argument of a minimal role of multivalent cation bridging in influencing foulant-membrane

interactions responsible for irreversible fouling. Thus, it can be argued that the backwash recoveries observed are primarily a result of hydraulic shear force leading to the physical removal of loosely attached foulants [244].

As the results indicate towards the minimal role of multivalent cation bridging of EfOM and membrane, direct membrane-foulant interactions likely play a more dominant role in irreversible fouling during wastewater effluent filtration. These interactions are influenced by the charge on the organic matter [107] which is a function of pH [245]. Therefore, the pH of the backwash water should affect the membrane-foulant interactions. Thus, in the following section, I analyze the efficacy of backwashing under acidic (HCl) and alkaline (NaOH) conditions.

Effect of backwash water pH

Backwashing with 0.01 N NaOH resulted in significant improvement in TMP recovery compared to ultrapure water (~90% as opposed to ~70%), **Figure 41** and **Figure 40b**. Thus, the hydrolysis and solubilization of organic matter by NaOH and electrostatic repulsions between the deprotonated organic matter in the fouling layer and membranes under alkaline pH conditions resulted in the breaking of the EfOM-membrane interactions [246]. The better performance in conjunction with the proposed mechanism suggests the dominant role of non-electrostatic direct membrane-foulant interactions in irreversible fouling. In contrast, HCl i.e. acidic pH led to a significant reduction in TMP recovery compared to recovery after ultrapure water backwashing (~40% as opposed to ~70%). Acidic conditions can decrease the net charge of the organic matter through protonation

[247]. The reduced recovery under these conditions implies that the possible protonation that may have occurred was ineffective in breaking the existing EfOM-foulant interactions and possibly resulted in the formation of newer non-electrostatic interactions between the neutralized organics and the membrane.

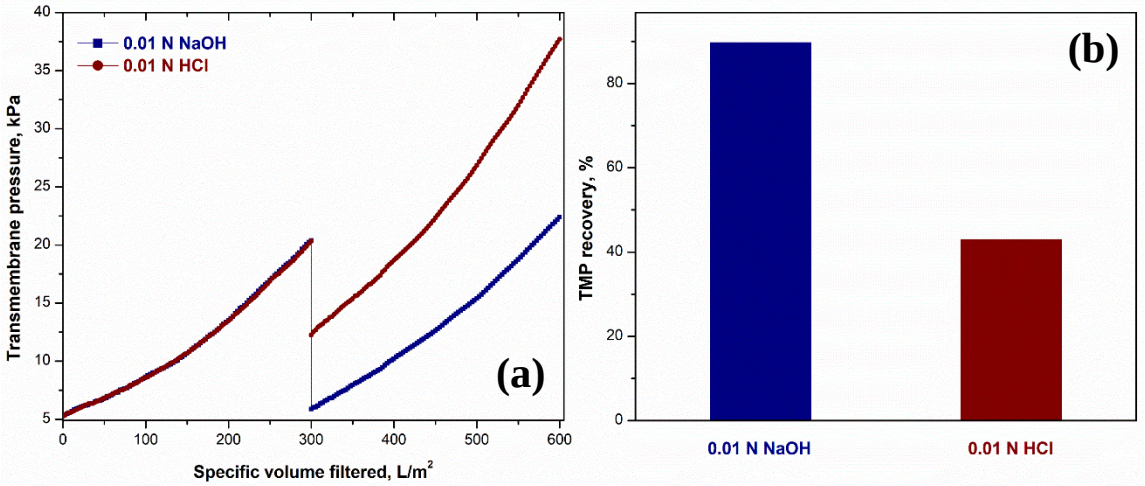

Figure 41 (a) TMP profiles during wastewater effluent filtration with NaOH and HCl backwashing, and (b) % TMP recoveries achieved after 1st backwash.

The recovery trends after backwashing with an acid and an alkali further accentuate the argument of the dominance of non-electrostatic direct EfOM-membrane interactions in irreversible fouling, for example, hydrophobic interactions [115, 234]. Therefore, it can be argued that the nature (functionality) of the organic matter dominates the EfOM-membrane interactions responsible for irreversible fouling. Therefore, to improve recovery during backwashing, the functionality of the organic species needs to be altered to break the non-electrostatic membrane-foulant interactions seemingly responsible for the irreversible fouling. An oxidizer like NaClO oxidizes organic species

to their more hydrophilic form [234]. In the next section, I look at the efficacy of NaClO in backwashing.

Effect of NaClO in backwashing

Backwashing with NaClO resulted in ~100% recovery, the highest recovery amongst all the tested backwash water compositions including ultrapure water, **Figure 42**. The result confirms our supposition that the dominant EfOM-membrane interactions are non-electrostatic and primarily dominated by the nature of the organic species and thus, by specifically interacting organic moieties [123]. Oxidation of the organic matter, i.e., hydrophilization of the organic matter, resulted in disrupting the EfOM-membrane interactions and thereby highest recovery. These results confirm our supposition regarding the nature of interactions primarily responsible for irreversible fouling. This confirmation is significant especially in the backdrop of two previously published reports which essentially put into contention the oxidative role of NaClO in fouling mitigation and gives credence to the prevalent use of the NaClO for chemically enhanced backwashing (CEB).

Now, although NaClO is widely used in industrial practice, interestingly, the results presented here are in contradiction to some previous reports. Wang et al. [241] in their membrane cleaning study, concluded that the alkaline effect of NaClO was more dominant rather than the oxidative reaction of active chlorine. Similarly, Kim et al. [247] showed that using NaOH was more effective compared to NaClO for backwashing and cleaning of ultrafiltration membranes fouled by specific biofilm components. However, as shown, NaClO (pH = 10) performed better than NaOH (pH = 12), ~100% as opposed

to ~90%. I believe that that the use of model foulants in these previous reports is likely the reason for the discrepancy from our results. This is important, as I show later (see **Model foulant mixture filtration and salt backwashing**) the dominant fouling mechanism during model foulant filtration is different from that during wastewater effluent filtration.

In the next section, I validated our process data regarding the backwash efficacy of different backwash water using analytical measurements.

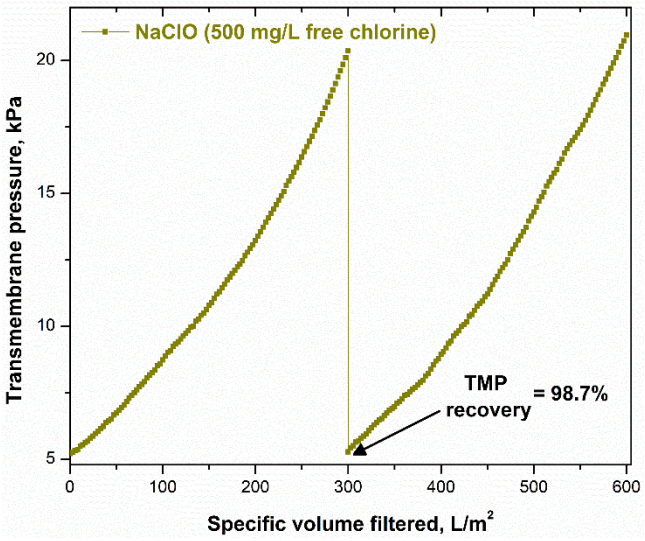

Figure 42 TMP profile during wastewater effluent filtration with NaClO backwashing and % TMP recovery achieved after 1st backwash.

Backwashing effluent DOC and membrane FTIR reflect backwash recovery trends

The DOC in backwashing effluent depended on the type of backwash water employed and closely followed the trends of the backwashing recovery, **Figure 43a**. For example, the highest DOC was obtained with NaClO backwashing which showed TMP highest recovery among all backwash waters. Similarly, the lowest DOC was obtained with HCl backwashing which showed the lowest TMP recovery. The trends in the removal of foulants evinced from the TMP recovery data and backwashing effluent DOC values

were further validated through the FTIR spectra of the fouled membranes. The order of the intensity of foulant peaks (O-H/N-H peaks at 3700-3300 cm^{-1} [81]) on the membrane surface was NaClO < NaOH < Ultrapure water < NaCl < $CaCl_2$ < HCl, **Figure 43b**. This peak intensity order follows that of DOC removal and TMP recovery with the different backwashing solutions.

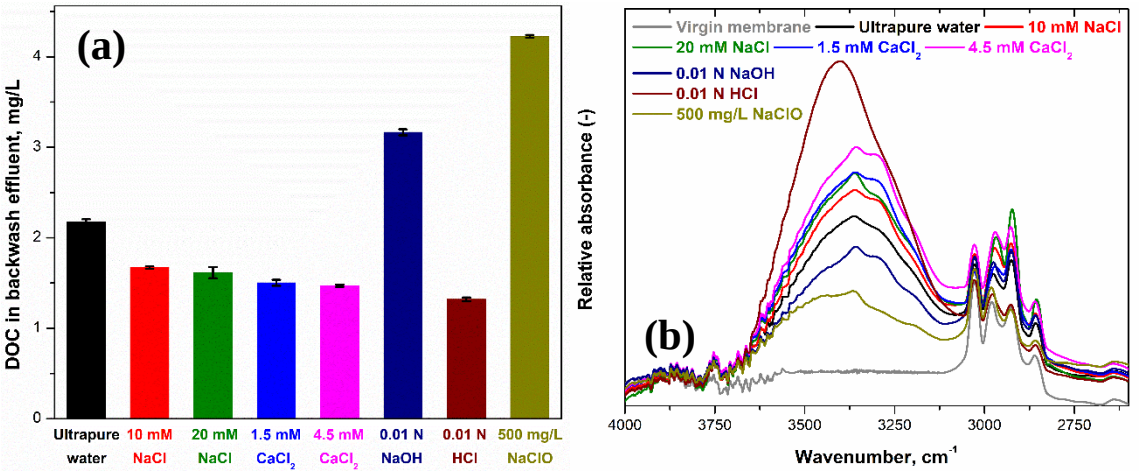

Figure 43 (a) mg/L DOC in backwashing effluent, and (b) FTIR spectra of the virgin and fouled membrane surface.

The analytical measurements validated the process data and therefore, the derived arguments. Thus, validating the supposition that non-electrostatic membrane foulant interactions are dominantly responsible for irreversible fouling.

Although our results and proposed fouling mechanism explain previously reported observations for natural water and wastewater effluents [235, 243], they are inconsistent with previous reports employing model foulants [57, 248]. To understand these discrepancies, I also looked at the effect of salt backwashing on the TMP recovery during filtration of a model foulant mixture.

Model foulant mixture filtration and salt backwashing

Salt backwashing of membranes fouled by model foulant mixture revealed a different behavior from wastewater effluent in terms of recovery. NaCl backwashing led to close to 90% recovery, followed by ultrapure water with 70% recovery, and 40% recovery with $CaCl_2$, **Figure 44**. The order of recovery is distinctly different from that obtained during wastewater effluent filtration (NaCl > ultrapure water > $CalCl_2$ as opposed to Ultrapure water > NaCl ≈ $CalCl_2$). However, similar to wastewater effluent filtration, no difference was observed between salt solutions of higher and lower concentrations, **Figure 44**.

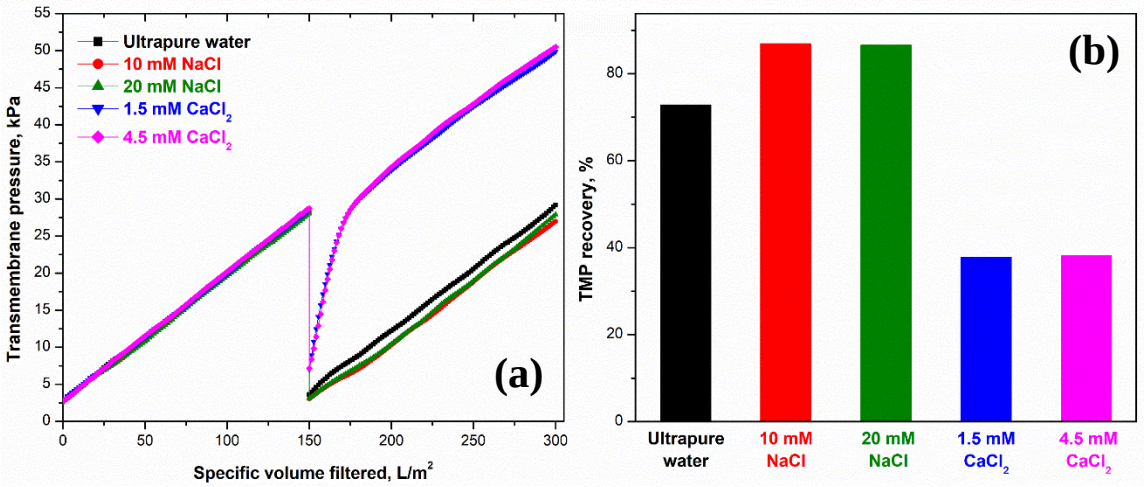

Figure 44 (a) TMP profile during model feed water filtration with ultrapure water and salt solution backwashing, and (b) % TMP recoveries achieved after 1st backwash.

The results obtained here are in line with previous reports [57, 248]. This distinct difference between the two feed water under the same backwashing conditions implies the existence of different mechanisms of fouling. In the case of model foulant filtration, previous reports have argued that Na^+ ions in backwashing water break down the

multivalent cation influenced bridging between membrane and foulants by ion-exchange for TMP recovery. In contrast, ultrapure water only results in the change of the ionic strength of the fouling layer and only partially affects the membrane-foulant multivalent cation bridging. Whereas, Ca^{2+} doesn't alter these interactions and therefore, minimal recovery. Thus, as a corollary, it implies that the primary mechanism of fouling during model foulant filtration is the multivalent cation facilitated membrane-foulant bridging as opposed to the dominance of non-electrostatic membrane foulant interactions during wastewater effluent filtration as argued previously. This is a critical inference and puts into contention the use of model organic materials as surrogates for EfOM, e.g., for understanding the fouling mechanisms or drawing inferences regarding membrane cleaning. For example, alginate was shown to be a poor representative for EfOM [151].

Conclusions

Analysis of the efficacy of different backwash water compositions (salts, acid, alkali, and oxidizer) revealed insights about dominant fouling mechanisms during wastewater effluent microfiltration. Similar efficiencies of ultrapure water and salt (NaCl and $CaCl_2$) backwashing showed that the EfOM-membrane bridging by multivalent cations had a minimal role in the irreversible fouling of microfilters. In contrast, the excellent efficiency of NaOH (90% TMP recovery) and NaClO (≈100% TMP recovery) highlighted the need for degradation of organic matter to achieve fouling reversal. Thus, establishing that irreversible fouling during wastewater effluent microfiltration was dominantly influenced by specific EfOM-membrane interactions, disrupted only by a

change in EfOM character brought about by NaOH (solubilization and hydrolysis) and NaClO (hydrophilization by oxidation).

Additionally, the distinct difference between the salt backwash efficiency trends during wastewater effluent and model foulant mixture (SA + BSA + HA) filtration implied the different fouling mechanisms for the two feed water. While salt backwashing and ultrapure water had similar efficiency during wastewater effluent filtration, during model foulant filtration there were clear differences between the three backwashing compositions. NaCl backwashing performed the best with nearly 90% TMP recovery, followed by ultrapure water and $CaCl_2$ backwashing with 70% and 40% TMP recovery, respectively. The significantly distinct efficacies indicate that EfOM-membrane cation bridging plays a critical role during model foulant filtration, unlike wastewater effluent filtration. Therefore, the use of model foulants as representatives for wastewater effluent, especially in studies investigating backwashing and cleaning efficiencies need to be carefully considered.

CHAPTER VII

CONCLUSIONS AND RECOMMENDATIONS FOR FUTURE WORK

Conclusions

The irreversible fouling of PVDF (and similarly hydrophobic) microfilters during wastewater effluent filtration progresses in two steps. Initially, relatively hydrophobic EfOM species attach to the membrane surface and pores. These relatively hydrophobic organic moieties 'condition' the membrane for the attachment of relatively hydrophilic moieties, namely proteins and polysaccharides in the second step. EfOM characterization using high-resolution mass spectrometry revealed the possible identity of the initially attaching relatively hydrophobic species as belonging to the lipid chemical class, which includes fatty acids, aliphatic hydrocarbons, terpenes, and sterols. The percentage contribution of the lipid chemical class in different feed water samples was strongly correlated to their respective irreversible fouling resistance and expectedly as was the protein chemical class. Identification of the previously unreported role of lipids chemical class in fouling provides avenues for the development of targeted pretreatment strategies for fouling control. However, it is cautioned that the prominent role of lipids was inferred from only four distinct samples (two drinking water supplies and two wastewater effluents). Additional samples and independent measurement of lipids by gas chromatography [156, 193] would lend further credibility to our findings.

Probing fouling mechanisms using adsorption pretreatment revealed the relatively different contributions of surface and pore foulants to productivity loss. The apparent

attachment of foulants to pore surfaces was less reversible and consequently more detrimental to the long-term loss in membrane permeability. Besides, foulants attached to the outer membrane surface can act as a dynamic secondary membrane reducing exposure of pores to the foulants, thereby reducing irreversible fouling. Thus, EfOM size distribution can be a potential indicator of the feed water fouling propensity.

Additionally, the fouling extent and total EfOM loading after adsorption pretreatment were not correlated indicating that a specifically interacting fraction of EfOM largely determined fouling. Importantly, this fraction constituted only approximately 5% of the total EfOM. The critical role of specific EfOM-membrane interactions was further validated operationally by evaluating the efficacy of different backwash water compositions (ultrapure water, salts, acid, alkali, and oxidizer). Similar efficacy with ultrapure water and salt (Na^+ and Ca^{2+}) backwashing (≈70 % transmembrane pressure recovery) revealed the minimal role of divalent cation influenced EfOM-membrane bridging. In contrast, excellent backwashing efficiencies of NaOH and NaClO (90 and 100% TMP, respectively) showed that specific EfOM-membrane interactions were dominantly responsible for irreversible fouling. Essentially, EfOM degradation (NaOH leads to hydrolysis and solubilization and NaClO oxidizes to hydrophilic form) was required for breakage of the specific interactions and thus, fouling reversal. The results add credence to the use of chemically enhanced backwashing with NaClO for fouling mitigation.

Importantly, irreversible foulants not removed by chemical cleaning may play a role in the aging of membranes over long-term operation. Progressive decline in both

membrane productivity (increased fouling propensity and reduced permeability) and membrane mechanical strength (estimated as Young's modulus and dynamic storage modulus) over multiple fouling-cleaning cycles was interpreted as aging. In contrast, analysis of microfilters after direct chemical exposure resulted in minimal aging, highlighting the high chemical resistance of PVDF membranes. While minimal modifications in the membrane surface functionality were observed, no changes were observed in either membrane productivity or mechanical strength. These distinct differences in the two experimental designs revealed the critical and detrimental role progressive chemically irreversible fouling plays in the aging of membranes. Therefore, utilities employing PVDF membranes can employ regular and extensive chemical cleaning ensuring long-term efficiency. However, it is emphasized that our results strictly pertain only to PVDF membranes and different behavior can be expected for other compositions based on their chemical and pH compatibility.

Lastly, pre-chlorination can be an effective pretreatment strategy to mitigate fouling during filtration of wastewater effluent. However, the extent of fouling mitigation or aggravation was dependent on the dose of sodium hypochlorite or free chlorine. Filtration experiments with a broad range of doses revealed the existence of a threshold dose below which the fouling was exacerbated but fouling was alleviated as the dose was increased further. This dose-dependent behavior was a result of the dose-dependent transformations of different EfOM species. For example, proteins and humic material at low doses become relatively more hydrophobic resulting in increased adsorption to membranes and consequently increased fouling. However, upon further increasing the

dose, more chemical transformations rendered them relatively more hydrophilic, thereby reduced sorption and consequently reduced fouling. The adsorption behavior was quantified in terms of free energy of adhesion between membrane and EfOM using XDLVO theory, trends of which closely followed the fouling trends observed. Thus, pre-chlorination can be a useful strategy for fouling mitigation but with careful assessment of required dosing, which will differ for individual wastewaters.

Recommendations for future work

Based on this research work, the following ideas can be used as directions for future work:

EfOM Characterization

High-resolution mass spectrometry-based characterization of the DOM across multiple sources of water revealed previously unreported lipid chemical class as major foulants. However, the technique is constrained by the DOM extraction method. For example, solid-phase extraction (SPE) recoveries of DOM are too low (40 to 60%) and the DOM character is influenced by the type of cartridges used. This constraint of DOM extraction is closely related to different extraction methods that result in significantly different compositions [249]. Therefore, the use of a broad range of SPE cartridges or other methods (e.g. rotary evaporation, freeze-drying) for DOM extraction and their further analysis will provide a more detailed molecular fingerprint of DOM and its role in fouling.

Membrane aging mechanisms

The present work showed that the progressive accumulation of chemically irreversible foulants led to a progressive decline in the mechanical strength of the membranes. The study proposes that this irreversible attachment of foulants disrupts secondary intermolecular bonding (responsible for inhibition of relative chain motion) within the polymer resulting in reduced mechanical strength. However, a better and potentially quantitative understanding of this mechanism needs to be established. The preliminary hypothesis for this research is: Different types of foulants interact differently with different membrane materials and thus, would impact the mechanical properties differently. For example, polymers with polar groups (e.g. Cl, OH, and CN) have stronger secondary bonds and therefore, larger elastic moduli [233].

REFERENCES

1. Sousa, P.M., et al., *The 'Day Zero' Cape Town drought and the poleward migration of moisture corridors.* Environmental Research Letters, 2018. **13**(12): p. 124025.

2. *Australian Associated Press, Sydney faces tougher water restrictions as NSW grapples with drought*, in *The Guardian*. November 2019.

3. Rosane, O. *India's Sixth-Largest City Is Almost Out of Water*. 2019 [cited 2020 July]; Available from: https://www.ecowatch.com/chennai-india-water-shortage-2638940908.html?rebelltitem=1#rebelltitem1.

4. *The United Nations World Water Development Report 2019: Leaving No One Behind*. United Nations World Water Development Programme 2019, Paris: UNESCO.

5. Hering, J.G., et al., *A Changing Framework for Urban Water Systems.* Environmental Science & Technology, 2013. **47**(19): p. 10721-10726.

6. *National Research Council. Water Reuse: Potential for Expanding the Nation's Water Supply Through Reuse of Municipal Wastewater*. 2012, Washington, DC: The National Academies Press. 276.

7. *The United Nations World Water Development Report 2017: Wastewater, The Untapped Resource.* United Nations World Water Development Programme 2017, Paris: UNESCO.

8. Gerrity, D., et al., *Potable reuse treatment trains throughout the world.* Journal of Water Supply Research and Technology-Aqua, 2013. **62**(6): p. 321-338.

9. *Potable reuse: Guidance for producing safe drinking-water. World Health Organization, (2017).* Retrieved from: https://apps.who.int/iris/handle/10665/258715.

10. Mosher, J.J., G.M. Vartanian, and G. Tchobanoglous, *Potable reuse research compilation: Synthesis of findings*. 2016: Water Environment and Reuse Foundation.

11. Warsinger, D.M., et al., *A review of polymeric membranes and processes for potable water reuse.* Progress in Polymer Science, 2016. **81**: p. 209-237.

12. Zeman, L.J. and A. Zydney, *Microfiltration and ultrafiltration: Principles and applications*. 2017: CRC Press.

13. Cheryan, M., *Ultrafiltration and microfiltration handbook*. 1998: CRC press.

14. Wintgens, T., et al., *The role of membrane processes in municipal wastewater reclamation and reuse.* Desalination, 2005. **178**(1-3): p. 1-11.

15. Anthony, W., *Membrane Processes for Water Reuse*. 2012: McGraw-Hill Professional.

16. Howe, K.J. and M.M. Clark, *Fouling of microfiltration and ultrafiltration membranes by natural waters.* Environmental Science & Technology, 2002. **36**(16): p. 3571-6.

17. Koros, W.J., Y.H. Ma, and T. Shimidzu, *Terminology for membranes and membrane processes (Reprinted from Pure & Appl Chem, vol 68, pg 1479-1489, 1996).* Journal of Membrane Science, 1996. **120**(2): p. 149-159.

18. Chellam, S., J.G. Jacangelo, and T.P. Bonacquisti, *Modeling and experimental verification of pilot-scale hollow fiber, direct flow microfiltration with periodic backwashing.* Environmental Science & Technology, 1998. **32**(1): p. 75-81.

19. Chang, H.Q., et al., *Hydraulic backwashing for low-pressure membranes in drinking water treatment: A review.* Journal of Membrane Science, 2017. **540**: p. 362-380.

20. Kimura, K., H. Yamamura, and Y. Watanabe, *Irreversible fouling in MF/UF membranes caused by natural organic matters (NOMs) isolated from different origins.* Separation Science and Technology, 2006. **41**(7): p. 1331-1344.

21. Gamage, N.P. and S. Chellam, *Mechanisms of physically irreversible fouling during surface water microfiltration and mitigation by aluminum electroflotation pretreatment.* Environmental Science & Technology, 2014. **48**(2): p. 1148-57.

22. Chellam, S. and J.G. Jacangelo, *Existence of critical recovery and impacts of operational mode on potable water microfiltration.* Journal of Environmental Engineering, 1998. **124**(12): p. 1211-1219.

23. Laabs, C.N., G.L. Amy, and M. Jekel, *Understanding the size and character of fouling-causing substances from effluent organic matter (EfOM) in low-pressure membrane filtration.* Environmental Science & Technology, 2006. **40**(14): p. 4495-9.

24. Kim, H.C. and B.A. Dempsey, *Effects of wastewater effluent organic materials on fouling in ultrafiltration.* Water Research, 2008. **42**(13): p. 3379-84.

25. Shon, H.K., et al., *Fouling of ultrafiltration membrane by effluent organic matter: A detailed characterization using different organic fractions in wastewater.* Journal of Membrane Science, 2006. **278**(1-2): p. 232-238.

26. Bessiere, Y., et al., *Effect of hydrophilic/hydrophobic fractions of natural organic matter on irreversible fouling of membranes.* Desalination, 2009. **249**(1): p. 182-187.

27. Filloux, E., H. Gallard, and J.-P. Croue, *Identification of effluent organic matter fractions responsible for low-pressure membrane fouling.* Water Research, 2012. **46**(17): p. 5531-5540.

28. Filloux, E., et al., *Investigating the relative contribution of colloidal and soluble fractions of secondary effluent organic matter to the irreversible fouling of MF and UF hollow fibre membranes.* Separation and Purification Technology, 2016. **170**: p. 109-115.

29. Zheng, X., M.T. Khan, and J.P. Croue, *Contribution of effluent organic matter (EfOM) to ultrafiltration (UF) membrane fouling: isolation, characterization, and fouling effect of EfOM fractions.* Water Research, 2014. **65**: p. 414-24.

30. Haberkamp, J., et al., *Complexity of ultrafiltration membrane fouling caused by macromolecular dissolved organic compounds in secondary effluents.* Water Research, 2008. **42**(12): p. 3153-61.

31. Tian, J.Y., et al., *Correlations of relevant membrane foulants with UF membrane fouling in different waters.* Water Research, 2013. **47**(3): p. 1218-28.

32. Kimura, K., K. Tanaka, and Y. Watanabe, *Microfiltration of different surface waters with/without coagulation: clear correlations between membrane fouling and hydrophilic biopolymers.* Water Research, 2014. **49**: p. 434-43.

33. Peiris, R.H., et al., *Assessing the role of feed water constituents in irreversible membrane fouling of pilot-scale ultrafiltration drinking water treatment systems.* Water Research, 2013. **47**(10): p. 3364-74.

34. Michael-Kordatou, I., et al., *Dissolved effluent organic matter: Characteristics and potential implications in wastewater treatment and reuse applications.* Water Research, 2015. **77**: p. 213-248.

35. Yamamura, H., K. Kimura, and Y. Watanabe, *Mechanism involved in the evolution of physically irreversible fouling in microfiltration and ultrafiltration membranes used for drinking water treatment.* Environmental Science & Technology, 2007. **41**(19): p. 6789-94.

36. Regula, C., et al., *Chemical cleaning/disinfection and ageing of organic UF membranes: a review.* Water Research, 2014. **56**: p. 325-65.

37. Liu, C., et al., *Membrane Chemical Cleaning: From Art to Science.* Pall Corporation, Port Washington, NY, 2001. **11050**.

38. Robinson, S., et al., *Ageing of membranes for water treatment: Linking changes to performance.* Journal of Membrane Science, 2016. **503**: p. 177-187.

39. Akhondi, E., et al., *The Performance and Fouling Control of Submerged Hollow Fiber (HF) Systems: A Review.* Applied Sciences, 2017. **7**(8): p. 765.

40. Charles, L., J. Campbell, and J. Moy, *Assessing the long-term performance of membranes via membrane autopsy*, in *AMTA/AWWA Joint Membrane Technology Conference*. 2015: Orlando, Florida.

41. Robinson, S. and P.R. Berube, *Membrane ageing in full-scale water treatment plants.* Water Research, 2019. **169**: p. 115212.

42. Phuntsho, S., et al., *Membrane autopsy of a 10year old hollow fibre membrane from Sydney Olympic Park water reclamation plant.* Desalination, 2011. **271**(1-3): p. 241-247.

43. Darton, E. and M. Fazel. *A statistical review of 150 membrane autopsies*. in *62nd Annual International Water Conference, Pittsburgh*. 2001.

44. Huang, H., K. Schwab, and J.G. Jacangelo, *Pretreatment for low pressure membranes in water treatment: a review.* Environmental Science & Technology, 2009. **43**(9): p. 3011-9.

45. Hilal, N., et al., *Methods Employed for Control of Fouling in MF and UF Membranes: A Comprehensive Review.* Separation Science and Technology, 2005. **40**(10): p. 1957-2005.

46. Bagga, A., S. Chellam, and D.A. Clifford, *Evaluation of iron chemical coagulation and electrocoagulation pretreatment for surface water microfiltration.* Journal of Membrane Science, 2008. **309**(1-2): p. 82-93.

47. Chellam, S., et al., *Effect of pretreatment on surface water nanofiltration.* Journal AWWA, 1997. **89**(10): p. 77-89.

48. Burris, D.L., *2018 Groundwater Replenishment System Annual Report, (2019).* Retrieved from https://www.ocwd.com/media/7934/2018-gwrs-annual-report.pdf.

49. Rizzo, L., et al., *Best available technologies and treatment trains to address current challenges in urban wastewater reuse for irrigation of crops in EU countries.* Science of The Total Environment, 2020. **710**: p. 136312.

50. Zhou, Z., et al., *Chemically induced alterations in the characteristics of fouling-causing bio-macromolecules - Implications for the chemical cleaning of fouled membranes.* Water Research, 2017. **108**: p. 115-123.

51. Zeng, T., C.J. Wilson, and W.A. Mitch, *Effect of chemical oxidation on the sorption tendency of dissolved organic matter to a model hydrophobic surface.* Environmental Science & Technology, 2014. **48**(9): p. 5118-26.

52. Fan, L.H., et al., *Low-pressure membrane filtration of secondary effluent in water reuse: Pre-treatment for fouling reduction.* Journal of Membrane Science, 2008. **320**(1-2): p. 135-142.

53. Jarusutthirak, C., G. Amy, and J.P. Croue, *Fouling characteristics of wastewater effluent organic matter (EfOM) isolates on NF and UF membranes.* Desalination, 2002. **145**(1-3): p. 247-255.

54. Shon, H.K., et al., *The effect of pretreatment to ultrafiltration of biologically treated sewage effluent: A detailed effluent organic matter (EfOM) characterization.* Water Research, 2004. **38**(7): p. 1933-9.

55. Kim, H.C. and B.A. Dempsey, *Comparison of two fractionation strategies for characterization of wastewater effluent organic matter and diagnosis of membrane fouling.* Water Research, 2012. **46**(11): p. 3714-22.

56. Zhu, H.T., X.H. Wen, and X. Huang, *Membrane organic fouling and the effect of pre-ozonation in microfiltration of secondary effluent organic matter.* Journal of Membrane Science, 2010. **352**(1-2): p. 213-221.

57. Chang, H.Q., et al., *Role of backwash water composition in alleviating ultrafiltration membrane fouling by sodium alginate and the effectiveness of salt backwashing.* Journal of Membrane Science, 2016. **499**: p. 429-441.

58. Chen, J.P., S.L. Kim, and Y. Ting, *Optimization of membrane physical and chemical cleaning by a statistically designed approach.* Journal of Membrane Science, 2003. **219**(1-2): p. 27-45.

59. Decarolis, J., S.K. Hong, and J. Taylor, *Fouling behavior of a pilot scale inside-out hollow fiber UF membrane during dead-end filtration of tertiary wastewater.* Journal of Membrane Science, 2001. **191**(1-2): p. 165-178.

60. Huang, H., T. Young, and J.G. Jacangelo, *Novel approach for the analysis of bench-scale, low pressure membrane fouling in water treatment.* Journal of Membrane Science, 2009. **334**(1-2): p. 1-8.

61. Smith, P.J., et al., *A new approach to backwash initiation in membrane systems.* Journal of Membrane Science, 2006. **278**(1-2): p. 381-389.

62. You, S.H., D.H. Tseng, and W.C. Hsu, *Effect and mechanism of ultrafiltration membrane fouling removal by ozonation.* Desalination, 2007. **202**(1-3): p. 224-230.

63. Zhu, H.T., X.H. Wen, and X. Huang, *Characterization of membrane fouling in a microfiltration ceramic membrane system treating secondary effluent.* Desalination, 2012. **284**: p. 324-331.

64. Zheng, X., et al., *Biopolymer fouling in dead-end ultrafiltration of treated domestic wastewater.* Water Research, 2010. **44**(18): p. 5212-21.

65. Laabs, C., et al., *Fouling of low-pressure (MF and UF) membranes by wastewater effluent organic matter (EfOM): Characterization of EfOM foulants in relation to membrane properties.* Water science and technology: Water supply, 2003. **3**(5-6): p. 229-235.

66. Ayache, C., et al., *Impact of effluent organic matter on low-pressure membrane fouling in tertiary treatment.* Water Research, 2013. **47**(8): p. 2633-42.

67. Basile, A., A. Cassano, and N.K. Rastogi, *Advances in membrane technologies for water treatment: materials, processes and applications*. 2015: Elsevier.

68. Shon, H.K., et al., *Effect of pretreatment on the fouling of membranes: Application in biologically treated sewage effluent.* Journal of Membrane Science, 2004. **234**(1-2): p. 111-120.

69. *Water for Texas: 2017 State Water Plan*. 2016, Austin (TX): Texas Water Development Board.

70. Leenheer, J.A. and J.P. Croue, *Peer Reviewed: Characterizing Aquatic Dissolved Organic Matter.* Environmental Science & Technology, 2003. **37**(1): p. 18A-26A.

71. Nam, S.N., S.W. Krasner, and G.L. Amy, *Differentiating Effluent Organic Matter (EfOM) from Natural Organic Matter (NOM): Impact of EfOM on Drinking Water Sources*, in *Advanced Environmental Monitoring*, Y.J. Kim and U. Platt, Editors. 2008, Springer: Dordrecht. p. 259-270.

72. Gonsior, M., et al., *Molecular characterization of effluent organic matter identified by ultrahigh resolution mass spectrometry.* Water Research, 2011. **45**(9): p. 2943-53.

73. Cai, Z., J. Kim, and M.M. Benjamin, *NOM removal by adsorption and membrane filtration using heated aluminum oxide particles.* Environmental Science & Technology, 2008. **42**(2): p. 619-23.

74. Clark, M.M., et al., *Formation of polysulfone colloids for adsorption of natural organic foulants.* Langmuir, 2005. **21**(16): p. 7207-13.

75. Aubry, J., et al., *Nanoprecipitation of polymethylmethacrylate by solvent shifting: 1. Boundaries.* Langmuir, 2009. **25**(4): p. 1970-9.

76. Chellam, S. and N.G. Cogan, *Colloidal and bacterial fouling during constant flux microfiltration: Comparison of classical blocking laws with a unified model combining pore blocking and EPS secretion.* Journal of Membrane Science, 2011. **382**(1-2): p. 148-157.

77. Luxbacher, T., *Assessment of surface charge for polymer hollow fibre membranes.* Euromembrane Conference 2012, 2012. **44**: p. 1440-1442.

78. Chellam, S. and W. Xu, *Blocking laws analysis of dead-end constant flux microfiltration of compressible cakes.* Journal of Colloid and Interface Science, 2006. **301**(1): p. 248-57.

79. Tiller, F.M. and C.S. Yeh, *The role of porosity in filtration. Part X: Deposition of compressible cakes on external radial surfaces.* AIChE Journal, 1985. **31**(8): p. 1241-1248.

80. Thakur, V.K., et al., *Green aqueous modification of fluoropolymers for energy storage applications.* Journal of Materials Chemistry, 2012. **22**(13): p. 5951-5959.

81. Smith, B.C., *Infrared Spectral Interpretation: A Systematic Approach*. 1999, Boca Raton: CRC Press LLC.

82. Choi, K.Y.J. and B.A. Dempsey, *Bench-scale evaluation of critical flux and TMP in low-pressure membrane filtration.* Journal American Water Works Association, 2005. **97**(7): p. 134-143.

83. Li, C.W. and Y.S. Chen, *Fouling of UF membrane by humic substance: Effects of molecular weight and powder-activated carbon (PAC) pre-treatment.* Desalination, 2004. **170**(1): p. 59-67.

84. Li, K., et al., *Membrane fouling in an integrated adsorption–UF system: Effects of NOM and adsorbent properties.* Environmental Science: Water Research & Technology, 2020.

85. Ran, N., et al., *Powdered Activated Carbon Exacerbates Fouling in MBR Treating Olive Mill Wastewater.* Water, 2019. **11**(12): p. 2498.

86. Koh, L.C., W.Y. Ahn, and M.M. Clark, *Selective adsorption of natural organic foulants by polysulfone colloids: Effect on ultrafiltration fouling.* Journal of Membrane Science, 2006. **281**(1-2): p. 472-479.

87. Cho, J.W., et al., *Characterization of clean and natural organic matter (NOM) fouled NF and UF membranes, and foulants characterization.* Desalination, 1998. **118**(1-3): p. 101-108.

88. Howe, K.J., K.P. Ishida, and M.M. Clark, *Use of ATR/FTIR spectrometry to study fouling of microfiltration membranes by natural waters.* Desalination, 2002. **147**(1-3): p. 251-255.

89. He, Z., et al., *The effects of salt concentration and foulant surface charge on hydrocarbon fouling of a poly(vinylidene fluoride) microfiltration membrane.* Water Research, 2017. **117**: p. 230-241.

90. Xiao, F., et al., *Identification of key factors affecting the organic fouling on low-pressure ultrafiltration membranes.* Journal of Membrane Science, 2013. **447**: p. 144-152.

91. Kwon, B., et al., *Organic nanocolloid fouling in UF membranes.* Journal of Membrane Science, 2006. **279**(1-2): p. 209-219.

92. Kimura, K., et al., *Surface water biopolymer fractionation for fouling mitigation in low-pressure membranes.* Journal of Membrane Science, 2018. **554**: p. 83-89.

93. Wang, F. and V.V. Tarabara, *Pore blocking mechanisms during early stages of membrane fouling by colloids.* Journal of Colloid and Interface Science, 2008. **328**(2): p. 464-9.

94. Chin, W.-C., M.V. Orellana, and P. Verdugo, *Spontaneous assembly of marine dissolved organic matter into polymer gels.* Nature, 1998. **391**(6667): p. 568-572.

95. Verdugo, P., et al., *Marine biopolymer self-assembly: implications for carbon cycling in the ocean.* Faraday Discussions, 2008. **139**(0): p. 393-398.

96. Xu, H. and L. Guo, *Intriguing changes in molecular size and composition of dissolved organic matter induced by microbial degradation and self-assembly.* Water Research, 2018. **135**: p. 187-194.

97. Crozes, G., C. Anselme, and J. Mallevialle, *Effect of Adsorption of Organic-Matter on Fouling of Ultrafiltration Membranes.* Journal of Membrane Science, 1993. **84**(1-2): p. 61-77.

98. Ishida, K.P. and W.J. Cooper, *Analysis of Parameters Affecting Process Efficiency, Energy Consumption, and Carbon Footprint in Water Reuse*. 2015, Alexandria, VA: WateReuse Research Foundation.

99. Ding, Q., et al., *Characteristics of meso-particles formed in coagulation process causing irreversible membrane fouling in the coagulation-microfiltration water treatment.* Water Research, 2016. **101**: p. 127-136.

100. Howe, K.J. and M.M. Clark, *Effect of coagulation pretreatment on membrane filtration performance.* Journal American Water Works Association, 2006. **98**(4): p. 133-146.

101. Jarusutthirak, C. and G. Amy, *Understanding soluble microbial products (SMP) as a component of effluent organic matter (EfOM).* Water Research, 2007. **41**(12): p. 2787-93.

102. Guo, J., et al., *Dissolved organic matter in biologically treated sewage effluent (BTSE): Characteristics and comparison.* Desalination, 2011. **278**(1-3): p. 365-372.

103. Li, K., et al., *Effect of pre-oxidation on low pressure membrane (LPM) for water and wastewater treatment: A review.* Chemosphere, 2019. **231**: p. 287-300.

104. Deborde, M. and U. von Gunten, *Reactions of chlorine with inorganic and organic compounds during water treatment-Kinetics and mechanisms: a critical review.* Water Research, 2008. **42**(1-2): p. 13-51.

105. Zhang, H., et al., *Study on transformation of natural organic matter in source water during chlorination and its chlorinated products using ultrahigh resolution mass spectrometry.* Environmental Science & Technology, 2012. **46**(8): p. 4396-402.

106. Taniguchi, M., J.E. Kilduff, and G. Belfort, *Modes of natural organic matter fouling during ultrafiltration.* Environmental Science & Technology, 2003. **37**(8): p. 1676-83.

107. Costa, A.R., M.N. de Pinho, and M. Elimelech, *Mechanisms of colloidal natural organic matter fouling in ultrafiltration.* Journal of Membrane Science, 2006. **281**(1-2): p. 716-725.

108. Amy, G., *Fundamental understanding of organic matter fouling of membranes.* Desalination, 2008. **231**(1-3): p. 44-51.

109. Wan, Y., et al., *Comparative study on the pretreatment of algae-laden water by UV/persulfate, UV/chlorine, and UV/H2O2: Variation of characteristics and alleviation of ultrafiltration membrane fouling.* Water Research, 2019. **158**: p. 213-226.

110. Chae, S.R., et al., *Comparison of fouling characteristics of two different poly-vinylidene fluoride microfiltration membranes in a pilot-scale drinking water treatment system using pre-coagulation/sedimentation, sand filtration, and chlorination.* Water Research, 2008. **42**(8-9): p. 2029-42.

111. Xing, J., et al., *Application of low-dosage UV/chlorine pre-oxidation for mitigating ultrafiltration (UF) membrane fouling in natural surface water treatment.* Chemical Engineering Journal, 2018. **344**: p. 62-70.

112. Yu, W., et al., *Pre-treatment for ultrafiltration: effect of pre-chlorination on membrane fouling.* Scientific Reports, 2014. **4**: p. 6513.

113. Cornelissen, E.R., T. van den Boomgaard, and H. Strathmann, *Physicochemical aspects of polymer selection for ultrafiltration and microfiltration membranes.* Colloids and Surfaces A: Physicochemical and Engineering Aspects, 1998. **138**(2-3): p. 283-289.

114. Brant, J.A. and A.E. Childress, *Assessing short-range membrane-colloid interactions using surface energetics.* Journal of Membrane Science, 2002. **203**(1-2): p. 257-273.

115. Subhi, N., et al., *Assessment of physicochemical interactions in hollow fibre ultrafiltration membrane by contact angle analysis.* Journal of Membrane Science, 2012. **403**: p. 32-40.

116. Fu, W., et al., *Polyvinyl chloride (PVC) ultrafiltration membrane fouling and defouling behavior: EDLVO theory and interface adhesion force analysis.* Journal of Membrane Science, 2018. **564**: p. 204-210.

117. Wang, H., et al., *Reducing ultrafiltration membrane fouling during potable water reuse using pre-ozonation.* Water Research, 2017. **125**: p. 42-51.

118. Li, R., et al., *Inkjet printing assisted fabrication of polyphenol-based coating membranes for oil/water separation.* Chemosphere, 2020. **250**: p. 126236.

119. Teng, J., et al., *Different fouling propensities of loosely and tightly bound extracellular polymeric substances (EPSs) and the related fouling mechanisms in a membrane bioreactor.* Chemosphere, 2020. **255**: p. 126953.

120. Liu, Y., et al., *A novel strategy based on magnetic field assisted preparation of magnetic and photocatalytic membranes with improved performance.* Journal of Membrane Science, 2020. **612**: p. 118378.

121. Wu, M., et al., *Membrane fouling caused by biological foams in a submerged membrane bioreactor: Mechanism insights.* Water Research, 2020. **181**: p. 115932.

122. Blatchley, E.R., et al., *Effects of disinfectants on wastewater effluent toxicity.* Water Research, 1997. **31**(7): p. 1581-1588.

123. Gupta, K. and S. Chellam, *Contributions of surface and pore deposition to (ir)reversible fouling during constant flux microfiltration of secondary municipal wastewater effluent.* Journal of Membrane Science, 2020. **610**: p. 118231.

124. Yin, Z., et al., *Pre-ozonation for the mitigation of reverse osmosis (RO) membrane fouling by biopolymer: The roles of Ca(2+) and Mg(2+).* Water Research, 2020. **171**: p. 115437.

125. Norde, W. and E. Rouwendal, *Streaming potential measurements as a tool to study protein adsorption kinetics.* Journal of Colloid and Interface Science, 1990. **139**(1): p. 169-176.

126. van Oss, C.J., *Acid—base interfacial interactions in aqueous media.* Colloids and Surfaces A: Physicochemical and Engineering Aspects, 1993. **78**: p. 1-49.

127. van Oss, C.J., *Interfacial Forces in Aqueous Media*. 2nd ed. 2006, Boca Raton: CRC Press.

128. Liu, F., et al., *Progress in the production and modification of PVDF membranes.* Journal of Membrane Science, 2011. **375**(1-2): p. 1-27.

129. DuBois, M., et al., *Colorimetric Method for Determination of Sugars and Related Substances.* Analytical Chemistry, 1956. **28**(3): p. 350-356.

130. Jirka, A.M. and M.J. Carter, *Micro semiautomated analysis of surface and waste waters for chemical oxygen demand.* Analytical Chemistry, 1975. **47**(8): p. 1397-1402.

131. Zhai, S., et al., *Sodium hypochlorite assisted membrane cleaning: Alterations in the characteristics of organic foulants and membrane permeability.* Chemosphere, 2018. **211**: p. 139-148.

132. Korshin, G.V., C.-W. Li, and M.M. Benjamin, *Use of UV Spectroscopy To Study Chlorination of Natural Organic Matter*, in *Water Disinfection and Natural Organic Matter*. 1996, American Chemical Society. p. 182-195.

133. Myllykangas, T., et al., *Molecular size fractions of treated aquatic humus.* Water Research, 2002. **36**(12): p. 3045-3053.

134. Swietlik, J., et al., *Reactivity of natural organic matter fractions with chlorine dioxide and ozone.* Water Research, 2004. **38**(3): p. 547-58.

135. Hawkins, Clare L., *Hypochlorous acid-mediated modification of proteins and its consequences.* Essays in Biochemistry, 2020. **64**(1): p. 75-86.

136. Hawkins, C.L., D.I. Pattison, and M.J. Davies, *Hypochlorite-induced oxidation of amino acids, peptides and proteins.* Amino Acids, 2003. **25**(3): p. 259-274.

137. Dahl, J.-U., M.J. Gray, and U. Jakob, *Protein Quality Control under Oxidative Stress Conditions.* Journal of Molecular Biology, 2015. **427**(7): p. 1549-1563.

138. Lowry, O.H., et al., *Protein Measurement with the Folin Phenol Reagent.* Journal of Biological Chemistry, 1951. **193**(1): p. 265-275.

139. Davies, M.J., *Oxidative Damage to Proteins*, in *Encyclopedia of Radicals in Chemistry, Biology and Materials*. 2012.

140. Hawkins, C.L. and M.J. Davies, *Hypochlorite-induced damage to proteins: formation of nitrogen-centred radicals from lysine residues and their role in protein fragmentation.* Biochemical Journal, 1998. **332**(3): p. 617-625.

141. Cumpstey, I., *Chemical modification of polysaccharides.* ISRN Organic Chemistry, 2013: p. 417672-417672.

142. Floor, M., A.P.G. Kieboom, and H. van Bekkum, *Preparation and Calcium Complexation of Oxidized Polysaccharides. Part I: Oxidation of Maltodextrins and Starch with Alkaline Sodium Hypochlorite.* Starch - Stärke, 1989. **41**(9): p. 348-354.

143. Rees, M.D., C.L. Hawkins, and M.J. Davies, *Polysaccharide Fragmentation Induced by Hydroxyl Radicals and Hypochlorite*, in *Hyaluronan*. 2002, Woodhead Publishing. p. 151-160.

144. Nielsen, S.S., *Phenol-Sulfuric Acid Method for Total Carbohydrates*, in *Food Analysis Laboratory Manual*. 2010, Springer US: Boston, MA. p. 47-53.

145. Mantsch, H.H. and D. Chapman, *Infrared spectroscopy of biomolecules*. 1996, New York: John Wiley & sons.

146. Makovskaya, V., et al., *Octanol-water partition coefficients of substituted phenols and their correlation with molecular descriptors.* Analytica Chimica Acta, 1995. **315**(1): p. 193-200.

147. De Leer, E.W., et al., *Identification of intermediates leading to chloroform and C-4 diacids in the chlorination of humic acid.* Environmental science & Technology, 1985. **19**(6): p. 512-522.

148. Gao, F., et al., *Interaction energy and competitive adsorption evaluation of different NOM fractions on aged membrane surfaces.* Journal of Membrane Science, 2017. **542**: p. 195-207.

149. Tan, Y., et al., *Effect of organic molecular weight distribution on membrane fouling in an ultrafiltration system with ozone oxidation from the perspective of interaction energy.* Environmental Science: Water Research & Technology, 2017. **3**(6): p. 1132-1142.

150. Zamani, F., et al., *Impact of the surface energy of particulate foulants on membrane fouling.* Journal of Membrane Science, 2016. **510**: p. 101-111.

151. Kim, H.-C. and B.A. Dempsey, *Membrane fouling due to alginate, SMP, EfOM, humic acid, and NOM.* Journal of Membrane Science, 2013. **428**(Supplement C): p. 190-197.

152. Stetefeld, J., S.A. McKenna, and T.R. Patel, *Dynamic light scattering: a practical guide and applications in biomedical sciences.* Biophysical reviews, 2016. **8**(4): p. 409-427.

153. Morote, Á.-F., J. Olcina, and M. Hernández, *The Use of Non-Conventional Water Resources as a Means of Adaptation to Drought and Climate Change in Semi-Arid Regions: South-Eastern Spain.* Water, 2019. **11**(1): p. 93.

154. Berbel, J. and E. Esteban, *Droughts as a catalyst for water policy change. Analysis of Spain, Australia (MDB), and California.* Global Environmental Change, 2019. **58**: p. 101969.

155. Sari, M.A. and S. Chellam, *Electrocoagulation process considerations during advanced pretreatment for brackish inland surface water desalination:*

Nanofilter fouling control and permeate water quality. Desalination, 2017. **410**: p. 66-76.

156. Park, S., et al., *Evaluating membrane fouling potentials of dissolved organic matter in brackish water.* Water Research, 2019. **149**: p. 65-73.

157. Zularisam, A.W., A.F. Ismail, and R. Salim, *Behaviours of natural organic matter in membrane filtration for surface water treatment: A review.* Desalination, 2006. **194**(1-3): p. 211-231.

158. Brezonik, P.L. and W.A. Arnold. *Water Chemistry: An Introduction to the Chemistry of Natural and Engineered Aquatic Systems*. 2011.

159. Cottrell, B.A., et al., *A regional study of the seasonal variation in the molecular composition of rainwater.* Atmospheric Environment, 2013. **77**: p. 588-597.

160. Phungsai, P., et al., *Molecular characterization of low molecular weight dissolved organic matter in water reclamation processes using Orbitrap mass spectrometry.* Water Research, 2016. **100**: p. 526-536.

161. Lv, J., et al., *Molecular-Scale Investigation with ESI-FT-ICR-MS on Fractionation of Dissolved Organic Matter Induced by Adsorption on Iron Oxyhydroxides.* Environmental Science & Technology, 2016. **50**(5): p. 2328-36.

162. Riedel, T., H. Biester, and T. Dittmar, *Molecular Fractionation of Dissolved Organic Matter with Metal Salts.* Environmental Science & Technology, 2012. **46**(8): p. 4419-4426.

163. Galindo, C. and M. Del Nero, *Chemical fractionation of a terrestrial humic acid upon sorption on alumina by high resolution mass spectrometry.* RSC Advances, 2015. **5**(89): p. 73058-73067.

164. Shi, W., et al., *Monitoring dissolved organic matter in wastewater and drinking water treatments using spectroscopic analysis and ultra-high resolution mass spectrometry.* Water Research, 2021. **188**: p. 116406.

165. Urai, M., et al., *Molecular characterization of dissolved organic matter in various urban water resources using Orbitrap Fourier transform mass spectrometry.* Water Supply, 2014. **14**(4): p. 547-553.

166. Hawkes, J.A., et al., *Evaluation of the Orbitrap Mass Spectrometer for the Molecular Fingerprinting Analysis of Natural Dissolved Organic Matter.* Analytical Chemistry, 2016. **88**(15): p. 7698-7704.

167. Dittmar, T., et al., *A simple and efficient method for the solid-phase extraction of dissolved organic matter (SPE-DOM) from seawater.* Limnology and Oceanography: Methods, 2008. **6**(6): p. 230-235.

168. Koch, B.P., et al., *Fundamentals of Molecular Formula Assignment to Ultrahigh Resolution Mass Data of Natural Organic Matter.* Analytical Chemistry, 2007. **79**(4): p. 1758-1763.

169. Tolić, N., et al., *Formularity: Software for Automated Formula Assignment of Natural and Other Organic Matter from Ultrahigh-Resolution Mass Spectra.* Analytical Chemistry, 2017. **89**(23): p. 12659-12665.

170. Kujawinski, E.B. and M.D. Behn, *Automated Analysis of Electrospray Ionization Fourier Transform Ion Cyclotron Resonance Mass Spectra of Natural Organic Matter.* Analytical Chemistry, 2006. **78**(13): p. 4363-4373.

171. Kind, T. and O. Fiehn, *Seven Golden Rules for heuristic filtering of molecular formulas obtained by accurate mass spectrometry.* BMC bioinformatics, 2007. **8**: p. 105-105.

172. Stenson, A.C., A.G. Marshall, and W.T. Cooper, *Exact Masses and Chemical Formulas of Individual Suwannee River Fulvic Acids from Ultrahigh Resolution Electrospray Ionization Fourier Transform Ion Cyclotron Resonance Mass Spectra.* Analytical Chemistry, 2003. **75**(6): p. 1275-1284.

173. Kim, S., R.W. Kramer, and P.G. Hatcher, *Graphical Method for Analysis of Ultrahigh-Resolution Broadband Mass Spectra of Natural Organic Matter, the Van Krevelen Diagram.* Analytical Chemistry, 2003. **75**(20): p. 5336-5344.

174. Badertscher, M., et al., *A Novel Formalism To Characterize the Degree of Unsaturation of Organic Molecules.* Journal of Chemical Information and Computer Sciences, 2001. **41**(4): p. 889-893.

175. Koch, B.P. and T. Dittmar, *From mass to structure: an aromaticity index for high-resolution mass data of natural organic matter.* 2006. **20**(5): p. 926-932.

176. Maizel, A.C. and C.K. Remucal, *The effect of advanced secondary municipal wastewater treatment on the molecular composition of dissolved organic matter.* Water Research, 2017. **122**: p. 42-52.

177. MacCarthy, P. and I.H. Suffet, *Aquatic Humic Substances*, in *Advances in Chemistry Series*. 1988, American Chemical Society. p. xiii-xxx.

178. Hockaday, W.C., et al., *Electrospray and photoionization mass spectrometry for the characterization of organic matter in natural waters: a qualitative assessment.* Limnology and Oceanography: Methods, 2009. **7**(1): p. 81-95.

179. Kujawinski, E.B., et al., *Identification of possible source markers in marine dissolved organic matter using ultrahigh resolution mass spectrometry.* Geochimica et Cosmochimica Acta, 2009. **73**(15): p. 4384-4399.

180. Yu, H., et al., *Relationship between soluble microbial products (SMP) and effluent organic matter (EfOM): characterized by fluorescence excitation emission matrix coupled with parallel factor analysis.* Chemosphere, 2015. **121**: p. 101-9.

181. Qu, F., et al., *Tertiary treatment of secondary effluent using ultrafiltration for wastewater reuse: correlating membrane fouling with rejection of effluent organic matter and hydrophobic pharmaceuticals.* Environmental Science: Water Research & Technology, 2019. **5**(4): p. 672-683.

182. Ramesh, A., D.-J. Lee, and S.G. Hong, *Soluble microbial products (SMP) and soluble extracellular polymeric substances (EPS) from wastewater sludge.* Applied Microbiology and Biotechnology, 2006. **73**(1): p. 219-225.

183. Shon, H.K., S. Vigneswaran, and S.A. Snyder, *Effluent Organic Matter (EfOM) in Wastewater: Constituents, Effects, and Treatment.* Critical Reviews in Environmental Science and Technology, 2006. **36**(4): p. 327-374.

184. Peiris, R.H., et al., *Understanding fouling behaviour of ultrafiltration membrane processes and natural water using principal component analysis of fluorescence excitation-emission matrices.* Journal of Membrane Science, 2010. **357**(1): p. 62-72.

185. Yamamura, H., et al., *Affinity of functional groups for membrane surfaces: implications for physically irreversible fouling.* Environmental Science & Technology, 2008. **42**(14): p. 5310-5.

186. Trzaskus, K., et al., *Understanding the role of nanoparticle size and polydispersity in fouling development during dead-end microfiltration.* Journal of Membrane Science, 2016. **516**: p. 152-161.

187. Katsoufidou, K., S.G. Yiantsios, and A.J. Karabelas, *A study of ultrafiltration membrane fouling by humic acids and flux recovery by backwashing: Experiments and modeling.* Journal of Membrane Science, 2005. **266**(1-2): p. 40-50.

188. Fan, L., et al., *Influence of the characteristics of natural organic matter on the fouling of microfiltration membranes.* Water Research, 2001. **35**(18): p. 4455-63.

189. Raeke, J., et al., *Selectivity of solid phase extraction of freshwater dissolved organic matter and its effect on ultrahigh resolution mass spectra.* Environmental Science: Processes & Impacts, 2016. **18**(7): p. 918-927.

190. Wünsch, U.J., et al., *Quantifying the impact of solid-phase extraction on chromophoric dissolved organic matter composition.* Marine Chemistry, 2018. **207**: p. 33-41.

191. Barry, M.C., K. Hristovski, and P. Westerhoff, *Membrane Fouling by Vesicles and Prevention through Ozonation.* Environmental Science & Technology, 2014. **48**(13): p. 7349-7356.

192. Ding, G. and J.A. Rice, *Effect of lipids on sorption/desorption hysteresis in natural organic matter.* Chemosphere, 2011. **84**(4): p. 519-526.

193. Al-Halbouni, D., W. Dott, and J. Hollender, *Occurrence and composition of extracellular lipids and polysaccharides in a full-scale membrane bioreactor.* Water Research, 2009. **43**(1): p. 97-106.

194. Dereli, R.K., et al., *Influence of high lipid containing wastewater on filtration performance and fouling in AnMBRs operated at different solids retention times.* Separation and Purification Technology, 2015. **139**: p. 43-52.

195. Kimura, K., T. Kakuda, and H. Iwasaki, *Membrane fouling caused by lipopolysaccharides: A suggestion for alternative model polysaccharides for MBR fouling research.* Separation and Purification Technology, 2019. **223**: p. 224-233.

196. *IUPAC. Compendium of Chemical Terminology, 2nd ed. (the "Gold Book"). Compiled by A. D. McNaught and A. Wilkinson.* 1997: Blackwell Scientific Publications, Oxford.

197. Aoustin, E., et al., *Ultrafiltration of natural organic matter.* Separation and Purification Technology, 2001. **22-23**: p. 63-78.

198. Wang, X., et al., *Characterization of wastewater effluent organic matter with different solid phase extraction sorbents.* Chemosphere, 2020: p. 127235.

199. Reemtsma, T., *Determination of molecular formulas of natural organic matter molecules by (ultra-) high-resolution mass spectrometry: Status and needs.* Journal of Chromatography A, 2009. **1216**(18): p. 3687-3701.

200. Yang, J., et al., *Membrane-Based Processes Used in Municipal Wastewater Treatment for Water Reuse: State-Of-The-Art and Performance Analysis.* Membranes, 2020. **10**(6): p. 131.

201. Ravereau, J., et al., *Ageing of polyvinylidene fluoride hollow fiber membranes in sodium hypochlorite solutions.* Journal of Membrane Science, 2016. **505**: p. 174-184.

202. Abdullah, S.Z. and P.R. Berube, *Filtration and cleaning performances of PVDF membranes aged with exposure to sodium hypochlorite.* Separation and Purification Technology, 2018. **195**: p. 253-259.

203. Causserand, C., et al., *Ageing of polysulfone membranes in contact with bleach solution: Role of radical oxidation and of some dissolved metal ions.* Chemical Engineering and Processing: Process Intensification, 2008. **47**(1): p. 48-56.

204. Robinson, S.J. and P.R. Bérubé, *Seeking realistic membrane ageing at bench-scale.* Journal of Membrane Science, 2020: p. 118606.

205. Arkhangelsky, E., D. Kuzmenko, and V. Gitis, *Impact of chemical cleaning on properties and functioning of polyethersulfone membranes.* Journal of Membrane Science, 2007. **305**(1-2): p. 176-184.

206. Puspitasari, V., et al., *Cleaning and ageing effect of sodium hypochlorite on polyvinylidene fluoride (PVDF) membrane.* Separation and Purification Technology, 2010. **72**(3): p. 301-308.

207. Hajibabania, S., et al., *Relative impact of fouling and cleaning on PVDF membrane hydraulic performances.* Separation and Purification Technology, 2012. **90**: p. 204-212.

208. Wang, P., et al., *Effect of hypochlorite cleaning on the physiochemical characteristics of polyvinylidene fluoride membranes.* Chemical Engineering Journal, 2010. **162**(3): p. 1050-1056.

209. Jucker, C. and M.M. Clark, *Adsorption of Aquatic Humic Substances on Hydrophobic Ultrafiltration Membranes.* Journal of Membrane Science, 1994. **97**: p. 37-52.

210. Zondervan, E., A. Zwijnenburg, and B. Roffel, *Statistical analysis of data from accelerated ageing tests of PES UF membranes.* Journal of Membrane Science, 2007. **300**(1): p. 111-116.

211. Gao, F., et al., *Effects of sodium hypochlorite on structural/surface characteristics, filtration performance and fouling behaviors of PVDF membranes.* Journal of Membrane Science, 2016. **519**: p. 22-31.

212. Yang, D., et al., *Aging of poly(vinylidene fluoride) hollow fibers in light hydrocarbon environments.* Journal of Membrane Science, 2012. **409-410**: p. 302-317.

213. Stalder, A.F., et al., *A snake-based approach to accurate determination of both contact points and contact angles.* Colloids and Surfaces A: Physicochemical and Engineering Aspects, 2006. **286**(1): p. 92-103.

214. Yu, H., et al., *Performance of hollow fiber ultrafiltration membrane in a full-scale drinking water treatment plant in China: A systematic evaluation during 7-year operation.* Journal of Membrane Science, 2020: p. 118469.

215. Rabuni, M.F., et al., *Effects of alkaline environments at mild conditions on the stability of PVDF membrane: An experimental study.* Industrial & Engineering Chemistry Research, 2013. **52**(45): p. 15874-15882.

216. Wu, Q., X. Zhang, and G. Cao, *Impacts of sodium hydroxide and sodium hypochlorite aging on polyvinylidene fluoride membranes fabricated with different methods.* Journal of Environmental Sciences, 2018. **67**: p. 294-308.

217. Rajabzadeh, S., et al., *Effect of additives on the morphology and properties of poly(vinylidene fluoride) blend hollow fiber membrane prepared by the thermally induced phase separation method.* Journal of Membrane Science, 2012. **423-424**: p. 189-194.

218. Bacchin, P. and P. Aimar, *Critical fouling conditions induced by colloidal surface interaction: from causes to consequences.* Desalination, 2005. **175**(1): p. 21-27.

219. Bottino, A., G. Capannelli, and A. Comite, *Novel porous membranes from chemically modified poly(vinylidene fluoride).* Journal of Membrane Science, 2006. **273**(1): p. 20-24.

220. Awanis Hashim, N., Y. Liu, and K. Li, *Stability of PVDF hollow fibre membranes in sodium hydroxide aqueous solution.* Chemical Engineering Science, 2011. **66**(8): p. 1565-1575.

221. Grasselli, M. and N. Betz, *Making porous membranes by chemical etching of heavy-ion tracks in β-PVDF films.* Nuclear Instruments and Methods in Physics Research Section B: Beam Interactions with Materials and Atoms, 2005. **236**(1): p. 501-507.

222. Ross, G.J., et al., *Surface modification of poly(vinylidene fluoride) by alkaline treatment1. The degradation mechanism.* Polymer, 2000. **41**(5): p. 1685-1696.

223. Schulze, A., M. Went, and A. Prager, *Membrane Functionalization with Hyperbranched Polymers.* Materials, 2016. **9**(8): p. 706.

224. Zimmermann, R., S. Dukhin, and C. Werner, *Electrokinetic Measurements Reveal Interfacial Charge at Polymer Films Caused by Simple Electrolyte Ions.* The Journal of Physical Chemistry B, 2001. **105**(36): p. 8544-8549.

225. Zimmermann, R., et al., *Hydroxide and hydronium ion adsorption — A survey.* Current Opinion in Colloid & Interface Science, 2010. **15**(3): p. 196-202.

226. Bettelheim, F.A., et al., *Introduction to general, organic and biochemistry*. 2012: Nelson Education.

227. Childress, A.E., et al., *Mechanical analysis of hollow fiber membrane integrity in water reuse applications.* Desalination, 2005. **180**(1-3): p. 5-14.

228. Gijsbertsen-Abrahamse, A.J., E.R. Cornelissen, and J.A.M.H. Hofman, *Fiber failure frequency and causes of hollow fiber integrity loss.* Desalination, 2006. **194**(1): p. 251-258.

229. Chartoff, R.P., J.D. Menczel, and S.H. Dillman, *Dynamic Mechanical Analysis (DMA)*, in *Thermal Analysis of Polymers*. 2008, John Wiley & Sons, Inc. p. 387-495.

230. Yadav, K., K. Morison, and M.P. Staiger, *Effects of hypochlorite treatment on the surface morphology and mechanical properties of polyethersulfone ultrafiltration membranes.* Polymer Degradation and Stability, 2009. **94**(11): p. 1955-1961.

231. Wang, K., et al., *Mechanical properties of water desalination and wastewater treatment membranes.* Desalination, 2017. **401**: p. 190-205.

232. Powell, L.C., N. Hilal, and C.J. Wright, *Atomic force microscopy study of the biofouling and mechanical properties of virgin and industrially fouled reverse osmosis membranes.* Desalination, 2017. **404**: p. 313-321.

233. Callister, W.D. and D.G. Rethwisch, *Materials science and engineering: An introduction*. Vol. 9. 2018: Wiley New York.

234. Gupta, K. and S. Chellam, *Pre-chlorination effects on fouling during microfiltration of secondary municipal wastewater effluent.* Journal of Membrane Science, 2021. **620**: p. 118969.

235. Li, S., et al., *Impact of backwash water composition on ultrafiltration fouling control.* Journal of Membrane Science, 2009. **344**(1-2): p. 17-25.

236. Li, S., et al., *Fouling control mechanisms of demineralized water backwash: Reduction of charge screening and calcium bridging effects.* Water Research, 2011. **45**(19): p. 6289-300.

237. Li, S., S.G.J. Heijman, and J.C. van Dijk, *A pilot-scale study of backwashing ultrafiltration membrane with demineralized water.* Journal of Water Supply: Research and Technology-Aqua, 2010. **59**(2-3): p. 128-133.

238. Qin, J.J., et al., *Dead-end ultrafiltration for pretreatment of RO in reclamation of municipal wastewater effluent.* Journal of Membrane Science, 2004. **243**(1-2): p. 107-113.

239. Vial, D., G. Doussau, and R. Galindo, *Comparison of three pilot studies using Microza® membranes for Mediterranean seawater pre-treatment.* Desalination, 2003. **156**(1): p. 43-50.

240. Zhang, Y., et al., *The influence of chemically enhanced backwash by-products (CEBBPs) on water quality in the coagulation-ultrafiltration process.* Environ Sci Pollut Res Int, 2016. **23**(2): p. 1805-19.

241. Wang, X.Y., et al., *Reinvestigation of membrane cleaning mechanisms using NaOCl: Role of reagent diffusion.* Journal of Membrane Science, 2018. **550**: p. 278-285.

242. Teychene, B., G. Collet, and H. Gallard, *Modeling of combined particles and natural organic matter fouling of ultrafiltration membrane.* Journal of Membrane Science, 2016. **505**: p. 185-193.

243. Li, S., et al., *Influence of Ca and Na ions in backwash water on ultrafiltration fouling control.* Desalination, 2010. **250**(2): p. 861-864.

244. Pramanik, B.K., F.A. Roddick, and L. Fan, *Long-term operation of biological activated carbon pre-treatment for microfiltration of secondary effluent: Correlation between the organic foulants and fouling potential.* Water Research, 2016. **90**: p. 405-414.

245. Benjamin, M.M. and D.F. Lawler, *Water quality engineering: Physical/chemical treatment processes*. 2013: John Wiley & Sons.

246. Ang, W.S., et al., *Chemical cleaning of RO membranes fouled by wastewater effluent: Achieving higher efficiency with dual-step cleaning.* Journal of Membrane Science, 2011. **382**(1-2): p. 100-106.

247. Kim, C.Y., et al., *Impact of Physical and Chemical Cleaning Agents on Specific Biofilm Components and the Implications for Membrane Biofouling Management.* Industrial & Engineering Chemistry Research, 2018. **57**(9): p. 3359-3370.

248. Chang, H.Q., et al., *Hydraulic irreversibility of ultrafiltration membrane fouling by humic acid: Effects of membrane properties and backwash water composition.* Journal of Membrane Science, 2015. **493**: p. 723-733.

249. Moody, C.S., *A comparison of methods for the extraction of dissolved organic matter from freshwaters.* Water Research, 2020: p. 116114.

APPENDIX A

SUPPORTING INFROMATION FOR CHAPTER II

Adsorption pretreatment

Equilibrium time and adsorption capacity

The equilibrium time for the removal of EfOM (measured as DOC) by the three adsorbents was estimated in batch experiments, shown in **Figure A-1 (left)**. As can be seen the equilibrium for all the adsorbents was achieved well within 24 hours. Additionally, the adsorption isotherm plot is also shown, **Figure A-1 (right)**.

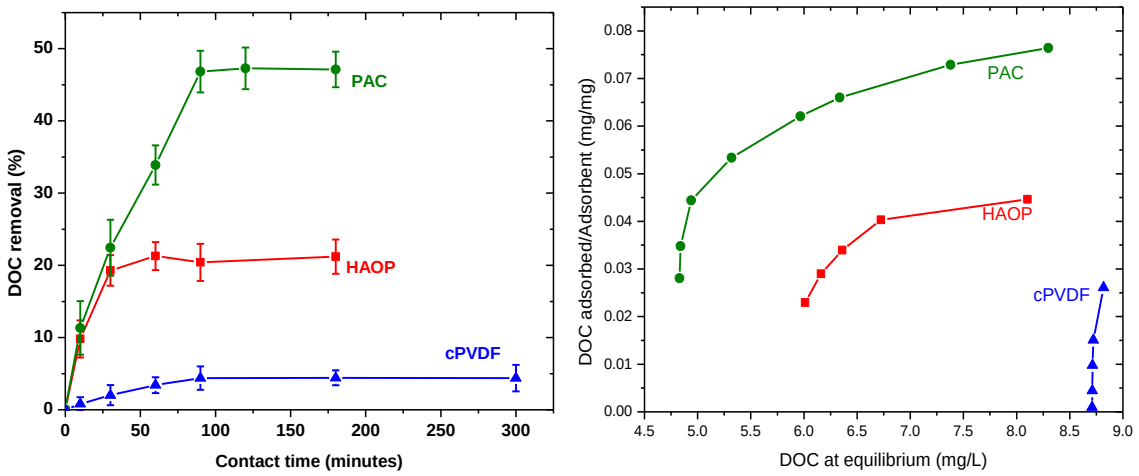

Figure A-1 (Left) DOC removal by the three adsorbents at 100 ppm dosage as a function of time. (Right) Adsorption isotherms for the different adsorbents.

Centrifugation times for the adsorbent particles

Centrifugation times were calculated according to the equation: $t = \frac{18\eta}{\omega^2 d^2 \Delta\rho} \frac{L}{R_{av}}$ (Livshits et al. Scientific Reports 2015), **Table A-1**, where,

η is viscosity of water at 20 °C = 1 cP

ω is the angular velocity at 10,000 g = 953 rad/s (for Eppendorf rotor FA-34-6-38)

$\Delta\rho$ is the density difference = $\rho_{particle} - \rho_{water}$ = $(\rho_{particle} - 1)$ g/cm^3

L is the sedimentation path length for FA rotors ≈ 2.74 cm for FA-34-6-38

R_{av} is the average radius of centrifugation ≈ 6 cm for FA-34-6-38 rotor

Table A-1 shows the calculated centrifugation times for the smallest adsorbent particle size, particle size distribution of the adsorbents is shown in **Figure A-2**.

Table A-1 Required sedimentation times for the different adsorbents at 10000 g.

Adsorbent	Smallest detected size (µm)	Density (g/cm^3)	Sedimentation time for complete removal (seconds)
PAC	4.8	1.8	0.49
HAOP	1.68	2.42	2.26
cPVDF	0.18	1.78	358

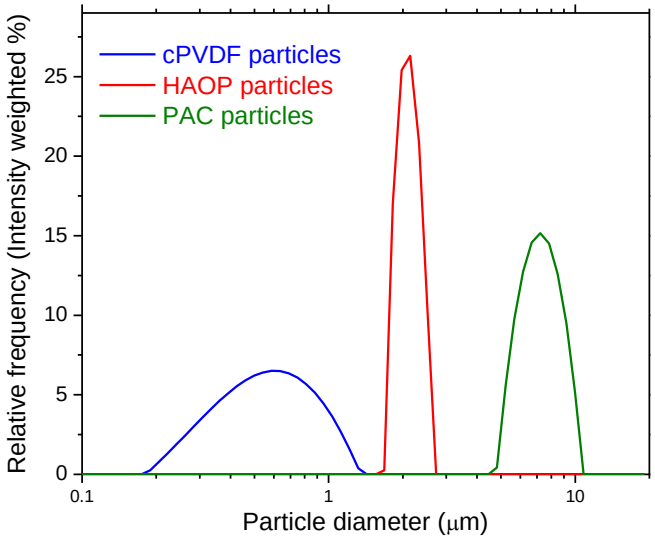

Figure A-2 Particle size distribution of the adsorbent particles. cPVDF (blue), HAOP (red), and PAC (green)

Effect of pretreatments on the fouling of microfilters

The effect of pretreatments on the fouling behavior of microfilters was evaluated in terms of the percentage increase in TMP over individual cycles i.e. total fouling (**Equation A1**) and percentage of virgin membrane TMP recovered (**Equation A2**) i.e. backwashing efficiency.

$$Increase\ in\ TMP\ (\%) = \frac{TMP^{i}_{final} - TMP^{i}_{initial}}{TMP^{i}_{initial}} \times 100 \qquad \text{(A1)}$$

$$Recovery\ by\ backwashing\ (\%) = \frac{TMP^{1}_{initial}}{TMP^{i}_{initial}} \times 100 \qquad \text{(A2)}$$

where, $TMP^{i}_{initial}$ and TMP^{i}_{final} are the transmembrane pressure at the start and end of i^{th} cycle, respectively. The same has been shown in **Figure A-3**.

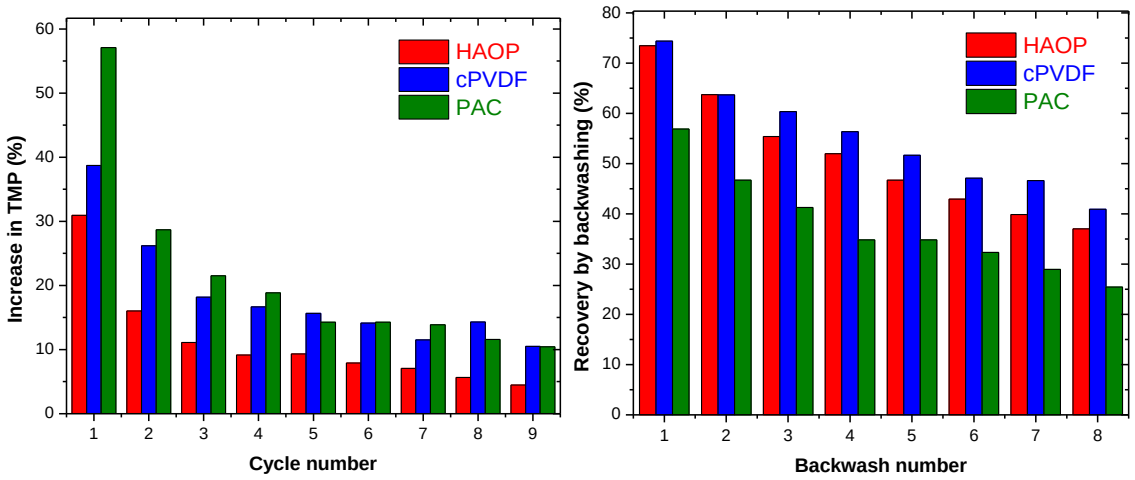

Figure A-3 Percentage increase in TMP during individual cycles for the three pretreatments (left), and percentage of virgin TMP recovered after each backwash (right).

The pretreatment of the wastewater and the following filtration also revealed a non-proportional relationship between the influent gross EfOM (measured as mg/L DOC) and the extent of fouling. As can be seen, in **Figure A-4**, neither maximum amount of influent EfOM lead to maximum fouling, nor minimum amount of EfOM led to minimum fouling. This behavior was consistently observed for all cycles.

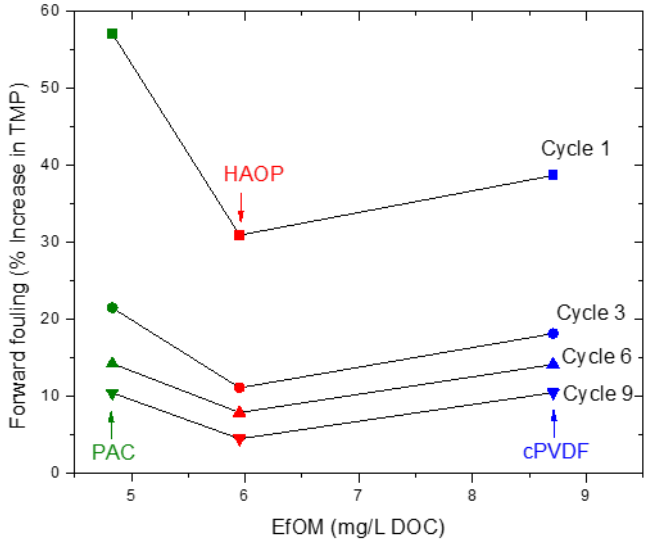

Figure A-4 Non-proportional relationship between the EfOM (measured as mg/L DOC) content and the extent of fouling over multiple cycles.

APPENDIX B

SUPPORTING INFROMATION FOR CHAPTER III

Table A-2 Water, formamide, and diiodomethane contact angles of the dissolved EfOM and membrane

Dose (mg/L)	Water	Formamide	Diiodomethane
0 (raw EfOM)	24.22 ± 0.27	30.58 ± 1.55	54.40 ± 0.71
1.5	22.79 ± 0.37	33.98 ± 0.36	50.35 ± 3.89
2.5	21.42 ± 0.18	41.54 ± 0.72	47.80 ± 1.41
5	18.95 ± 0.30	28.32 ± 0.11	53.30 ± 0.71
7.5	16.71 ± 0.22	27.36 ± 0.11	65.25 ± 0.64
10	13.64 ± 0.15	25.97 ± 0.24	69.00 ± 0.28
15	12.17 ± 0.26	25.34 ± 0.30	72.75 ± 0.35
Membrane	112.80 ± 0.14	88.81 ± 0.82	66.72 ± 0.57

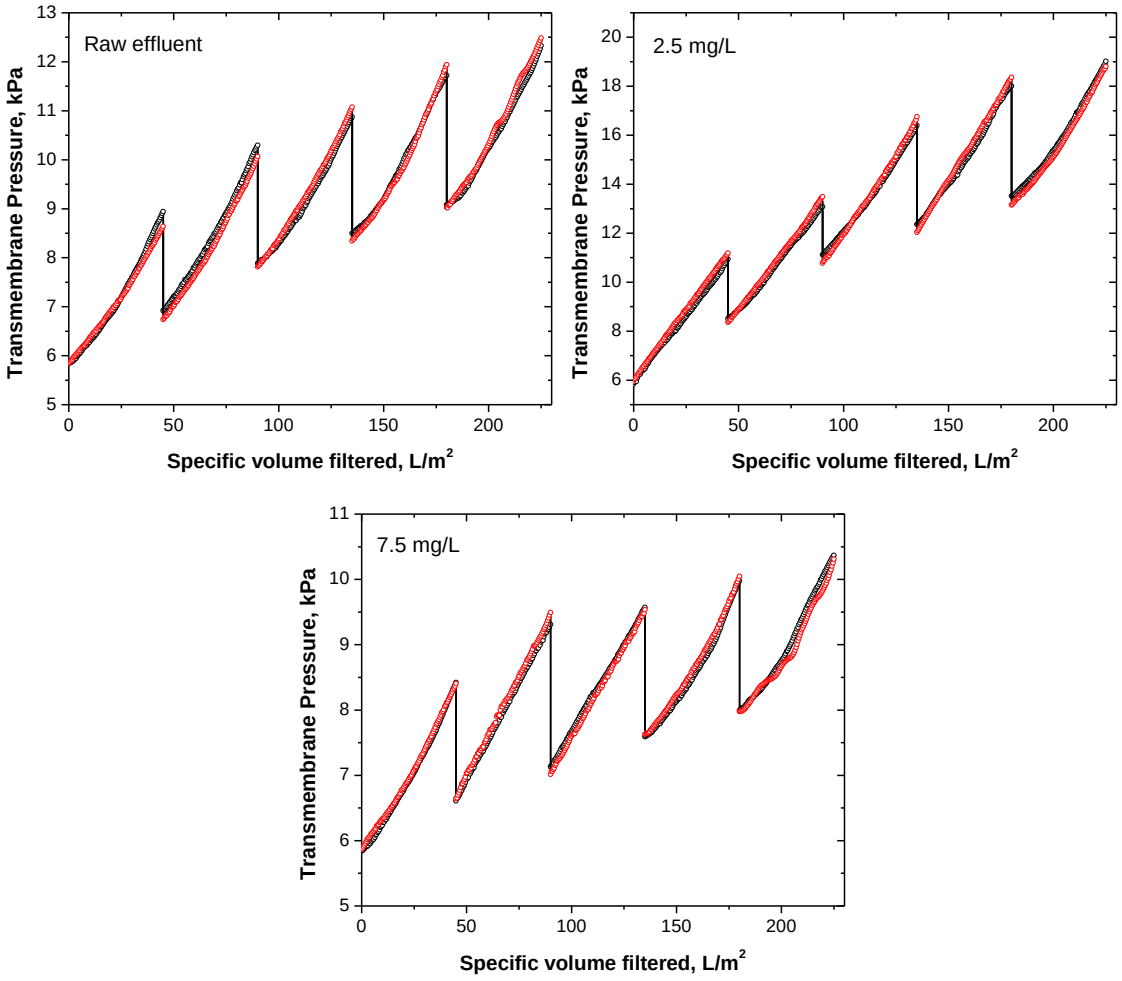

Figure A-5 Fouling profiles for filtration of raw and prechlorinated (2.5 and 7.5 mg/L) wastewater effluent at three different doses. The red and black plots represent duplicate experiments conducted on different days during the duration of this research. As observed, instantaneous pressure values under identical experimental conditions were very similar, indicating that the filtration behavior was closely reproducible.

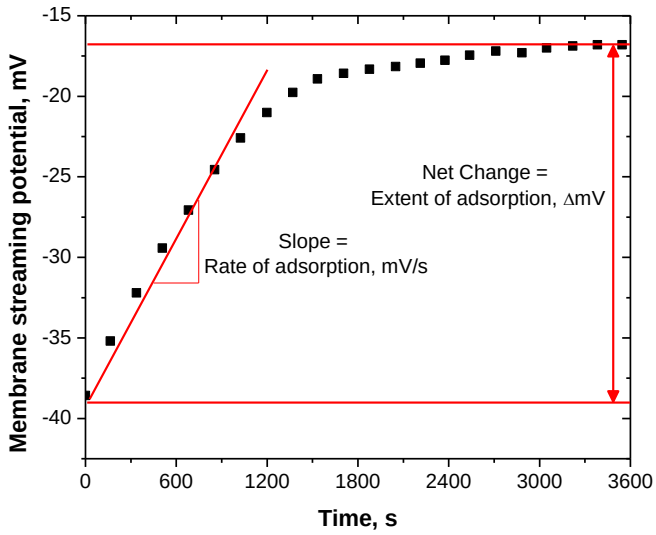

Figure A-6 Representative calculation for extent and rate of adsorption from streaming potential measurements.

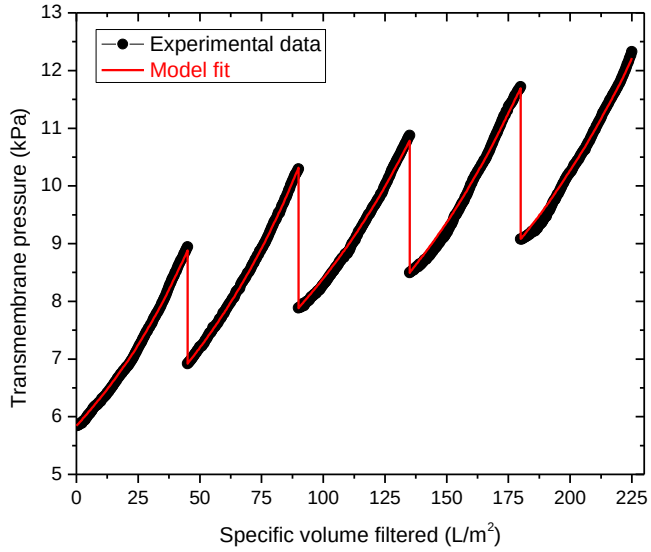

Figure A-7 Cake filtration model fits (red) to experimental transmembrane pressure profiles for the raw effluent (black)

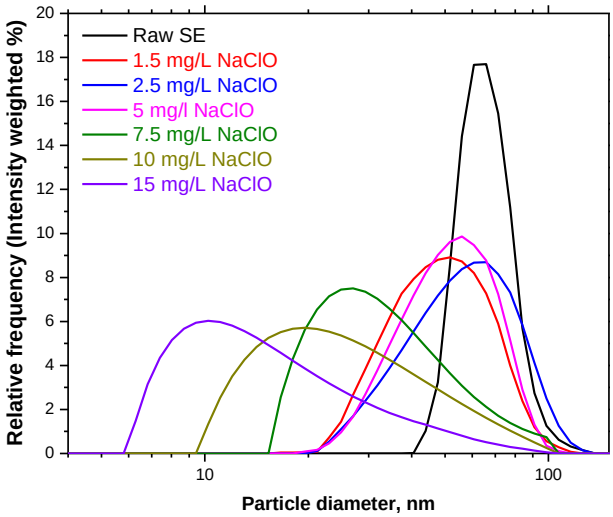

Figure A-8 Size distribution of the microfiltration permeate of raw and prechlorinated effluents.

Table A-3 The specific volume filtered (L/m^2) after which a transition from standard blocking to intermediate blocking occurred within a forward filtration cycle at different NaClO doses. "0" implies that intermediate blocking was the fouling mechanism throughout and "-" implies standard blocking was the fouling mechanism throughout, i.e., no transition occurred.

Dose (mg/L)	Cycle 1	Cycle 2	Cycle 3	Cycle 4	Cycle 5
1.5	-	18.9	16.65	13.5	0
2.5	21.15	5.85	0	0	0
5	-	27.45	18	14.4	12.6
7.5	-	-	23.4	15.75	14.85
10	-	-	-	-	17.1
15	-	-	-	-	-

APPENDIX C

SUPPORTING INFROMATION FOR CHAPTER IV

Table A-4 : Dissolved organic carbon (DOC, mg/L) based solid-phase extraction (SPE) efficiency for all feed water samples.

Sample	DOC in feed water (mg/L)	DOC in SPE extract (mg/L)	Efficiency (%)	Sample
SW	7.903	3.967	50.2	SW
BSW	7.239	4.329	59.8	BSW
MWE1	6.600	2.660	40.3	MWE1
MWE2	7.455	3.332	44.7	MWE2

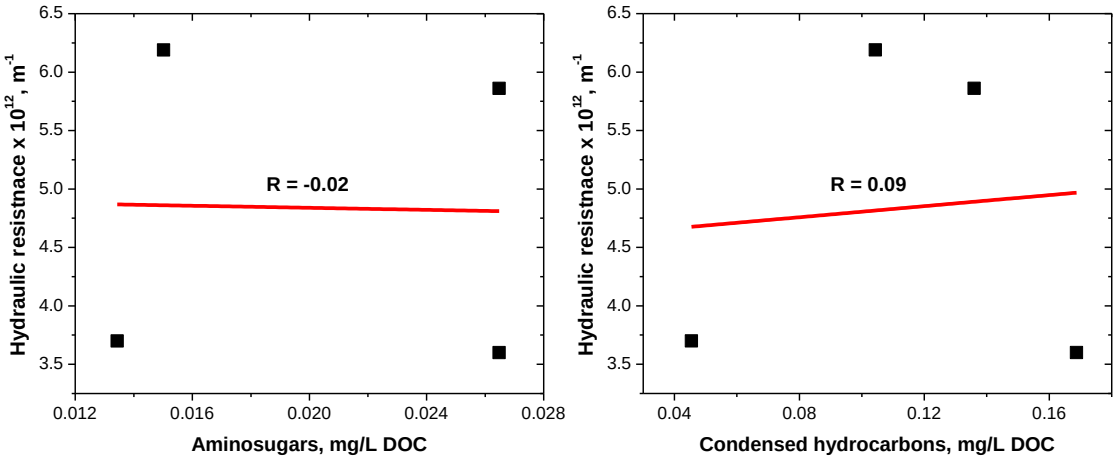

Figure A-9 Relationships between hydraulically irreversible resistance and percentage weighted concentration of different aminosugars and condensed hydrocarbon chemical classes.

Table A-5 H:C and O:C ranges used to define compound classes in van Krevelen diagrams.

Chemical Class	H:C	O:C
Lipids	1.5-2.2	0-0.3
Proteins	1.5-2.2	0.3-0.6
Aminosugars	1.5-1.7	0.6-0.7
Carbohydrates	>1.5	>0.67
Condensed hydrocarbons	0.5-1.1	0-0.25
Lignin	0.7-1.5	0.3-0.67
Tannin	0.5-1.3	0.6-0.9

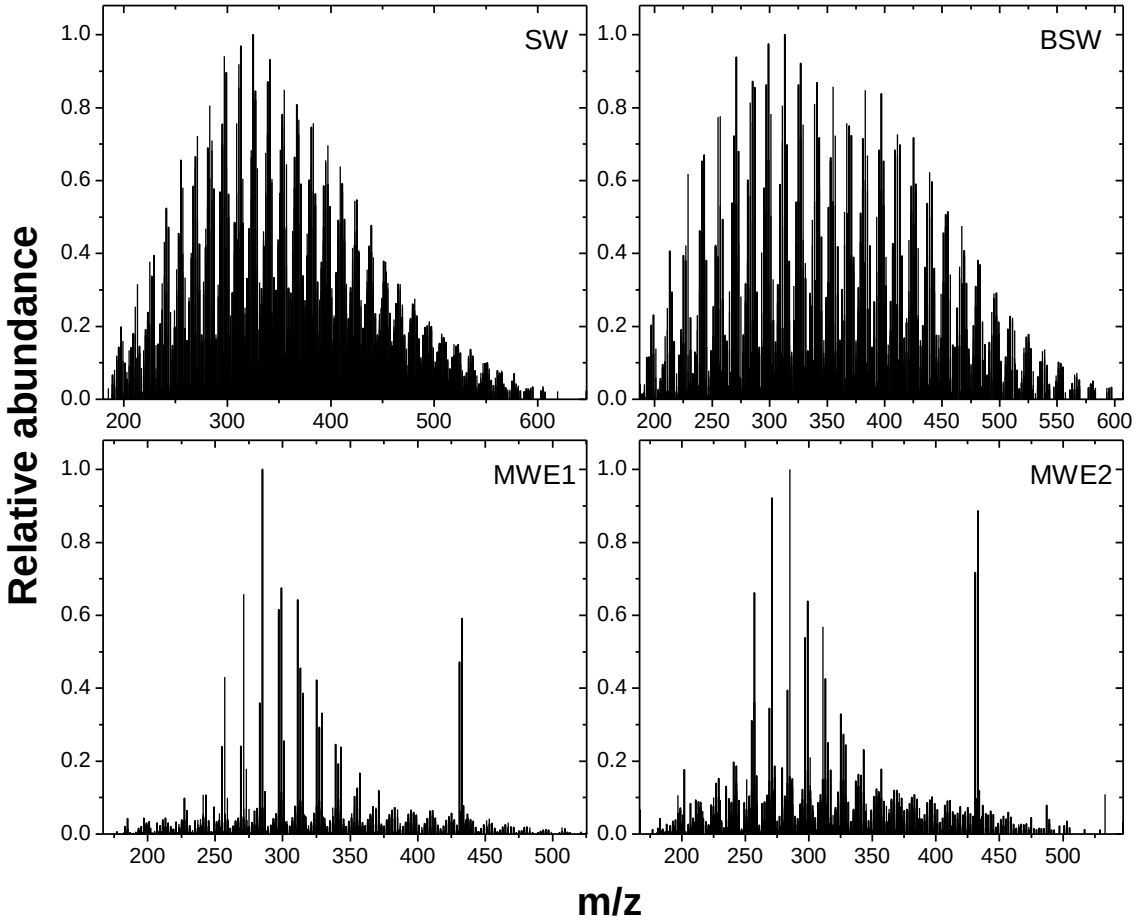

Figure A-10 Negative ESI Orbitrap mass spectra of each of the permeate after filtration of the different feed water samples showing the relative abundance of the identified peaks.

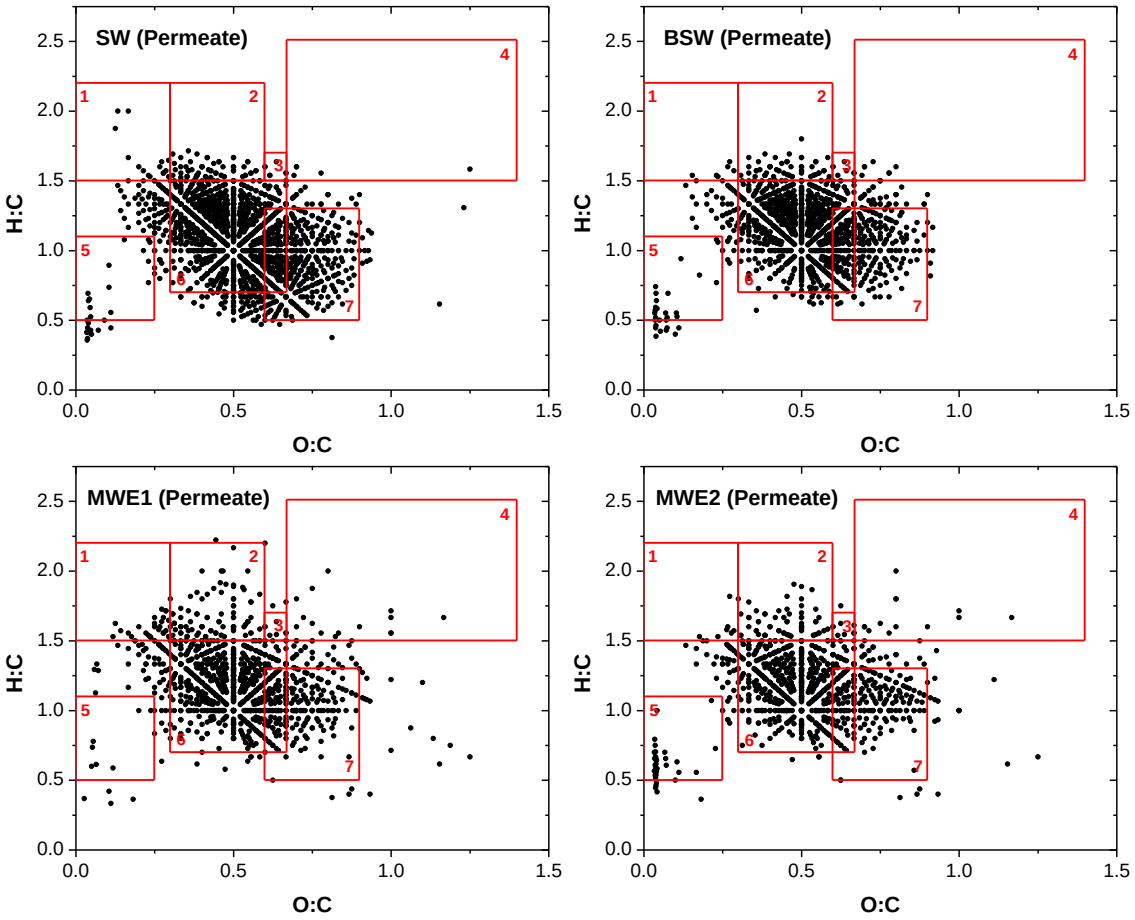

Figure A-11 The van Krevelen diagrams for all the four microfiltration permeates showing their respective chemical class distribution. The numbered rectangles mark the regions associated with (1) lipids, (2) proteins, (3) aminosugars, (4) carbohydrates, (5) condensed hydrocarbons, (6) lignins, and (7) tannins.

APPENDIX D

SUPPORTING INFROMATION FOR CHAPTER VI

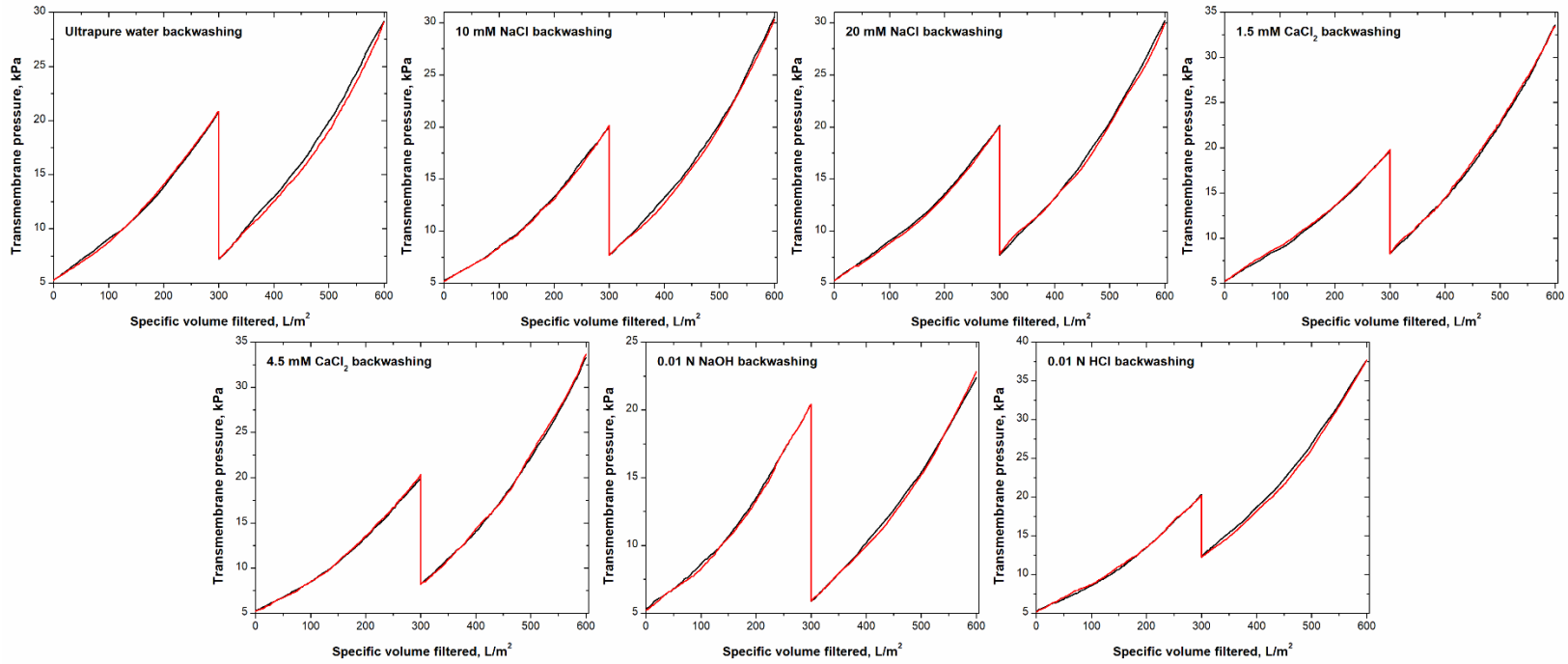

Figure A-12 Fouling profiles for filtration wastewater effluent with different backwashing water. The red and black plots represent duplicate experiments conducted on different days during the duration of this research. As observed, instantaneous pressure values under identical experimental conditions were very similar, indicating that the filtration behavior was closely reproducible.